FABRICATING MULTIFUNCTIONAL COATINGS USING LAYER-BY-LAYER LANGMUIR-BLODGETT PROCESSES

A Thesis

Presented to the Faculty of the Graduate School

of Cornell University

In Partial Fulfillment of the Requirements for the Degree of

Master of Science

By

Mun Sek Kim

May 2016

ABSTRACT

This thesis reports two new coating methods, Langmuir-Blodgett-Scooping (LBS) and Langmuir-Blodgett-Sequential-Dip-Coating (LBSDC), which allows one to efficiently create self-assembled, organized thin films of nanomaterials at the surface of water and to transfer these films onto nonreactive-supports in a layer-by-layer. The methods are used to create sophisticated coating configurations in *clip-like* and *laminated/stripped configurations* to impart explicit, desired functionality to membranes. LBS and LBSDC methods are used to integrate various forms of carbons, polymers and ceramics in specific configurations on conventional separators to enhance electrochemical performances of state-of-the-art lithium-sulfur cells. In essence, the coating methods utilize a self-assembly mechanism induced by spreading and mixing of water miscible solvents that create surface-tension-gradients caused by two different fluids known as the Marangoni effect. Utilizing this mechanism in a sequential fashion allows stacks of thin films composed of carbon/ceramic/polymer are successfully coated onto the porous polyolefin separator used in advanced energy storage devices, without the need for binders. It is shown that when the carbon/ceramic/polymer films are configured in the clip and laminated configurations, the resultant membranes are able to efficiently regulate mass and ion transport between the sulfur cathode and reactive lithium anode of a lithium-sulfur battery. Direct consequences of these improvements include enhanced capacity retention and Coulombic efficiency of rechargeable lithium-sulfur cells over a range of operating conditions.

BIOGRAPHICAL SKETCH

Mun Sek Kim was born in May 1992 in Seoul, the capital of the Republic of Korea. At the age of 13, he began his studies abroad. He first attended middle school in Ontario, Canada and subsequently moved to Seattle, USA to complete high school. He was admitted to the College of Chemistry at the University of California Berkeley to pursue a pre-dental program in 2010. However, after taking a few courses, he quickly became fascinated with engineering. As a result, he changed his major to Chemical Engineering after his first semester.

In the summer of 2011, Mun Sek joined Professor Roya Maboudian's Applied Materials & Surface Science Laboratory at UC Berkeley and began research in energy storage systems that focus on nanomaterial synthesis and application for microsupercapacitors. During his three years with Professor Maboudian, Mun Sek published two first-author and three second-author research papers, and co-authored four peer-reviewed conference papers. At the commencement in 2014, he received the John M. Prausnitz Award for outstanding undergraduate research in Chemical and Biomolecular Engineering, the highest honor given to one distinguished undergraduate researcher. Mun Sek's strong passion for energy storage systems research led him to pursue graduate studies in Chemical and Biomolecular Engineering at Cornell University. Under the tutelage of Professor Lynden A. Archer, he has devoted his graduate work to advancing the electrochemical performance of lithium sulfur batteries.

ACKNOWLEDGMENTS

First, I would like to express my most sincere gratitude to Professor Lynden A. Archer for his professional and helpful guidance on my research throughout my M.S. program. I have gained an incredible amount of knowledge and insight on battery research from the numerous meetings and conversations I have had with him. Professor Archer's energy and enthusiasm has continuously inspired me to grow as a mature independent researcher.

I would like to acknowledge my parents for their unconditional love and support, especially throughout my time of studying abroad. They have made numerous sacrifices for me over the years, and I would not be where I am today had it not been for their unwavering devotion. I am forever grateful for my parents.

I would also like to thank my friends across various continents who have always provided me with invaluable advice and encouraged me to pursue my dreams. My life has been deeply enriched by the trusting friendships these special individuals have given me.

Finally, I thank all my colleagues in the Archer Research Group. My research experience at Cornell was extremely productive, valuable and entertaining because of the amazing coworkers I have had the privilege of sharing this journey with.

TABLE OF CONTENTS

LIST OF FIGURES

CHAPTER 1

INTRODUCTION

1.1 Motivation

Throughout the 19th century, vast advances have been made in the field of electrification of human civilization, with the greatest advances evident in the technological improvement in electrical devices. These developments have enabled scientists and engineers to discover ways to effectively generate electricity for commercial use that further enhances peoples' quality of life.[1] Nowadays, most electrical power is generated by combustion processes where one fuel or another is consumed. Large amounts of energy consumed today come from combustion of coal and natural gas. Very recently, society has turned its attention to expanding this portfolio to include nuclear, hydropower, and renewable energy sources[2] including wind, solar, biomass and geothermal. As seen in Figure 1.1, the major sources of energy such as coal, natural gas and nuclear, are generated on demand through continuous processes and have no capacity to store electrical power. Furthermore, much of the generated energy is wasted due to the highly fluctuating energy consumption rates during day/night and different seasons.

There is no doubt that enough electricity power can be generated from the aforementioned fuel types using current technologies. However, there are still many pending issues as to how to store this tremendous amount of electricity into a system that must respond to random demand profiles even in a given day. Therefore, a system that could store energy efficiently, safely and economically will minimize energy waste and conveniently deliver energy at anytime and to any places. In this vein, the study of energy storage systems (ESS) can be considered the most important area of development in order to fulfill the future needs of sustainable energy.

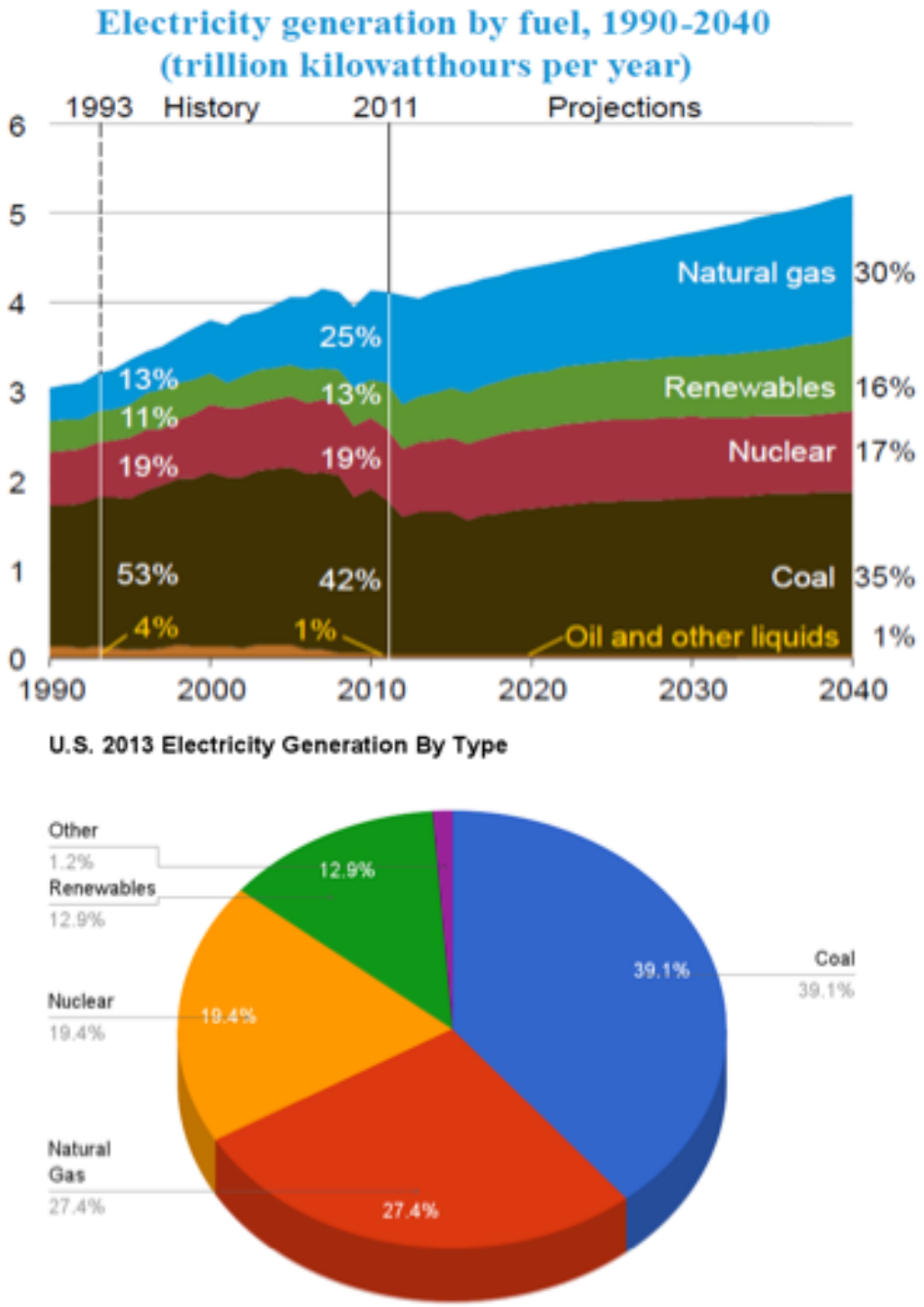

Figure 1.1. Trends in USA electricity generation. Petrina, Petru. "Renewable Energy." MSE 5150-Structures and Materials for Sustainable Energy Systems. 20 Jan. 2015. Lecture.

The first electric battery known as the voltaic pile was invented by Alessandro Volta in 1800. Since then, progress has been made continuously to enhance the efficacy of ESS and has resulted in chemical and physical batteries with several classifications such as primary (non-rechargeable), secondary (rechargeable), and tertiary (fuel cells) batteries. Primary and secondary batteries have received great attention from academia and industry to accommodate the soaring demand on portable electronic devises such as computers, mobile phones, autonomous sensors/actuators, and automobiles. To further facilitate the diverse and wide-ranging development of portable electronic devices, ESS technology must evolve to meet three important criteria: (i) high energy/power density, (ii) long cycle life and shelf time, and (iii) environmental/electrochemical safety.

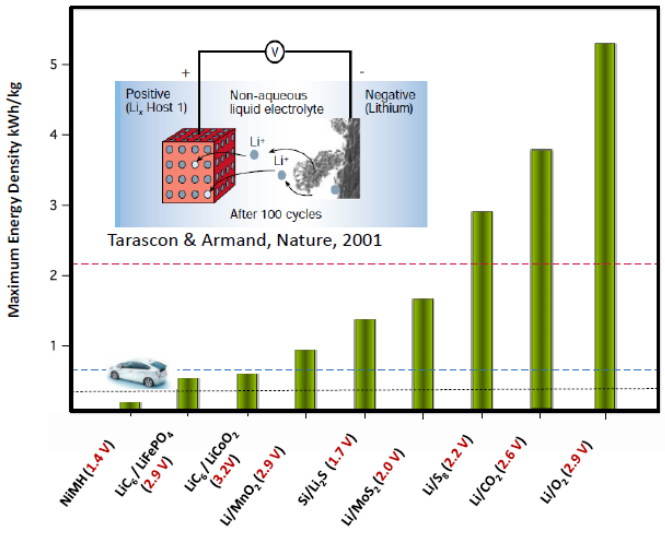

Figure 1.2. Comparison plot of theoretical energy density and discharge voltages for various lithium-based rechargeable batteries. The horizontal red and black lines indicate long- and short-term targets. The blue line represents the estimated energy density of gasoline for transportations. Reproduced with permission[3]. Copyright (2001) Nature Publishing Group.

Lithium-based secondary batteries are considered to be the most promising ESS that could safely store/deliver electrical energy with moderate operating/unit costs. In recent years, insertion-based lithium ion (Li-ion) and lithium ion polymer (Li-Po) rechargeable batteries have benefited greatly from a growing body of research and industrial processes able to create these cells in a reliable and cost effective manner.[4,5] Li-ion and Li-Po batteries have typical specific energies of 150 Wh kg^{-1} and 180 Wh kg^{-1}, respectively, and today, performance of practical batteries in either formal can easily achieve 90% of the respective theoretical capacity set by the chemistry of the materials in the battery anode, cathode, and electrolyte.[6] With the rapid advancement in mobile phones, electrical vehicles, grid energy systems and space/aircraft, however, post-secondary batteries (such as Li metal, lithium-sulfur (LiS), lithium-air, and sodium/aluminum-based batteries) are now attracting more attention due to their large theoretical capacities.

Room-temperature LiS batteries are regarded as the next generation batteries for ESS and are targeted to replace traditional insertion-based Li-ion batteries due to their high theoretical capacity. LiS batteries have a tenfold higher theoretical capacity (2500 Wh kg^{-1}) compared to that of Li-ion batteries (See Figure 1.2). And because sulfur is an electrochemically active element that is environmentally benign, nontoxic, cheap, and readily available, LiS batteries are quickly becoming the research and investment focus of both academia and industry in regions all over the world.

Despite such advantages as high capacity and cost effectiveness, LiS batteries critically suffer from poor cycle life and low coulombic efficiency (CE).[6–11] The rapid fade in

capacity and low electrochemical utilization of sulfur are now known to originate from at least four inter-related problems: (1) sulfur and the discharge product of Li_2S are poor electronic/ionic conductors and thus require a highly conductive matrix such as carbon, polymer or metal in which incorporation of the matrices reduce the energy density of LiS cells; (2) the intermediate discharge products of sulfur, known as lithium polysulfides (LiPS), dissolve in an electrolyte; (3) the dissolved LiPS shuttle from cathode to anode during the battery cycles and this shuttling phenomenon results in a loss of active material sulfur and a low CE; and (4) the lithium metal anode degrades as LiPS, especially $Li_2S_{1\text{-}2}$, react and form an insoluble/inactive layer at the lithium surfaces, as this surface passivation induces unstable solid-electrolyte-interfaces that hinder the long cycle life of LiS batteries. All these critical problems need to be addressed in order to fabricate highly rechargeable LiS batteries that live up to the promise of this cell chemistry.

Many scientific and technical approaches have been made to resolve the aforementioned problems and to enhance the capacity retention rate and CE of LiS cells. These approaches include the encapsulation of sulfur using nanostructured physical confinements,[12–14] modifications of surface chemistries on conductive matrices,[15–17] optimizing electrolyte systems using chemical additives,[8] understanding of Li-S redox chemistries,[18] and separator modifications.[19–31] As a result of advances made in each of these areas, LiS cells able achieve stable cycling performance (>500 cycles) with a reasonable capacity (~1000 mAh g^{-1}) and CE (>90%) with sulfur loading and content of >2 mg cm^2 and >60% in the cathode have become possible in smaller format research

cells. Nevertheless, there is still much room for improvement in LiS systems in order to achieve the full potential of LiS and establish LiS ESS in practical devices.

To date, a large amount of research has been devoted to cathode and electrolyte engineering to improve stability of LiS batteries. Conventionally, cathode preparation requires the infusion and encapsulation of sulfur into a nanostructured carbon matrix. Also, a conventional electrolyte system, 1M of Bis(trifluoromethane)sulfonimide lithium salt (LiTFSI) in Dimethoxyethane (DME):1,3-dioxolane (DOL) (1:1 v/v) with $LiNO_3$ as co-salt, for LiS is established. In order to further optimize LiS cells, researchers have recently begun to expand their focus on modifying conventional polyolefin separators, which are readily available in the market and widely used in many battery systems as well as in research. These separators play a crucial role in the battery system as they could electrically separate the anode from the cathode. Therefore, it is important to note that improvements in separator design and performance also offer potential for enhancing battery safety, which from a commercializing perspective is as important as battery performance.

Since LiS cells undergo complex electrochemical reactions with the aforementioned problems limiting performance, novel cell configurations are required to successfully overcome the fundamental problems at the root of these issues. Considering the important role of transport of conversion products developed in the cathode on degradation pathways in LiS cells, strategies for modifying existing separators to regulate ion and mass transport are especially promising. However, the technical methods currently

available to the research/industry fields are insufficient in accomplishing this task and thus obstruct the advancement of LiS cells. Therefore, new technical approaches to modifying commercially available separators are urgently needed to surpass the current electrochemical performance threshold of the LiS cells.

1.2 Thesis Structure

In this thesis, new separator modification methods for LiS cells are reported. These new methods, namely Langmuir-Blodgett Scooping (LBS) and Langmuir-Blodgett-Sequential-Dip-Coating (LBSDC), utilize a self-assembly mechanism of nanoparticles and the Marangoni stresses of fluids on the surface of water. The approaches enable diverse nanomaterials to be integrated and coated on various solid substrates in layer-by-layer configurations. In order to optimize material loading on the separator and to maximize the utilization rate of the coated materials, clip and laminated coating structures are developed. In this process, carbon, polymer, and ceramic nanomaterials are mainly used to create an effective LiPS reservoir that can maintain a high capacity retention while mitigating the shuttling effect of LiS cells.

Chapter 1 provides a brief introduction to the importance of ESS and the leading literature on LiS batteries, along with some implications for the future design of LiS components. Chapter 2 presents a more detailed analysis on LiS batteries with a focus on the LiS system. A review on the development of the LiS technology is also reported in this chapter, followed by various approaches to overcoming the critical problems associated with LiS batteries. The chapter concludes with an explanation of the important aspects of separator modification for the purpose of further advancing state-of-the-art LiS batteries.

In Chapter 3, the LBS and LBSDC methods are illustrated and explained in detail, along with the appropriate application for LiS batteries. With these two methods, ordered multifunctional nanoparticle films are created on non-reactive support to facilitate fast ion/electron transport. Dense monolayers of multi-walled carbon nanotubes, spherical carbon nanopowders and metal-oxide nanospheres/particles are coated on solid substrates with different configurations. Also, these materials are stacked in a layer-by-layer configuration to create effective multifunctional membrane coatings. A clip like structure that contains layers of Carbon/Ceramic/Carbon is developed in this chapter, with coatings that have a gravimetrical areal coverage of ~130 $\mu g\ cm^{-2}$ and a thickness of ~3 μm. This clip configuration coating is advantageous for efficiently adsorbing dissolved LiPS, but maintaining electrical connectivity of the trapped LiPS, allowing its reutilization as the cell is cycled to improve electrochemical performance of LiS cells. The applicability of these invented coating methods for LiS separator modifications is shown in detail in this chapter.

In Chapter 4, the coating methods are extended to coat carbon, polymer, and ceramics with active functional groups on the polymer chains that help to adsorb LiPS via specific electrostatic/coulombic interactions. For this purpose, a laminated/stripped configuration coating that consists of a thin layer of carbon, highly electronically conducting polymer, and ceramic nanopowders is developed. These materials are integrated in a layer-by-layer to regulate fast mass and charge transport and subsequently create a LiPS reservoir on the separator for LiS cells. The LiPS reservoir effectively intercepts LiPS by electropositive

imine/amine groups on polyaniline (PANI) polymer and reutilizes them by conducting electrons during cell cycles. A thin, dense layer of titania nanoparticles is imbedded in PANI coatings to reduce LiPS migration flux via physical adsorption of LiPS on the titania surfaces. A highly packed and porous 3D network of titania nanoparticle coatings synergistically works with PANI coatings to efficiently capture LiPS and retain capacity for a large number of cycles. With this polymer/ceramic hybrid LiPS reservoir (~400 μg cm^{-2} and ~10 μm thickness), a high Coulombic efficiency is achieved without any additives/co-salt in an electrolyte. Finally, how to optimize material loading and the electrochemical performance of LiS cells via separator modifications is explained in this chapter.

REFERENCES

1. Johansson, T. B., Kelly, H., Reddy, A. K. . & Willliams, R. . Renewable Fuels and Electricity for a Growing World Economy: Defining and Achieving the Potential. *Energy Study Rev.* **4,** 201–212 (1992).
2. Sims, R. E. H., Rogner, H.-H. & Gregory, K. Carbon emission and mitigation cost comparision between fossil fuel, nuclear and renewable energy resources for electricity generation. *Energy Policy* **31,** 1315–1326 (2003).
3. Tarascon, J.-M. & Armand, M. Issues and challenges facing rechargeable lithium batteries. *Nature* **414,** 359–367 (2001).
4. Goodenough, J. B. Evolution of strategies for modern rechargeable batteries. *Acc. Chem. Res.* **46,** 1053–1061 (2013).
5. Bruce, P. G. Energy storage beyond the horizon: Rechargeable lithium batteries. *Solid State Ionics* **179,** 752–760 (2008).
6. Ma, L., Hendrickson, K. E., Wei, S. & Archer, L. A. Nanomaterials: Science and applications in the lithium–sulfur battery. *Nano Today* **10,** 315–338 (2015).
7. Manthiram, A., Fu, Y., Chung, S., Zu, C. & Su, Y. Rechargeable Lithium − Sulfur Batteries. *Chem. Rev.* **114,** 11751–11787 (2014).
8. Scheers, J., Fantini, S. & Johansson, P. A review of electrolytes for lithium-sulphur batteries. *J. Power Sources* **255,** 204–218 (2014).
9. Lin, Z. & Liang, C. Lithium–sulfur batteries: from liquid to solid cells. *J. Mater. Chem. A* **3,** 936–958 (2015).
10. Zhang, S., Ueno, K., Dokko, K. & Watanabe, M. Recent Advances in Electrolytes

for Lithium-Sulfur Batteries. *Adv. Energy Mater.* **5,** 1–28 (2015).

11. Manthiram, A., Chung, S.-H. & Zu, C. Lithium–Sulfur Batteries: Progress and Prospects. *Adv. Mater.* **27,** 1980–2006 (2015).
12. Jayaprakash, N., Shen, J., Moganty, S. S., Corona, A. & Archer, L. A. Porous hollow carbon@sulfur composites for high-power lithium-sulfur batteries. *Angew. Chemie* **50,** 5904–5908 (2011).
13. Ji, X., Lee, K. T. & Nazar, L. F. A highly ordered nanostructured carbon-sulphur cathode for lithium-sulphur batteries. *Nat. Mater.* **8,** 500–506 (2009).
14. Wang, H. *et al.* Graphene-Wrapped Sulfur Particles as a Rechargeable Lithium – Sulfur Battery Cathode Material with High Capacity and Cycling Stability. *Nano Lett.* **11,** 2644–2647 (2011).
15. Ma, L. *et al.* Enhanced Li–S Batteries Using Amine-Functionalized Carbon Nanotubes in the Cathode. *ACS Nano* **10,** 1050–1059 (2015).
16. Ma, L. *et al.* Hybrid cathode architectures for lithium batteries based on TiS 2 and sulfur. *J. Mater. Chem. A* **3,** 19857–19866 (2015).
17. Ma, L. *et al.* Tethered Molecular Sorbents: Enabling Metal-Sulfur Battery Cathodes. *Adv. Energy Mater.* **4,** 390–399 (2014).
18. Barchasz, C. *et al.* Lithium/sulfur cell discharge mechanism: An original approach for intermediate species identification. *Anal. Chem.* **84,** 3973–3980 (2012).
19. Hendrickson, K. E., Ma, L., Cohn, G., Lu, Y. & Archer, L. A. Model Membrane-Free Li-S Batteries for Enhanced Performance and Cycle Life. *Adv. Sci.* **2,** 68–77 (2015).
20. Yao, H. Bin *et al.* Improved lithium-sulfur batteries with a conductive coating on

the separator to prevent the accumulation of inactive S-related species at the cathode-separator interface. *Energy Environ. Sci.* **7,** 3381 (2014).

21. Balach, J. *et al.* Functional Mesoporous Carbon-Coated Separator for Long-Life, High-Energy Lithium-Sulfur Batteries. *Adv. Funct. Mater.* **25,** 5285–5291 (2015).
22. Wang, G., Lai, Y., Zhang, Z., Li, J. & Zhang, Z. Enhanced rate capability and cycle stability of lithium–sulfur batteries with a bifunctional MCNT@PEG-modified separator. *J. Mater. Chem. A* **3,** 7139–7144 (2015).
23. Zhang, Z., Lai, Y., Zhang, Z. & Li, J. A functional carbon layer-coated separator for high performance lithium sulfur batteries. *Solid State Ionics* **278,** 166–171 (2015).
24. Wei, H., Li, B., Zuo, Y. & Xia, D. Enhanced Cycle Performance of Lithium-Sulfur Battereis Using a Separator Modified with a PVDF-C Layer. *ACS Appl. Mater. Interfaces* **6,** 20276–20281 (2014).
25. Li, F. *et al.* A graphene-pure-sulfur sandwich structure for ultrafast, long-life lithium-sulfur batteries. *Adv. Mater.* **26,** 625–631 (2014).
26. Xiao, Z. *et al.* A Lightweight TiO2/Graphene Interlayer, Applied as a Highly Effective Polysulfide Absorbent for Fast, Long-Life Lithium-Sulfur Batteries. *Adv. Mater.* **27,** 2891–2898 (2015).
27. Zhang, Z., Lai, Y., Zhang, Z., Zhang, K. & Li, J. Al2O3-coated porous separator for enhanced electrochemical performance of lithium sulfur batteries. *Electrochim. Acta* **129,** 55–61 (2014).
28. Chen, Y. *et al.* Chitosan as a functional additive for high-performance lithium–sulfur batteries. *J. Mater. Chem. A* **3,** 15235–15240 (2015).

29. Zhang, Z., Zhang, Z., Li, J. & Lai, Y. Polydopamine-coated separator for high-performance lithium-sulfur batteries. *J. Solid State Electrochem.* **19,** 1709–1715 (2015).

30. Huang, J.-Q. *et al.* Ionic shield for polysulfides towards highly-stable lithium–sulfur batteries. *Energy Environ. Sci.* **7,** 347 (2014).

31. Jin, Z., Xie, K., Hong, X., Hu, Z. & Liu, X. Application of lithiated Nafion ionomer film as functional separator for lithium sulfur cells. *J. Power Sources* **218,** 163–167 (2012).

CHAPTER 2

BACKGROUND ON LITHIUM SULFUR BATTERY

2.1 About lithium sulfur batteries

In 1962, D. Herbert and J. Ulam first introduced sulfur as a cathode material in electric dry cells and storage batteries.[1] Since then, progressive developments have been made on primary lithium-sulfur (LiS) batteries. During the late 1900's, researchers found important electrolyte solvents that contain aliphatic amines,[1] propylene carbonate,[2] tetrahydrofuran-toluene,[3] and dioxolane[4,5] for LiS batteries, and demonstrated the rechargeability of LiS cells.[5] LiS batteries continue to attract more attention because of the high theoretical capacity of sulfur (1650 mAh g^{-1}) and lithium (3860 mAh g^{-1}) as electrodes and the low cost of sulfur. In the 21st century, scientists and engineers are continuing to devote great efforts into developing highly rechargeable LiS cells.

LiS batteries are classified as secondary chemical batteries that can store/deliver electricity via a chemical reaction between sulfur and lithium. A conventional LiS cell is composed of an electrochemically active elemental sulfur cathode, a lithium (Li) metal anode, an insulating membrane/separator, and non-aqueous organic electrolytes with salts. The electrical current is produced during the cell discharge, wherein the Li metal anode is oxidized by loss of electrons to form Li^+ ions that travel internally via the electrolyte to react with the cyclic sulfur in the cathode. The produced electrons from the anode travel via a metallic current collector to an external circuit (See Figure 2.1 a) to power a device. During charging, the reverse process occurs. The reversible chemical reaction between lithium and cyclic sulfur shown below is therefore a requirement for

rechargeable cell performance. It is based on the assumption of a complete reaction between Li and S_8.

$$16Li + S_8 \leftrightarrow 8Li_2S$$

This reaction of Li and sulfur is responsible for the high theoretical energy of 2500 Wh kg^{-1} that able to be reversibly stored in the LiS battery, which is approximately ten times higher than that of conventional Li-ion cells.

Figure 2.1 b shows the galvanostatic discharge/charge voltage profiles of LiS cells. During discharge, two voltage plateaus at 2.3V and 2V are observed. The discharge voltage profile shows a reduction of the cyclic sulfur to form intermediate species of high-order LiPS (Li_2S_x $4 < x \leq 8$) at a high plateau (2.3V) and low-order LiPS (Li_2S_x $2 < x \leq 4$) at low plateau (2V) with the final product of Li_2S. The reverse process occurs during battery charge, and two plateaus are observed at 2.2V and 2.4V, respectively, based on the phase transition mechanism (lithium sulfides to longer LiPS - liquid, ending with cyclic sulfur - solid).[6] A schematic illustration of the reduction process of sulfur with intermediate LiPS formation is shown in Figure 2.1 c. It is found that LiPS (Li_2S_x $2 < x \leq 8$) dissolve in electrolytes[7] and, as a result, the actual process involves more complex reactions than the ideal process mentioned above. A summary of the representative discharge reaction mechanism of the LiS cell is shown in Figure 2.2.

(a)

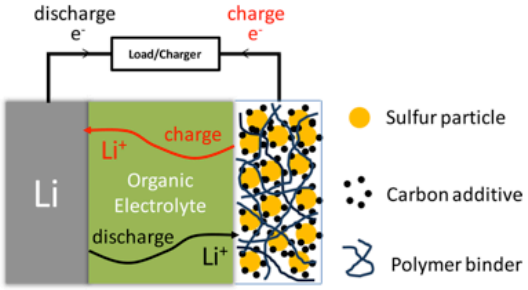

(b)

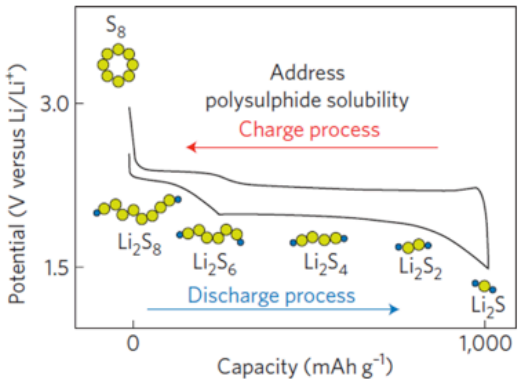

(c)

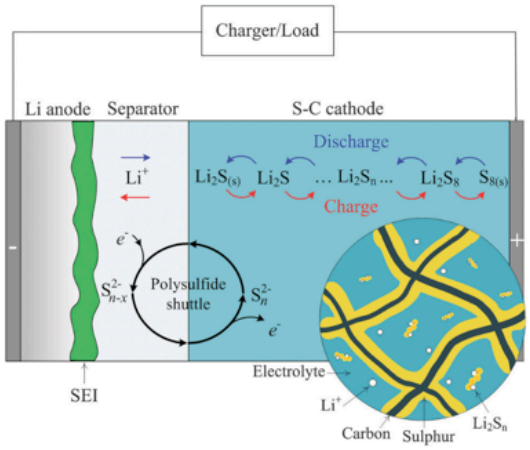

Figure 2.1. (**a**) Electrochemical process of LiS cell. Reproduced with permission[8]. Copyright (2014) American Chemical Society. (**b**) Galvanostatic discharge/charge voltage profiles of LiS cell. Reproduced with permission[9]. Copyright (2012) Macmillan Publishers Ltd. (**c**) Illustration of LiPS dissolution and shuttling phenomenon. Reproduced with permission[7]. Copyright (2015) Royal Society of Chemistry

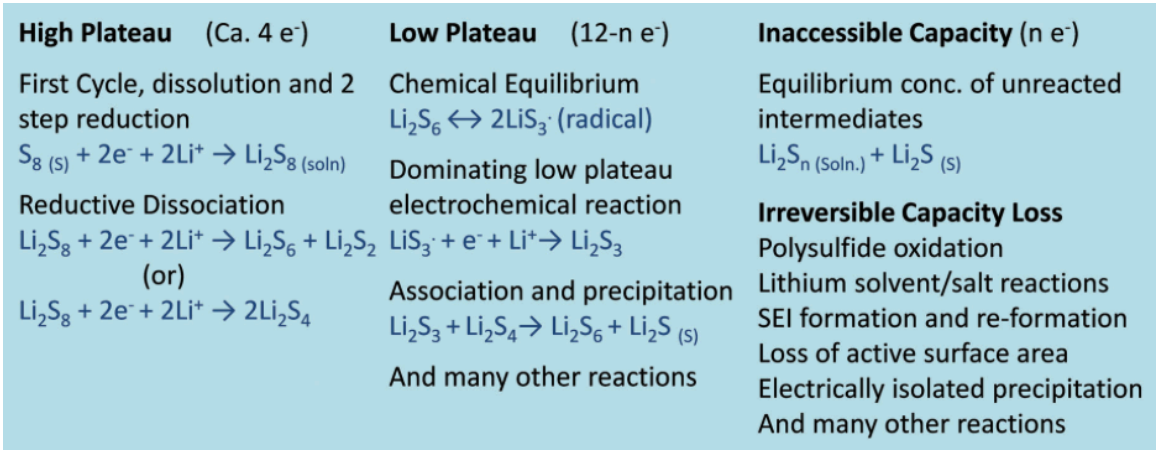

Figure 2.2. Representative discharge reaction mechanism of LiS cell. Reproduced with permission[7]. Copyright (2015) Royal Society of Chemistry.

In spite of having such advantages as large capacity, low active material cost, and the nontoxicity of sulfur, the LiS battery faces a number of technical challenges that impede commercialization. The greatest concern is the resistive nature of sulfur (5×10^{-30} S cm^{-1} at room-temperature) and its discharge products, which lead to poor electrode kinetics and causes low material utilization and rate capability. To mitigate this, highly electrically conductive materials must be incorporated with sulfur to reduce electron transport lengths in sulfur so the timescales for charge transfer are reasonable. However, the addition of new materials not only reduces the energy density of the LiS cell, but may also compromise access of the electrolyte to sulfur. For this, liquid electrolytes able to wet sulfur and other materials incorporated in the cathode are a requirement. Unfortunately, most liquid electrolytes have a high solubility of LiPS, and electrolytes with a high utilization of sulfur tend to have high solubility of LiPS, thereby creating another critical challenge called LiPS shuttling.

Electrolyte	Typical example	Advantages	Limitations
Carbonate solvents	1 M $LiPF_6$ in EC/DMC (1:1 v/v)	Applicable for sulfur/microporous carbon, PAN-S, and polymer gel electrolyte, high dielectric constant and low viscosity	Incompatible with polysulfides, evaporation
Ether solvents	1 M LiTFSI in DOL/DME (1:1 v/v)	Stable toward polysulfides, applicable for all cathodes, low viscosity, high donor number and conductivity, high polysulfide solubility, good rate capability	Severe shuttle effect, easy evaporation
Fluorinated ethers	1.0 M LiTFSI in DOL/HFE (1:2 v/v)	Low melting points, low viscosities, low flammabilities, depressed shuttle effect, low polysulfide solubility	Low conductivity, easy evaporation, high cost
Sulfone homologs	EMS or TMS	Lower volatility than ethers, low cost, superior safety, high dielectric constant, high oxidation potential, low toxicity	More viscous and lower donor number than ethers
Concentrated electrolytes	solvent-in-salt electrolyte (7 M LiTFSI in DME/DOL)	High Li^+ concentration, low solubility of polysulfides, very high coulombic efficiency	High viscosity, low Li^+ diffusion rate, high potential polarization, low rate capability
Aprotic ionic liquids	1 M LiTFSI in [PP14][TFSI]	Negligibly volatility, low flammability, high thermal stability, wide electrochemical potential window, low volatility, low polysulfide solubility	Need additional lithium salt, high viscosity, low conductivity, low Li^+ transference numbers, high cost, complicated synthesis, high cell polarization, poor rate capability
Solvate ionic liquids	[Li(G4)][TFSI]	Containing only Li cations, high Li^+ transference numbers, low cost, low volatility, easy preparation, low polysulfide solubility, high coulombic efficiency	High viscosity, low conductivity, slow Li^+ transport, high cell polarization, poor rate capability
Ionic liquids-organic solvent mixtures	1 M LiTFSI in DME/[PP13][TFSI] or [Li(G4)][TFSI]/4HFE	High conductivity, large capacity, high coulombic efficiency, improved capacity retention, and suppressed shuttling.	Easy evaporation
Aqueous electrolytes	0.2 M LiOH aqueous solution	Non-toxic, low cost, noncombustible, high conductivities	Narrower electrochemical window, complex redox reaction of sulfur
Solid polymer electrolytes	10 wt% ZrO_2 in PEO_{20}-$LiCF_3SO_3$ complex	Solvent-free, superior temperature and mechanical stabilities, prevention of Li dendrite formation, depressed shuttle effect,	High operation temperature, very low conductivity at room temperature, high cell polarization, poor cycling lifetimes, poor rate capability
Polymer gel electrolytes	PVdF–HFP incorporating 0.5 M LiTFSI–[P14][TFSI]	Higher conductivity than solid polymer electrolytes, mechanically stable,	Evaporation, still leakage, poorer battery performance than organic liquid electrolytes
Inorganic solid electrolytes	Li_2S–P_2S_5 or Thio-LISICONs	High Li^+ transference numbers, no leakage, no vapor pressure and non-flammability of electrolytes	High operation temperature, low conductivity, sluggish electrochemical reaction, poor rate capability,

Figure 2.3. Characteristics of various electrolyte systems for LiS cells. Reproduced with permission[10]. Copyright (2015) WILEY-VCH Verlag GmbH & Co. KGaA, Weinheim.

Even though many electrolyte systems for LiS batteries have been studied, the dissolution of LiPS is inevitable especially with glyme-based and dioxolane-based liquid electrolytes. Recent advancements in the LiS electrolyte system are summarized in Figure 2.3. The shuttling phenomenon arises from the dissolution and migration of intermediate LiPS species from the cathode to the anode via electrolytes and vice versa during the

cycling of the LiS cell. Furthermore, the migrated LiPS from the cathode reacts with the Li anode[6] to cause a chemical short, meaning the material is electrochemically inactive, due to passivation of the Li surfaces, and as a result reduces the material utilization and coulombic efficiency (CE). The main reason for the low CE is shuttling, which occurs when the high-order LiPS dissolve in the electrolyte, migrate to and react with the Li metal, transform into low-order LiPS, which in turn may diffuse back to the cathode to react with sulfur to recreate higher order LiPS in a parasitic, cyclic process that consumes both the active material in the cathode and anode without generating electrical energy.[11] The attempts to model the shuttling process mathematically were made by Y. Mikhaylik and J. Akridge to quantitatively analyze the shuttle phenomenon in the LiS cells.[6] The charge-shuttle Factor (f_c) in Equation 1 evaluates shuttling with two different charge behaviors based on the ratio of the charge current I_c, shuttle constant k_s, high plateau specific capacity (quarter of the theoretical capacity) q_H, and total sulfur concentration S_{total}:

$$\frac{k_s q_H S_{total}}{I_c} = f_c \qquad (1)$$

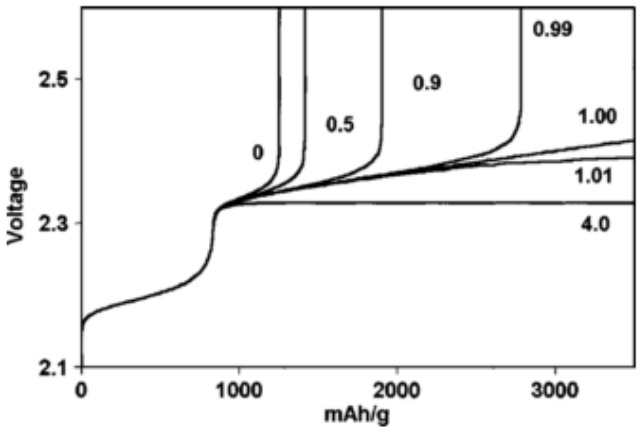

Figure 2.4. Simulated charge voltage profiles of LiS at different f_c values. Reproduced with permission[6]. Copyright (2004) The Electrochemical Society.

Figure 2.4 shows the simulated results for the charging behavior in a LiS cell with different f_c values ranging from 0 to 4. Complete charging is observed for f_c <1 with high enough I_c or small k_s and S_{total}. However, when the shuttle factor reaches a value of one or above, a high overcharge protection is observed, horizontal voltage leveling without a sharp voltage increase. This extension of the charging voltage profile causes the corrosion of the Li metal and furthermore the consumption of electrons from the LiPS migration, which result in the poor cycling and low CE of the LiS cell. The reciprocal shuttle constant is interpreted with a differential equation as shown in Equation 2 to observe relationship between shuttle constant and shuttling phenomenon:

$$\frac{1}{k_s} = \frac{dQ_H}{dI_c} \qquad (2)$$

Equation 2 is the simplified equation from the high plateau accumulated capacity equation (Q_H)[6] assuming low charging current. The shuttle constant can be calculated by

using a small charging current and measuring the upper plateau charging capacity. In corollary, the shuttle constant, k_s, is proportionally related to the shuttle effect (i.e. the lower the shuttle constant for LiS system, the weaker the shuttling effect).

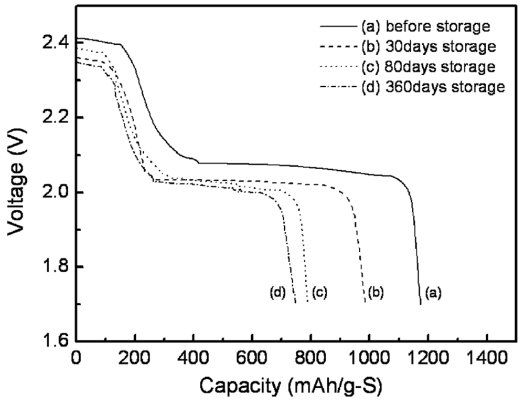

Figure 2.5. Self-discharge demonstration of LiS cells using tetra ethylene glycol dimethylether electrolyte at room temperature. Reproduced with permission[12]. Copyright (2006) Elsevier.

The instability and high reactivity of LiPS in LiS battery cause a short shelf time due to the high self-discharge process, which is an important factor for possible commercialization. As observed in Figure 2.5, the LiS cells tend to discharge by themselves, resulting in a capacity fade by the dissolution of LiPS in the liquid electrolyte; diffusion to the anode and reaction with Li to form lower order LiPS. The self-discharge of the LiS cell is more severe with ether-based electrolytes, which possess a high solubility of LiPS. The mathematical formula that illustrates the relationship among the shuttle constant k_s, high plateau capacity Q_H, and resting time t_r, is developed by Y. Mikhaylik et al. as shown below:

$$-k_s = \frac{dQ_H}{dt_r} \qquad (3)$$

Equation 3 shows the strong correlation between the self-discharge (t_r) and the shuttling effect (k_s), which means that both problems originate from the dissolution of the LiPS in the electrolytes. For this reason, mitigating and stopping LiPS dissolution in the electrolyte is not only highly desirable, but also necessary in order to eliminate prominent challenges. Hence, a great amount of research has been focused on suppressing LiPS dissolution by developing novel electrode materials/structures and cell configurations/components.

2.2 Lithium sulfur cathodes

A conventional LiS cathode consists of pure sulfur and a carbon mixture with an electrochemically inactive binder.[13] This conventional cathode unfortunately suffers from low sulfur utilization and unstable electrochemical reactions. Because sulfur is highly resistive, only sulfur that is in contact with the carbon/current collector and electrolyte is electrochemically accessible and able to participate in redox reactions in the cathode. Also, sulfur undergoes an 80% volumetric change during its conversion reaction with Li, which puts significant strain on the components in the cathode and ultimately destroys the particles' interconnected junctions among the sulfur, carbon, binder, and current collector during the first few cycles that lead to a rapid capacity decay.[11,14,15] As LiPS readily dissolve into the electrolyte and shuttle, this phenomenon impedes the stable redeposition of sulfur onto a conductive platform and initiates the formation of sulfur clusters/aggregates that are inactive in the cathode. Thus, an ideal cathode for LiS batteries should have a high electronic conductivity, tolerate volumetric changes, and encapsulate the LiPS during the redox reactions. To overcome these prominent challenges, scientists and engineers first started to physically/chemically modify the morphologies of conductive matrices and sulfur particles. Since adding conductive materials is unavoidable in the sulfur cathode, adjusting the sulfur loading and content in the cathode is needed to achieve a reasonable performance that can maximize the utility of sulfur in LiS batteries.

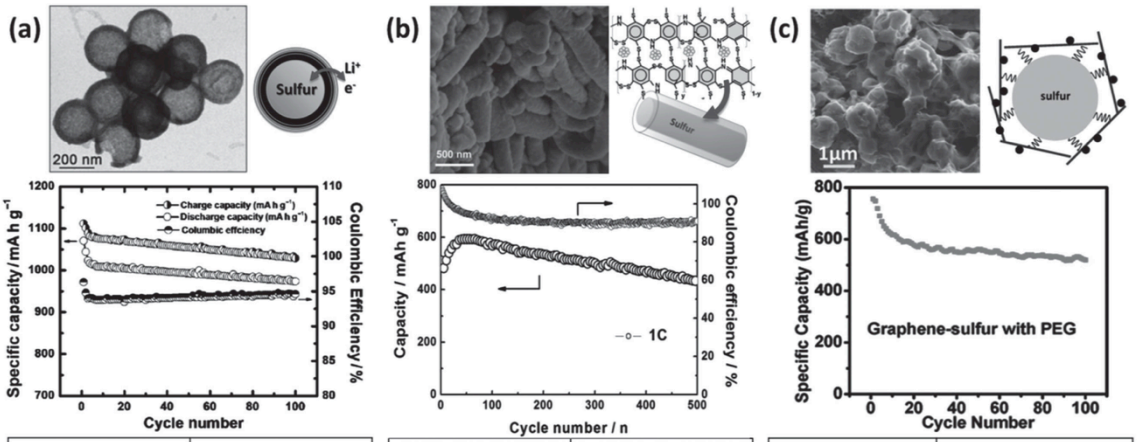

Sulfur content	64.75 wt. %
Initial discharge capacity	1071 $mAhg^{-1}$ at a C/2 rate
Cycle life	100 cycles
Capacity fading rate	0.09 % per cycle
Capacity retention rate	91 %

Sulfur content	49.60 wt. %
Initial discharge capacity	511 $mAhg^{-1}$ at a 1C rate
Cycle life	500 cycles
Capacity fading rate	0.03 % per cycle
Capacity retention rate	85 %

Sulfur content	56.00 wt. %
Initial discharge capacity	750 $mAhg^{-1}$ at a C/5 rate
Cycle life	100 cycles
Capacity fading rate	0.30 % per cycle
Capacity retention rate	70 %

Figure 2.6. (**a**) porous hollow carbon@sulfur nanocomposite, (**b**) sulfur–polyaniline nanotube, and (**c**) poly(ethylene glycol) (PEG)-wrapped graphene–sulfur nanocomposite. (**a**) Reproduced with permission[16]. Copyright 2011, WILEY-VCH Verlag GmbH & Co. KGaA, Weinheim. (**b**) Reproduced with permission[17]. Copyright 2012, WILEY-VCH Verlag GmbH & Co. KGaA, Weinheim. (**c**) Reproduced with permission[18]. Copyright 2011, American Chemical Society.

Researchers have proposed several methods[16,19,20] to sequester sulfur in various carbon[16,18,19,21–31] and polymer[17,32–34] nanomaterials. First, the melt-diffusion process of sulfur to synthesize sulfur/carbon nanocomposite was introduced by Ji et al.[19] In brief, pristine sulfur is melted at 155 ^{o}C (the temperature at which liquid sulfur exhibits lowest viscosity), and diffuse into mesoporous network of carbon, CMK-3, with pore size and volume of 3 nm and 2.1 $cm^3 g^{-1}$. By infusing liquid sulfur into the mesoporous conductive matrix, a good encapsulation of sulfur is obtained and thus stable reversible capacity of the LiS cells is achieved. Jayaprakash et al. proposed a vapor infusion method to encapsulate vaporized sulfur into mesoporous hollow carbon cores.[16] For the first time, high-performance LiS cells were fabricated with porous hollow carbon@sulfur nanocomposite with a high reversible capacity, sulfur content, as well as cycling number

(Figure 2.6 a). The mesoporous hollow carbon shells provide an excellent encapsulation of sulfur that can sequester up to 70% of the sulfur, maximize sulfur utilization, minimize the LiPS dissolution, withstand volumetric changes, and regulate the rapid Li ion transport. Hence, a capacity retention rate of 91% and reversible capacity of ~1000 mAh g^{-1} at 0.5C are reported for 100 cycles. Additionally, a chemical synthesis method of developed by Su et al enables direct formation of sulfur-carbon nanocomposites able to sequester sulfur during LiS battery cycling.[20] This approach, which is different from the heat-treatment process, is utilized to chemically bind sulfur to synthesize sulfur-carbon composites. Despite its simpler and safer configuration, strong nucleation of sulfur is common on the carbon matrix, forming sulfur aggregates that become inactive after few redox reactions. Hence, a limited improvement in the electrochemical performance (~340 mAh g^{-1} at 0.5C) is achieved.

Polymers have also been considered to constitute a promising matrix for sulfur to facilitate the charge and ion transport.[35] Polymers with a high conductivity, chemically active functional groups, and mechanical flexibility are especially desired for encapsulating sulfur. Xiao et al. reported the encapsulation of sulfur using self-assembled polyaniline (PANI) nanotubes.[17] Unlike carbon, electropositive amine/imine groups on the polymer chains attract LiPS via electrostatic/coulombic interactions that reduces the solubility in and loss of LiPS in the cathode to the electrolyte. Also, the mechanical flexibility of PANI helps to tolerate high volume changes during cycling. With this sulfur-polymer nanocomposite, the initial discharge capacity of ~500 mAh g^{-1} at 1C is

achieved with an 85% capacity retention rate for 500 cycles (Figure 2.6 b). Although conducive and functional polymers can provide long-term cycling and bind LiPS more efficiently than carbon in the cathode, the relatively low conductivity and pore-size/porosity of the polymer means that the improvement in sulfur utilization possible with this method is limited.[36] Therefore, integrating and balancing the polymer with carbon materials can lead to a further advancement that efficiently sequesters sulfur for LiS batteries. Ji et al. proposed a functional polymer-supported, polyethylene glycol (PEG), sulfur/carbon composite cathode for LiS batteries.[19] In this context, PEG offers two advantages. First, it has a strong affinity for LiPS and second, it is easily swollen by electrolyte solvent in the battery to form a soft polymer coating able to tolerate large volume changes in the sulfur-CMK-3 composite. Further work by Wang et al.[18], synthesized the nanocomposite by wrapping graphene sheets on PEG coated sulfur particles. With this nanostructure, the composite can withstand the huge volume changes while maintaining conductivity throughout number of cycles resulting in reversible capacity of ~500 mAh g^{-1} at 0.2C over more than 100 cycles (Figure 2.6 c). Hence, a stable electrochemical performance of LiS is achieved by using the polymer as a supporting agent for sulfur/carbon nanocomposites. Since then, researchers have utilized this synergistic application of polymer and carbon to improve the sulfur utilization and LiPS trapping efficacy of LiS batteries. For instance, PANI coated sulfur/multiwalled carbon nanotubes (MWCNT)[37] and sulfur/polyethylenimine tethered MWCNT[38] nanocomposites are developed to increase LiPS trapping efficiency by utilizing amine functional groups on the polymer chains. Thus, functional polymers and sulfur/carbon nanocomposites are employed together in the cathodes that enable ~500 cycles with a

high utilization of sulfur. Overall, many important research findings have been reported on fabricating reversible LiS cathodes (high discharge capacity >1200 mAh g^{-1} with stable cycling >500)[19,30,39], applying sulfur infusion methods, and employing nanostructured carbon (i.e. porous carbon[16,19,21,39–45], carbon fibers[22,23,46,47], carbon nanotubes[24,30,48,49], graphene[24–26,28,31], carbide-derived carbon[27,29]) and functional polymers[17,32–34,37,50,51].

2.3 Separator modifications for lithium sulfur batteries

Separator membranes are used to prevent direct electronic transport between a battery anode and cathode, but to allow ions to move freely between the electrodes. The membranes are fabricated using electronically insulating materials and are designed to prevent direct contact between the cathode and anode, while facilitating ion transport via pores that are wetted by electrolyte. In comparison to the comprehensive studies on cathode and electrolyte designs for LiS batteries, relatively little work has been performed to engineer the separator despite its essential role in regulating ion and mass transport between the LiS battery electrodes. Additionally, because conventional LiS batteries use lithium metal as anode, complete and stable separation between the anode and cathode is required as metallic Li is notorious for unstable electrodeposition and dendrite formation during battery recharge. Lithium metal dendrites are mechanically strong enough to puncture most separator materials in common use, which causes internal short-circuiting and possibly battery explosion. Resolving problem of Li dendritic proliferation is therefore and important component in any commercial LiS battery design that is able to operate safely.

Nowadays, stretched polypropylene and polyethylene membranes such as Celgard are widely used as separators for LiS batteries. These membranes, depending on their characteristics such as thickness, pore size/density, electrolyte wettability, modulus and flexibility, largely affect the performance of the LiS cell. Furthermore, these parameters determine the ion transport and safety limit of LiS batteries. Due to the strong dissolution

and shuttling of the LiPS intermediates during cycling, concentration and electrochemical potential gradients, which drive ions to move in the electrolyte between the electrodes via pores of the membrane, are created. Therefore, the membrane's thickness, pore size and porosity can potentially be manipulated in systematic studies to help understand and control the diffusion of the LiPS species in the LiS cells. Additionally, the membrane's high mechanical strength and toughness are required to accommodate volume changes in the cathode during the charge/discharge of the LiS batteries. Also, as the separator is an important compartment of the battery (i.e. anode, cathode, electrolyte, sealing cage…), developing separators that are favorable to the LiS battery can further advance battery performance. Unfortunately, the traditional separators used in LiS cells allow LiPS to easily diffuse between the electrodes and subsequently degrade the electrochemical performance of the LiS batteries.

Since many battery separators are commercially available, researchers began to modify conventional separators to add desirable functionalities for specific battery systems. For LiS batteries, works on creating hybrid/bifunctional separators using polymers, carbons and ceramics have been reported to suppress the shuttling effect and to enhance the reutilization of active materials. Although several coating methods and configurations have been developed so far, none are able to achieve high enough efficiencies so as to minimize the mass of additional inactive materials in the battery

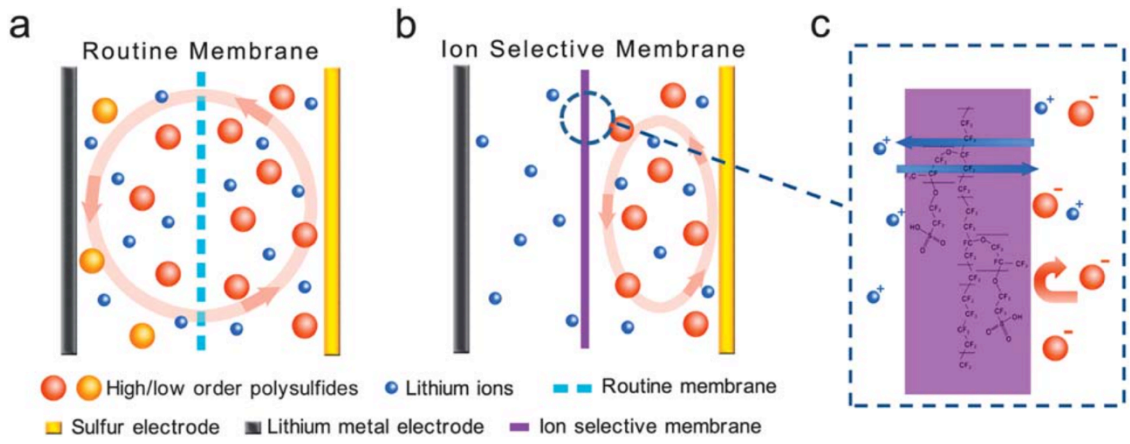

Figure 2.7. Illustration of lithiated Nafion ionomer film mechanism in LiS batteries. a. LiPS diffusion with a pristine separator, b. LiPS diffusion with the Nafion coated separator, c. close up mechanism of blocking LiPS. Produced with permission[52]. Copyright 2013, Royal Society of Chemistry.

Polymer coated separators are one possible choice for mitigating LiPS migration from the cathode. Ji et al. first demonstrated the use of lithiated Nafion ionomer coated separators for LiS batteries.[53] The Nafion membrane was reported to have an ionic conductivity of 2.1 x 10^{-5} S cm^{-1} at room temperature and selectively transport Li ions, with a transference number close to unity ($t_{Li} \approx 0.986$) once lithiated. Furthermore, -SO_3^- groups covalently attached on the Nafion chains allow cations, Li^+, to freely diffuse through the material while repulsing negatively charged anions, LiPS, by coulombic interactions (See Figure 2.7). Thus, with the lithiated Nafion ionomer coated separators, LiS cells are able to achieve ~97% of CE without the use of $LiNO_3$ additives in the electrolyte. However, the authors reported poor capacity retention of around 47% after 50 cycles due to the formation of a passivation layer, which covers the cathode surface with sulfur aggregates.[15]

Huang et al. further developed the idea of applying Nafion films using a solution-drying method that combines the separators with a S/CNT nanocomposite cathode to limit the LiPS diffusion.[52] With a Nafion coating of ~1 μm thickness on the separator with the composite cathode, a CE above 90% and a high capacity retention rate of 0.08% per cycle was achieved. Although this ionic shield for the LiPS produces stable electrochemical performances, the coating process is unreliable and the spreading/drying of Nafion solution at different concentrations on the separator results in poor control over the coating uniformity/thickness and loading. The coated separator was reported to have a Nafion loading of 0.7 mg cm^{-2}, which is relatively high compared to that of sulfur in the cathode, reducing the effective sulfur content from 50% to 30%. Also, the high resistance from the Nafion film is also problematic, as it would limit the ion transport rate in the cell, reducing utilization of the active material over a number of cycles.[52,53]

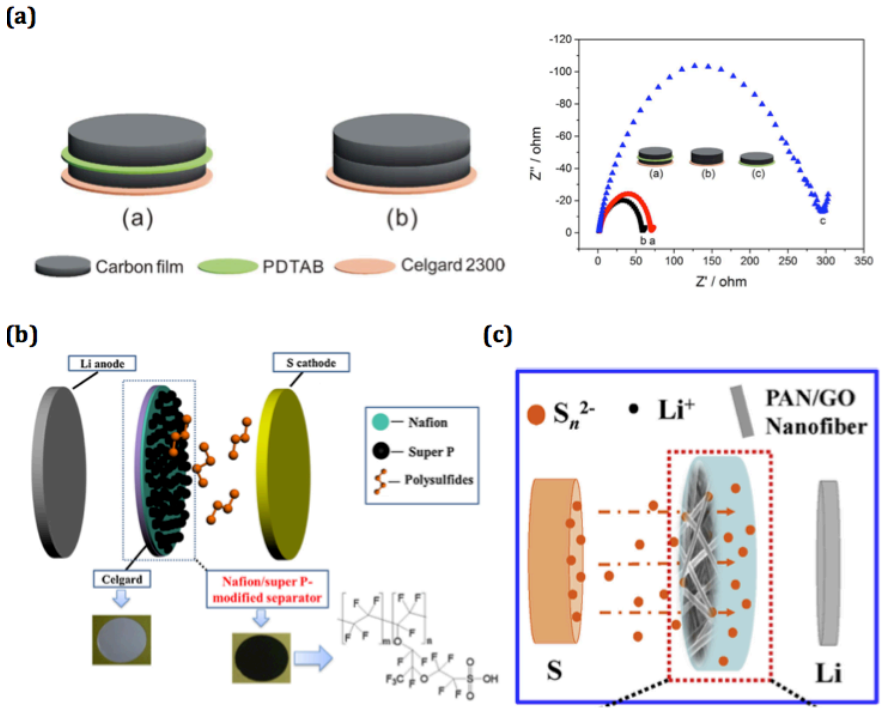

Figure 2.8. (**a**) Schematic illustration of sandwiched single ion conducting polymer electrolyte with carbon films on the separator and corresponding AC impedance analysis on different configurations (a-c), (**b**) Dual-functional separator configuration (**c**) PAN/GO emembrane sulfur schematic. (**a**) Reproduced with permission[54]. Copyright 2016, Nature Publishing Group. (**b**) Reproduced with permission[55]. Copyright 2016, Elsevier. (**c**) Reproduced with permission[56]. Copyright 2016, Elsevier.

Because of the limited active material utilization of the polymer by itself, combining polymers with carbon has been introduced recently as a strategy for managing shuttling without compromising active material utilization in LiS cells.[54,56,55] As shown in Figure 2.8a, Sun et al. discovered a novel configuration of sandwiching a single ion conducting polymer electrolyte film (sp^3 boron-based single ion polymer-PDTAB) with carbon films to create a composite separator for the LiS battery.[54] With this configuration, the negatively charged membrane electrolyte is able to electrostatically hinder LiPS shuttling and yield a high rate performance by introducing conductive carbon films, which reduce

interfacial impedance (See Figure 2.8a). A CE above 90% and >1000 mAh g^{-1} at 1C-3C are achieved with the sandwiched PDTAB separator for 100 cycles. Hence, combining single ion conductors with carbon layers appear to yield synergistic improvements that mitigate the shuttling effect and enhance the active material reutilization. Similarly, a dual-functional separator using Nafion and Super P carbon was reported by Hao et al.[55] As shown in Figure 2.8b, Nafion and carbon are coated together on the separator to reduce LiPS migration by introducing an electrostatic repulsion from the negatively charged Nafion chains and to increase the conductivity of the coating by adding spherical carbon powders. Thus, a higher capacity retention rate is achieved with the modified separator compared to that of a pristine case. However, the improvements were not substantial due to the high resistance of Nafion and the heterogeneous coating of the materials on the separator. Instead of using single ion conducting polymers, Zhu et al. introduced porous polyacronitrile/graphene oxide membranes that prevent self-discharge and high capacity retention rate (~95%) for 100 cycles[56] (See Figure 2.8c). Even though integrating polymers with carbon resulted in an improved material utilization and stabilized the cathode interface, the LiS cells still could not cycle and remain at a high capacity as well as CE. Only limited improvements were observed due to the poor coating qualities and the uncontrolled thicknesses of the coating materials on the separator. With incomplete and nonhomogeneous coatings, LiPS were still able to shuttle through the pores in the coatings and limit the accessible contact points for the active materials. Therefore, high quality coatings are required to achieve large improvements on the LiS cell performance.

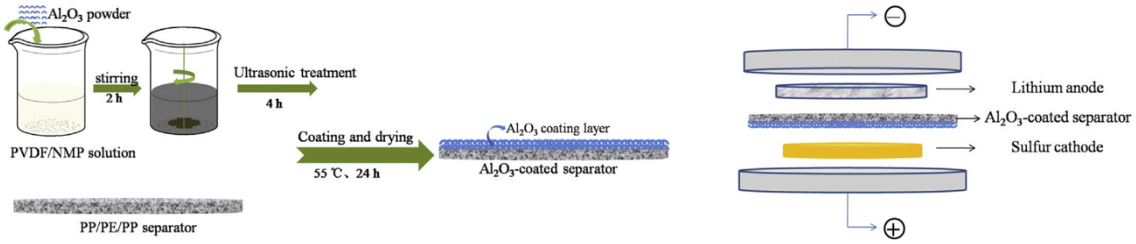

Figure 2.9. Schematics of alumina nanoparticle coating on the separator. Produced with permission[57]. Copyright 2014, Elsevier.

Efforts to modify separators with ceramics have been reported in the literature. Zheng et al. proposed alumina nanoparticle coated separators to provide physical adsorption for LiPS to agitate smooth migration (See Figure 2.9).[57] With the improved cell performance, a reversible capacity of ~600 mAh g^{-1} was reported for 50 cycles in LiS cells. These results, which resemble that of the polymer-coated separators, indicate that a similar problem may limit performance of the separators as the added weight and high resistance result in low utilization of the active material. The ceramic coating could nonetheless be advantageous in suppressing Li dendrite growth and proliferation in the metal anode due to a high modulus of alumina (152.8 GPa); the nonconductive organic materials however hinder reutilization of the redox species in LiS batteries. Therefore, highly conductive materials such as carbon or combinations of carbon/inorganics appear to provide a more suitable configuration to apply on the separators facing the cathode side in order to enhance the reutilization rate of the active material in LiS while providing effective blocking paths to LiPS.

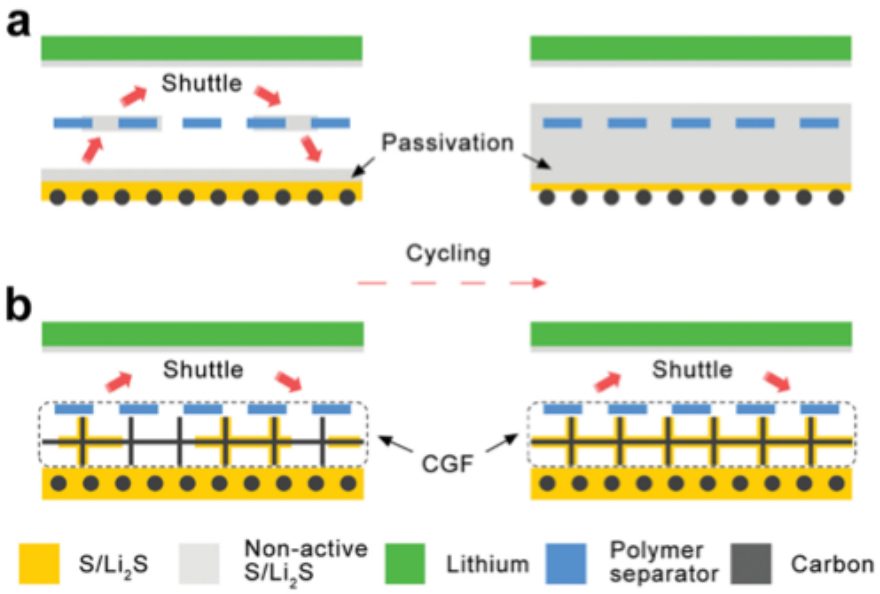

Figure 2.10. Illustration of effectiveness of upper current collector of carbon coatings on the separator. (a) Causing passivation layer of inactive zones on the cathode surface and (b) upper current collector helping redeposition of LiPS. Reproduced with permission[58]. Copyright 2016, WILEY-VCH Verlag GmbH & Co. KGaA, Weinheim.

Most separator modification works have been reported on the carbon coatings for LiS batteries. Carbon coatings on the separator may appear to place an empty/inactive cathode above the active cathode and reduce the active material content, but in truth this process highlights several benefits to enhancing the electrochemical performance of LiS batteries. The carbon coatings on the separator create an upper current collector for LiPS due to the electrically accessible platforms that enable the reutilization of the active materials that are dissolved in the electrolyte within the region around the cathode. This upper current collector space could further prevent the formation of inactive zones where sulfur starts to aggregate at the cathode interface by providing fresh regions for dissolved LiPS to redeposit during cycling (See Figure 2.10).[58] The nanostructured carbon materials not only provide physical polysulfide traps, but also enable fast electron

transport for the insulating redox products in the cathode. Several coating approaches (solution-drying[52], doctor-blade[59–61], tape-casting[62], vacuum filtration[62–64] methods) have been addressed to accommodate the various forms of carbon that exist (particle/spheres[45,60,61,65], fibers/tubes[62–64,66], sheets[67–71,58]).

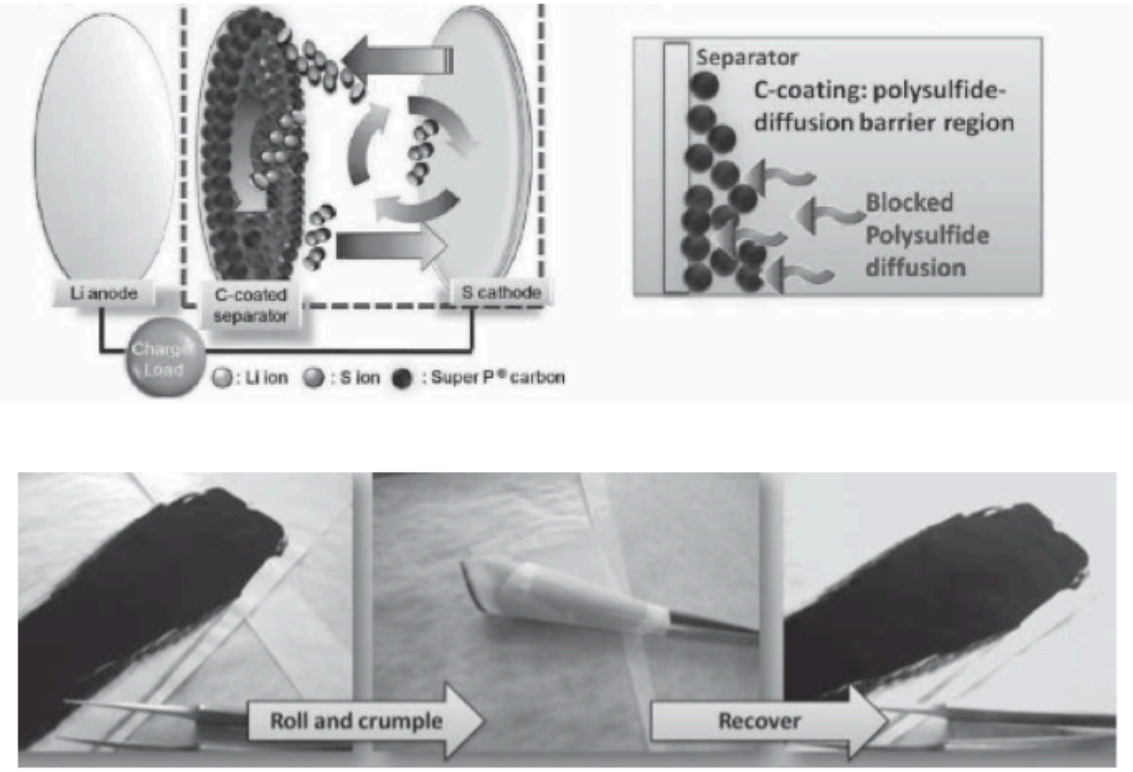

Figure 2.11. Demonstration of Super P carbon coated separator using tape-casting method for Li-S cell. Reproduced with permission[62]. Copyright 2014, WILEY-VCH Verlag GmbH & Co. KGaA, Weinheim.

Figure 2.11 shows a Super P carbon coated separator using a tape-casting method reported by Chung et al.[62] A spherical carbon coating facing the sulfur cathode is intended to intercept and immobilize the migrating LiPS as an effective upper current collector. Stable performances are achieved with these carbon-coated separators (initial

discharge capacity of 1220 mAh g^{-1} at 1C with capacity retention rate of 63% for 200 cycles). Also, a stable anti-self-discharge capability is observed for a three-month period. It is known that carbon coatings on the separator make smooth contact with the cathode and function as a protection layer that mitigates the loss of active sulfur during the resting period.

Carbon protection layers have been found to be most effective in suppressing self-discharge compared to other materials for LiS batteries.[6,12,72,73] However, a high carbon loading with a coating thickness of >20 μm and a nonuniform coating on the separator are undesirable for LiS batteries. Although carbon is light in weight, adding any unnecessary amount of carbon can still reduce the fair amount of active species in the cell. Furthermore, a nonuniform coating on the separator may require a higher loading of materials to achieve a reasonable cell performance as large gaps in the coatings allow LiPS to easily diffuse and shuttle between the electrodes. Hence, better coating methods are required to create effective separator coatings that fully utilize the coating materials. Chung et al. further introduced a vacuum filtration separator coating method that is suitable for fibrous materials such as carbon fibers and nanotubes.[63] No binder is used to coat MWCNT on the separator using a vacuum filtration. However, the coating was observed to have a very uncontrolled uniformity and thickness with a high loading of ~0.2 mg cm^{-2}. Also, this coating method is only suitable for porous substrates, as the method requires air suction.

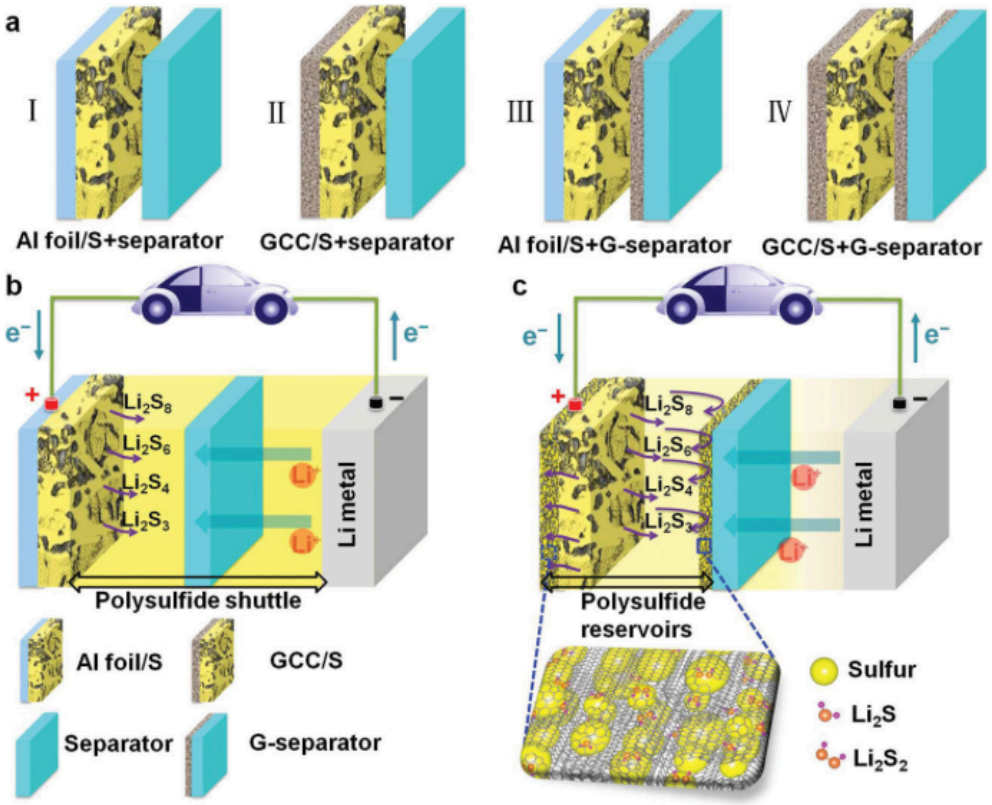

Figure 2.12. Graphene sandwiched sulfur/carbon nanocomposite for new structural design of the cathode on the separator. (a) several configurations of the cathode design, cycling mechanism of (b) pristine and (c) graphene sandwiched cathodes in LiS cells. Reproduced with permission[67]. Copyright 2014, WILEY-VCH Verlag GmbH & Co. KGaA, Weinheim.

Different novel cell configurations of sandwiched grapene electrodes are reported by Zhou et al.[67] A graphene current collector and graphene-coated separators are used to sandwich the sulfur/carbon nanocomposite cathode. With this configuration, the porous graphene coatings as the current collector and upper current collector yielded a more stable performance compared to a coating that uses an aluminum current collector (Figure 2.12 a III) as well as single-sided coatings (Figure 2.12 a II and III). This implies that porous conductive coatings are desired for LiS batteries to retain a high utilization rate of sulfur and to suppress shuttling.

Similarly, Wang et al. recently created these sandwiched structures on the separator so as to remove the current collector and directly fabricate the cathode on the separator.[74] The configuration of Carbon/Sulfur@Carbon/Carbon/Separator is created using slurry casting methods, which still yield nonuniform and thick coatings of the materials. Even though reasonably stable electrochemical performances were reported for this cathode-on-the-separator concept, the true performance of the materials was not fully utilized as can be observed in many material coated separators. Nevertheless, understanding how carbon and polymer coatings can be effective for LiS batteries, especially carbon which increases the reutilization of sulfur and polymer to suppress the shuttling effect, is an important step toward further advancing LiS technologies.

Different configurations of the coating structure largely impact the performance of LiS cells. Therefore, an important implication for the future of separator modification research may be in discovering facile coating methods that enable the coating of various forms and types of materials, especially carbons, polymers and ceramics and subsequently yield high quality and uniform coatings with a nice control over thickness. Material loading on the separator also has to be optimized (i.e. remove binders and reduce coating thicknesses) to accommodate/preserve high active material loading and content in the cathode. Additionally, creating diverse configurational designs of coating structures and integrating different materials should be examined in the near future to create truly effective multifunctional separators for LiS batteries.

EFERENCES

1. Herbert, D. & Ulam, J. Electric dry cells and storage batteries. *US Pat. 3,043,986,* July 10 (1962).
2. Rao, M. L. . Organic electrolyte cells. *US Pat. 3,413,154,* Nov 26 (1966).
3. Yamin, H. & Peled, E. Electrochemistry of a nonaqueous lithium/sulfur cell. *J. Power Sources* **9,** 281–287 (1983).
4. Peled, E., Sternberg, Y., Gorenshtein, A. & Lavi, Y. Lithium-Sulfur Battery : Evaluation of Dioxolane-Based Electrolytes. *J. Electrochem. Soc.* **136,** 2–6 (1989).
5. Peled, E., Gorenshtein, A., Segal, M. & Sternberg, Y. Rechargeable lithium sulfur battery. *J. Power Sources* **26,** 269–271 (1989).
6. Mikhaylik, Y. V. & Akridge, J. R. Polysulfide shuttle study in the Li/S battery system. *J. Electrochem. Soc.* **151,** A1969–A1976 (2004).
7. Wild, M. *et al.* Lithium sulfur batteries, a mechanistic review. *Energy Environ. Sci.* **8,** 3477–3494 (2015).
8. Manthiram, A., Fu, Y., Chung, S., Zu, C. & Su, Y. Rechargeable Lithium − Sulfur Batteries. *Chem. Rev.* **114,** 11751–11787 (2014).
9. Bruce, P. G., Freunberger, S. a., Hardwick, L. J. & Tarascon, J.-M. Li–O2 and Li–S batteries with high energy storage. *Nat. Mater.* **11,** 172–172 (2011).
10. Scheers, J., Fantini, S. & Johansson, P. A review of electrolytes for lithium-sulphur batteries. *J. Power Sources* **255,** 204–218 (2014).
11. Cheon, S.-E. *et al.* Rechargeable Lithium Sulfur Battery I. *J. Electrochem. Soc.* **150,** A800 (2003).

12. Ryu, H. S. *et al.* Self-discharge characteristics of lithium/sulfur batteries using TEGDME liquid electrolyte. *Electrochim. Acta* **52,** 1563–1566 (2006).

13. Shim, J., Striebel, K. a. & Cairns, E. J. The Lithium/Sulfur Rechargeable Cell. *J. Electrochem. Soc.* **149,** A1321 (2002).

14. Cheon, S.-E. *et al.* Rechargeable Lithium Sulfur Battery II. *J. Electrochem. Soc.* **150,** A800 (2003).

15. Cheon, S.-E. *et al.* Capacity Fading Mechanisms on Cycling a High-Capacity Secondary Sulfur Cathode. *J. Electrochem. Soc.* **151,** A2067 (2004).

16. Jayaprakash, N., Shen, J., Moganty, S. S., Corona, A. & Archer, L. A. Porous hollow carbon@sulfur composites for high-power lithium-sulfur batteries. *Angew. Chemie* **50,** 5904–5908 (2011).

17. Xiao, L. *et al.* A soft approach to encapsulate sulfur: Polyaniline nanotubes for lithium-sulfur batteries with long cycle life. *Adv. Mater.* **24,** 1176–1181 (2012).

18. Wang, H. *et al.* Graphene-Wrapped Sulfur Particles as a Rechargeable Lithium – Sulfur Battery Cathode Material with High Capacity and Cycling Stability. *Nano Lett.* **11,** 2644–2647 (2011).

19. Ji, X., Lee, K. T. & Nazar, L. F. A highly ordered nanostructured carbon-sulphur cathode for lithium-sulphur batteries. *Nat. Mater.* **8,** 500–506 (2009).

20. Su, Y. S. & Manthiram, A. A facile in situ sulfur deposition route to obtain carbon-wrapped sulfur composite cathodes for lithium-sulfur batteries. *Electrochim. Acta* **77,** 272–278 (2012).

21. Zhang, C., Wu, H. Bin, Yuan, C., Guo, Z. & Lou, X. W. Confining sulfur in double-shelled hollow carbon spheres for lithium-sulfur batteries. *Angew. Chemie*

- *Int. Ed.* **51,** 9592–9595 (2012).

22. Cheng, X. B. *et al.* Aligned carbon nanotube/sulfur composite cathodes with high sulfur content for lithium-sulfur batteries. *Nano Energy* **4,** 65–72 (2014).

23. Ji, L. *et al.* Porous carbon nanofiber–sulfur composite electrodes for lithium/sulfur cells. *Energy Environ. Sci.* **4,** 5053 (2011).

24. Chen, J. *et al.* A hierarchical architecture S/MWCNT nanomicrosphere with large pores for lithium sulfur batteries. *Phys. Chem. Chem. Phys.* **14,** 5376–5382 (2012).

25. Lin, T. *et al.* Scotch-tape-like exfoliation of graphite assisted with elemental sulfur and graphene–sulfur composites for high-performance lithium-sulfur batteries. *Energy Environ. Sci.* **6,** 1283 (2013).

26. Kim, H., Lim, H.-D., Kim, J. & Kang, K. Graphene for advanced Li/S and Li/air batteries. *J. Mater. Chem. A* **2,** 33 (2014).

27. Tao, X. *et al.* Bio-inspired fabrication of carbon nanotiles for high performance cathode of Li-S batteries. *J. Mater. Chem. A Mater. Energy Sustain.* **2,** 2290–2296 (2014).

28. Cells, L. S. *et al.* Graphene Oxide as a Sulfur Immobilizer in High Performance Lithium/Surfur cells. *J. Am. Chem. Soc.* **133,** 18522–18525 (2011).

29. Lee, J. T. *et al.* Sulfur-infiltrated micro- and mesoporous silicon carbide-derived carbon cathode for high-performance lithium sulfur batteries. *Adv. Mater.* **25,** 4573–4579 (2013).

30. Wang, L., Zhao, Y., Thomas, M. L. & Byon, H. R. In situ synthesis of bipyramidal sulfur with 3D carbon nanotube framework for lithium-sulfur batteries. *Adv. Funct. Mater.* **24,** 2248–2252 (2014).

31. Zu, C. & Manthiram, A. Hydroxylated graphene-sulfur nanocomposites for high-rate lithium-sulfur batteries. *Adv. Energy Mater.* **3,** 1008–1012 (2013).

32. Wang, J., Yang, J., Xie, J. & Xu, N. A novel conductive polymer-sulfur composite cathode material for rechargeable lithium batteries. *Adv. Mater.* **14,** 963–965 (2002).

33. Li, G. C., Li, G. R., Ye, S. H. & Gao, X. P. A Polyaniline-coated sulfur/carbon composite with an enhanced high-rate capability as a cathode material for lithium/sulfur batteries. *Adv. Energy Mater.* **2,** 1238–1245 (2012).

34. Zhou, W., Yu, Y., Chen, H. & Disalvo, F. J. Yolk − Shell Structure of Polyaniline-Coated Sulfur for Lithium − Sulfur Batteries. *J. Am. Chem. Soc.* 16736–16743 (2013).

35. Chen, L. & Shaw, L. L. Recent advances in lithium-sulfur batteries. *J. Power Sources* **267,** 770–783 (2014).

36. Yin, Y. X., Xin, S., Guo, Y. G. & Wan, L. J. Lithium-sulfur batteries: Electrochemistry, materials, and prospects. *Angew. Chemie - Int. Ed.* **52,** 13186–13200 (2013).

37. Wu, F., Chen, J., Li, L., Zhao, T. & Chen, R. Improvement of rate and cycle performence by rapid polyaniline coating of a MWCNT/sulfur cathode. *J. Phys. Chem. C* **115,** 24411–24417 (2011).

38. Ma, L. *et al.* Enhanced Li–S Batteries Using Amine-Functionalized Carbon Nanotubes in the Cathode. *ACS Nano* **10,** 1050–1059 (2015).

39. Ye, H., Yin, Y.-X., Xin, S. & Guo, Y.-G. Tuning the porous structure of carbon hosts for loading sulfur toward long lifespan cathode materials for Li–S batteries.

J. Mater. Chem. A **1,** 6602–6608 (2013).

40. Zhang, B., Qin, X., Li, G. R. & Gao, X. P. Enhancement of long stability of sulfur cathode by encapsulating sulfur into micropores of carbon spheres. *Energy Environ. Sci.* **3,** 1531 (2010).

41. Schuster, J. *et al.* Spherical ordered mesoporous carbon nanoparticles with high porosity for lithium-sulfur batteries. *Angew. Chemie - Int. Ed.* **51,** 3591–3595 (2012).

42. Zhang, Z. *et al.* 3D interconnected porous carbon aerogels as sulfur immobilizers for sulfur impregnation for lithium-sulfur batteries with high rate capability and cycling stability. *Adv. Funct. Mater.* **24,** 2500–2509 (2014).

43. Kim, J. *et al.* An advanced lithium-sulfur battery. *Adv. Funct. Mater.* **23,** 1076–1080 (2013).

44. Li, D. *et al.* High sulfur loading cathodes fabricated using peapodlike, large pore volume mesoporous carbon for lithium-sulfur battery. *ACS Appl. Mater. Interfaces* **5,** 2208–2213 (2013).

45. Song, J. *et al.* Nitrogen-doped Mesoporous carbon promoted chemical adsorption of sulfur and fabrication of high-Areal-capacity sulfur cathode with exceptional cycling stability for lithium-sulfur batteries. *Adv. Funct. Mater.* **24,** 1243–1250 (2014).

46. Choi, Y. J., Kim, K. W., Ahn, H. J. & Ahn, J. H. Improvement of cycle property of sulfur electrode for lithium/sulfur battery. *J. Alloys Compd.* **449,** 313–316 (2008).

47. Rao, M., Song, X. & Cairns, E. J. Nano-carbon/sulfur composite cathode materials with carbon nanofiber as electrical conductor for advanced secondary

lithium/sulfur cells. *J. Power Sources* **205,** 474–478 (2012).

48. Jia-Jia, C. *et al.* The preparation of nano-sulfur/MWCNTs and its electrochemical performance. *Electrochim. Acta* **55,** 8062–8066 (2010).

49. Wei, W. *et al.* CNT enhanced sulfur composite cathode material for high rate lithium battery. *Electrochem. commun.* **13,** 399–402 (2011).

50. Fisher, R. a. *et al.* Recent advances in polyaniline composites with metals, metalloids and nonmetals. *Energy Environ. Sci.* **3,** 4889–4899 (2013).

51. Li, W., Zhang, Z., Kang, W., Tang, Y. & Lee, C.-S. Rice-like Sulfur/Polyaniline Nanorods Wrapped by Reduced Graphene Oxide Nanosheets as High-Performance Cathode for Lithium-Sulfur Batteries. *ChemElectroChem* **3,** 1–8 (2016).

52. Huang, J.-Q. *et al.* Ionic shield for polysulfides towards highly-stable lithium–sulfur batteries. *Energy Environ. Sci.* **7,** 347 (2014).

53. Jin, Z., Xie, K., Hong, X., Hu, Z. & Liu, X. Application of lithiated Nafion ionomer film as functional separator for lithium sulfur cells. *J. Power Sources* **218,** 163–167 (2012).

54. Sun, Y., Li, G., Lai, Y., Zeng, D. & Cheng, H. High rate lithium-sulfur battery enabled by sandwiched single ion conducting polymer electrolyte. *Sci. Rep.* **6,** 22048 (2016).

55. Hao, Z. *et al.* High performance lithium-sulfur batteries with a facile and effective dual functional separator. *Electrochim. Acta* **200,** 197–203 (2016).

56. Zhu, J. *et al.* Highly porous polyacrylonitrile/graphene oxide membrane separator exhibiting excellent anti-self-discharge feature for high-performance lithium–sulfur batteries. *Carbon N. Y.* **101,** 272–280 (2016).

57. Zhang, Z., Lai, Y., Zhang, Z., Zhang, K. & Li, J. Al2O3-coated porous separator for enhanced electrochemical performance of lithium sulfur batteries. *Electrochim. Acta* **129,** 55–61 (2014).

58. Peng, H.-J. *et al.* Janus Separator of Polypropylene-Supported Cellular Graphene Framework for Sulfur Cathodes with High Utilization in Lithium–Sulfur Batteries. *Adv. Sci.* **3,** 268–279 (2015).

59. Balach, J. *et al.* Functional Mesoporous Carbon-Coated Separator for Long-Life, High-Energy Lithium-Sulfur Batteries. *Adv. Funct. Mater.* **25,** 5285–5291 (2015).

60. Zhang, Z., Lai, Y., Zhang, Z. & Li, J. A functional carbon layer-coated separator for high performance lithium sulfur batteries. *Solid State Ionics* **278,** 166–171 (2015).

61. Yao, H. Bin *et al.* Improved lithium-sulfur batteries with a conductive coating on the separator to prevent the accumulation of inactive S-related species at the cathode-separator interface. *Energy Environ. Sci.* **7,** 3381 (2014).

62. Chung, S.-H. & Manthiram, A. Bifunctional Separator with a Light-Weight Carbon-Coating for Dynamically and Statically Stable Lithium-Sulfur Batteries. *Adv. Funct. Mater.* **24,** 5299–5306 (2014).

63. Chung, S. & Manthiram, A. High-Performance Li − S Batteries with an Ultra-lightweight MWCNT- Coated Separator. *Phys. Chem. Lett.* **5,** 1987–1983 (2014).

64. Chung, S.-H., Han, P., Singhal, R., Kalra, V. & Manthiram, A. Electrochemically Stable Rechargeable Lithium-Sulfur Batteries with a Microporous Carbon Nanofiber Filter for Polysulfide. *Adv. Energy Mater.* (2015). doi:10.1002/aenm.201500738

65. Wei, H., Li, B., Zuo, Y. & Xia, D. Enhanced Cycle Performance of Lithium-Sulfur Battereis Using a Separator Modified with a PVDF-C Layer. *ACS Appl. Mater. Interfaces* **6,** 20276–20281 (2014).

66. Wang, G., Lai, Y., Zhang, Z., Li, J. & Zhang, Z. Enhanced rate capability and cycle stability of lithium–sulfur batteries with a bifunctional MCNT@PEG-modified separator. *J. Mater. Chem. A* **3,** 7139–7144 (2015).

67. Li, F. *et al.* A graphene-pure-sulfur sandwich structure for ultrafast, long-life lithium-sulfur batteries. *Adv. Mater.* **26,** 625–631 (2014).

68. Zhang, Y. *et al.* A graphene-oxide-based thin coating on the separator: an efficient barrier towards high-stable lithium–sulfur batteries. *2D Mater.* **2,** 024013 (2015).

69. Fang, R., Zhou, G., Pei, S., Li, F. & Cheng, H.-M. Localized polyselenides in a graphene-coated polymer separator for high rate and ultralong life lithium–selenium batteries. *Chem. Commun.* **51,** 3667–3670 (2015).

70. Lin, W. *et al.* Enhanced Performance of Lithium Sulfur Battery with a Reduced Graphene Oxide Coating Separator. *J. Electrochem. Soc.* **162,** 1624–1629 (2015).

71. Xiao, Z. *et al.* A Lightweight TiO2/Graphene Interlayer, Applied as a Highly Effective Polysulfide Absorbent for Fast, Long-Life Lithium-Sulfur Batteries. *Adv. Mater.* **27,** 2891–2898 (2015).

72. Chung, S. H. & Manthiram, A. Lithium-sulfur batteries with superior cycle stability by employing porous current collectors. *Electrochim. Acta* **107,** 569–576 (2013).

73. Ryu, H. S. *et al.* Self-discharge of lithium-sulfur cells using stainless-steel current-collectors. *J. Power Sources* **140,** 365–369 (2005).

74. Wang, H., Zhang, W., Liu, H. & Guo, Z. A Strategy for Configuration of an Integrated Flexible Sulfur Cathode for High-Performance Lithium – Sulfur Batteries. *Angew. Chemie - Int. Ed.* **55,** 3992–3996 (2016).

CHAPTER 3

FABRICATING MULTIFUNCTIONAL NANOPARTICLE MEMBRANES BY A FAST LAYER-BY-LAYER LANGMUIR-BLODGETT PROCESS: APPLICATION IN LITHIUM-SULFUR BATTERIES

3.1 Abstract

The Langmuir-Blodgett (LB) technique is a powerful, widely used method for preparing coatings of amphiphilic molecules at air/water interfaces with thickness control down to a single molecule. Here we report two new LB techniques designed to create ordered, multifunctional nanoparticle films on any non-reactive support. The methods utilize Marangoni stresses produced by surfactants at a fluid/solid/gas interface and self-assembly of nanoparticles to facilitate rapid creation of dense monolayers of multi-wall carbon nanotubes (MWCNT), metal-oxide nanoparticles, polymers, and combinations of these materials in a layer-by-layer configuration. Using the polyolefin separator in a lithium sulfur (Li-S) electrochemical cell as an example, we illustrate how the method can be used to create structured membranes for regulating mass and charge transport. We show that a layered MWCNT/SiO_2/MWCNT nanomaterial created in a clip-like configuration, with gravimetric areal coverage of ~130 μg cm^{-2} and a thickness of ~3 μm, efficiently adsorbs dissolved lithium polysulfide (LiPS) species and efficiently reutilize them for improving Li-S battery performance.

3.2 Introduction

The Langmuir-Blodgett (LB) technique is a method for preparing coatings of amphiphilic molecules at air/water interfaces with thickness of one molecule[1–3]. The method is attractive for a variety of reasons, including its ability to precisely control the thicknesses of coatings down to molecular dimensions, for the versatility of substrates that can be coated, and for its scalability. Ever since its discovery in the 1920s and its rise in popularity following Irving Langmuir's receipt of the Nobel prize in chemistry in 1932, it has been applied in numerous fields of science and technology to form thin micro patterns,[4,5] molecular-thick thin films,[6,7] and more recently monoparticle layers based on spheres,[8,9] rods,[10,11] and nanotubes,[12] which can be easily transferred onto various substrates. Recently, Nie et al proposed an electrospray method that extends the LB technique to yield high coverage of metallic nanospheres at the surface of water[13]. With LB assembly it is therefore now possible to produce monolayers of colloidal films that broadly range in particle sizes and shapes, which may be used to advantage for tuning film properties[14] as well as for coating applications to create thin film devices[15,16].

This article reports two new and versatile LB coating approaches - Langmuir-Blodgett sequential dip coating (LBSDC) and the Langmuir-Blodgett scooping (LBS), which facilitate efficient creation of multifunctional, layer-by-layer coatings of carbon, metal-oxides, polymers, and combinations of these materials on any non-reactive substrate. Unlike the conventional LB method, which uses a mechanical force applied to a disordered material at the air/water interface to create well-ordered assemblies of molecules or particles, LBSDC and LBS utilize surfactant and self-assembly,

respectively, to create ordered coatings that can be transferred to a solid or porous support. This difference allows highly organized coatings to be created in a fraction of the time and using any containment vessel (i.e. a LB mechanical barrier is not needed). The speed with which ordered monolayer coatings are created, the high quality and low thickness of the transferred coatings, and versatility of the process by which the coatings are formed mean that LBSDC and LBS can be applied in a repetitive fashion to create multi-functional coatings in a layer-by-layer format that enable design of new materials with surface features able to regulate mass and charge transport. Because the assembly occurs at a sharp gas/liquid interface, the methods nonetheless benefit from the inherent attributes of the LB technique - precise control over film thickness and structure, as well as the versatility of substrate choices. Moreover, numbers and positions of suspension injection nozzle and water surface area can be altered and customized to scale up the coating process.

The utility of the LBSDC and LBS approaches is illustrated in the present study using the polyolefin separator membrane of a standard Lithium-Sulfur (Li-S) electrochemical cell as a substrate. This choice is motivated by the promise such cells offer for cost-effective storage of large quantities of electrical energy and by the stubborn challenges associated with solubility and diffusion of long-chain (Li_2S_x; $x \geq 4$), lithium polysulfide (LiPS) species, to the electrolyte that limit performance of Li-S batteries.[17-48] We report that using LBSDC and LBS it is possible to create multifunctional coatings in multiple designs that enable conventional membranes to overcome the most difficult challenges.

We further report a novel "clip" separator membrane configuration in which a well-formed, but incomplete layer of structures of one chemistry is sandwiched between complete layers of another chemistry. This coating morphology allows one to engineer the surface of a membrane to simultaneously trap an undesired material (e.g. LiPS) and to maintain electrochemical access to it. In so doing, we show that it is possible to preserve the favorable attributes of the Li-S cell and address some of its most serious weaknesses.

3.3 Results and Discussions

The LBSDC and LBS coating methods enable creation of well-defined layers of materials in various physical forms and chemistries on a conventional polypropylene separator, without the need for chemical binders. LBSDC is a discontinuous process that utilizes a sodium dodecyl sulfate (SDS) surfactant, inducing Marangoni effect, to lower the surface tension of water and to provide a unidirectional force on floating particles or to a particulate LB film at the air-water interface to form a dense, close-packed structure. Care is needed in this step, for on the small length scales of these monolayer films the pressure provided by the surfactant can easily exceed the stability of the self-assembled LB film, causing it to rupture due to too strong surface tension gradient (Supplementary Figure S1). Grains that exceed 200 nm in size exhibit the greatest film stability and are able to form the most densely packed coatings through the LBSDC technique. The LBS method, on the other hand, is a continuous process that uses constant injection of a particle suspension during the coating process to maintain a closely-packed LB film by a self-assembly mechanism, which is induced by the simple spreading and mixing of the water miscible fluid. This approach enables particles smaller than 200 nm in size to be

coated on a mobile substrate due to the absence of the extra surface tension gradient provided by the surfactant and may be implemented in a roll-to-roll manufacturing process. The LBS method is therefore more flexible than the LBSDC method, but requires constant injection of the suspension during the coating process.

Surface pressure profiles obtained using the LBSDC and LBS approaches to assemble monoparticle layers of ~350 nm diameter sized nanospheres and multi-walled carbon nanotubes (MWCNT) at the air/water interface are reported in Supplementary Figure S2. Figure 3.1 compares the pressure profiles to those obtained using a conventional LB trough. Three different surface pressure points are chosen in Figure 3.1a to investigate the packing densities of the colloidal film onto a separator achieved with each of the approaches. The points A, B, and C correspond to the surface pressure of 60 mN m^{-1}, 33 mN m^{-1}, and 2 mN m^{-1}, respectively: Points A and C represent the surface pressure where the colloids are overly packed and inadequately packed, and point B represents the starting surface pressure from the LBSDC method. The inflection point of the surface pressure profile represents a transition point where the folding of the film starts, which is consistent with what is observed in the SEM images at point A. Point B shows the most uniform coating, which indicates that the surface pressure between 33 mN m^{-1} and 38 mN m^{-1} will yield the highest quality LB film. The surface pressure profile of the colloids from the LBSDC method starts at 33 mN m^{-1}, which represents the amount of pressure exerted by one 5μL drop of 3wt% SDS surfactant on the film.

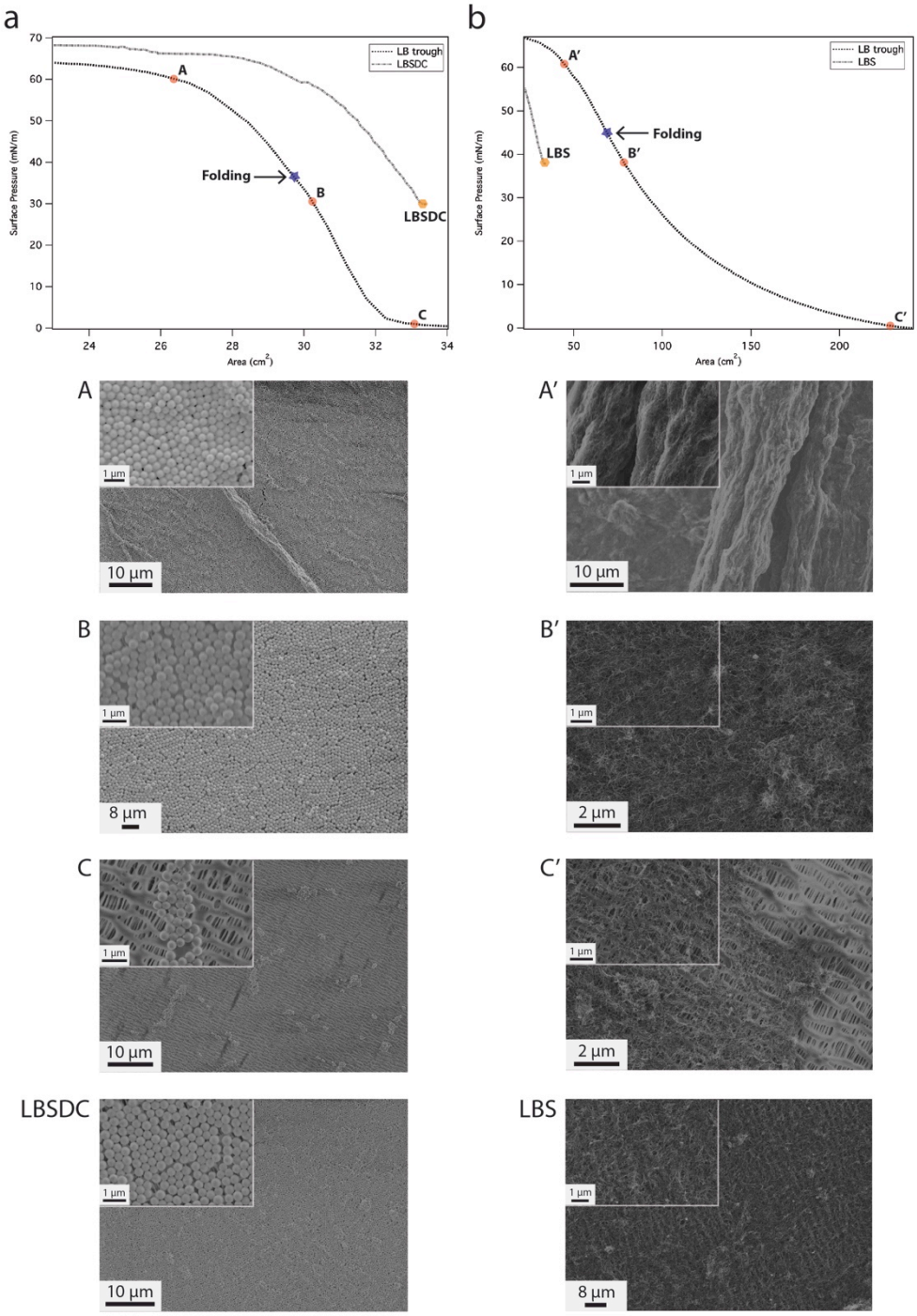

Figure 3.1. Langmuir-Blodgett surface pressure profiles and corresponding coating qualities of silica nanospheres and MWCNTs at designated surface pressures. (a) Silica nanosphere surface pressure profiles of conventional LB trough and LBSDC methods with SEM images of the coating qualities at 60 mN m^{-1}, 33 mN m^{-1}, and 2 mN m^{-1}. (b) MWCNT surface pressure profiles of conventional LB trough and LBS methods with SEM images of the coating qualities at 61 mN m^{-1}, 37 mN m^{-1}, and 1 mN m^{-1}.

This pressure from the surface tension gradient allows the colloids to be packed closely and remain stationary, and therefore, no inflection point is observed from the LBSDC profile. To confirm the packing density of the colloids using the LBSDC method, the colloids are coated onto the separator using the LB trough at 33 mN m^{-1} and using the LBSDC method. A coating quality of good agreement is observed from SEM images at point B and from LBSDC, which confirms that LBSDC starts from a highly packed colloidal LB film. To understand the role of the surfactant in the LBSDC method, the maximum amount of the pressure acting on the film is measured and its stability is observed (See Supplementary Figure S3a & S3b). The maximum pressure that the surfactant can provide is ~34 mN m^{-1} and tends to slowly fade over time. The maximum pressure exerted by the surfactant matches the starting surface pressure of the colloids using the LBSDC method, where the increased pressure is the same as obtained from one drop of the surfactant.

In Figure 3.1b, the surface pressure profiles of the MWCNT is compared from conventional LB trough and LBS methods, and three different surface pressure points, A', B', and C', are chosen at 61 mN m^{-1}, 37 mN m^{-1}, and 1 mN m^{-1}, respectively, to observe the coating quality. The MWCNT film tends to fold as shown in the SEM at point A', and poor coverage of the film is seen at point C'. A long compression region of the film is observed from the profile by comparing the area before and after the inflection point. This is because of the elastic behavior of the self-assembled MWCNT film as the film is comprised of nanotubes. Based on the geometry of the particle, different trends of

the surface pressure profiles can be obtained (See Supplementary Figure S3c).

To investigate where the coating quality of the LBS lies, the surface pressure profile of the LBS method is measured and compared to the profile obtained from the LB trough. The LBS method requires a constant injection of the suspension to maintain high packing density by self-assembly mechanism induced by spreading and mixing of the suspension solvent (ethanol) with water. To observe how much pressure is exerted during the self-assembly, the surface pressure was measured by saturating the surface of the trough with MWCNT. The measured pressure is 37 mN m^{-1}, which is the pressure exerted from the self-assembly. Since the spreading velocity depends on the distance traveled by the particle, the area on the trough is set to around 25 cm^2, which is a similar surface area for our experimental coating process. No inflection point is shown from the profile, which confirms that the fibers are closely packed and compressed from the starting point. Furthermore, congruent coating qualities are observed at point B' and from the LBS in Figure 3.1b, confirming that the LBS method yields a closely packed, high quality LB film. Moreover, surface pressure profiles of Ketjen Black (KB) and Super P (SP) carbons using the LB trough and LBS methods are measured to understand the stability of the film in the presence of the surfactant (See Supplementary Figure S3c). The starting surface pressure of MWCNT, KB, and SP from the LBS method is 37 mN m^{-1}, 20 mN m^{-1}, and 35 mN m^{-1}, respectively. One drop of the surfactant provides an instant pressure of 34 mN m^{-1}, similar to that of MWCNT and SP, while exceeding that of KB. As a result, the film starts to collapse in the presence of the extra surface tension gradient. As expected, the instant destruction of the KB film, ~1 second, is observed, while a longer destruction time, ~7 seconds, is observed for MWCNT and SP in the presence of the

surfactant (Supplementary Figure S1). The above results support that the LBSDC and LBS coating methods start in an optimized packing condition and yield high-quality LB films. Figure 3.2a illustrates the simplicity and effectiveness of the LBSDC and LBS methods. Multilayer coatings using the two approaches are reported in Figure 3.2b & 2c. The coatings and their processes are important not only because they exhibit an excellent close-packed morphology, but also because they are the thinnest and highest fidelity coatings reported on a battery separator. For example, thickness variations for silica nanospheres and MWCNT within a single monolayer of the silica particle size and ~80 nm of MWCNT (Supplementary Figure S4a) are achieved. This means that these coatings will add very little mass to a battery separator or electrode, yet significantly optimize the electrochemical performance in the batteries due to the uniform and densely-packed coating layers.

The polypropylene Celgard^{TM} membrane used as a separator in the Li-S battery is chosen as a substrate to illustrate the utility of the LBSDC and LBS approach for at least three reasons. First, the rechargeable Li-S battery is arguably one of the most important platforms for storing large amounts of electrical energy at a moderate cost. The redox reaction between lithium and sulfur, $16Li + S_8 \Leftrightarrow 8Li_2S$, occurs spontaneously, is reversible, and produces up to two electrons per formula unit of sulfur, without intervention with catalysts or other means. These features endow the Li-S battery with high theoretical specific energy, 2600 Wh kg^{-1}, and low material and operating costs[17–19].

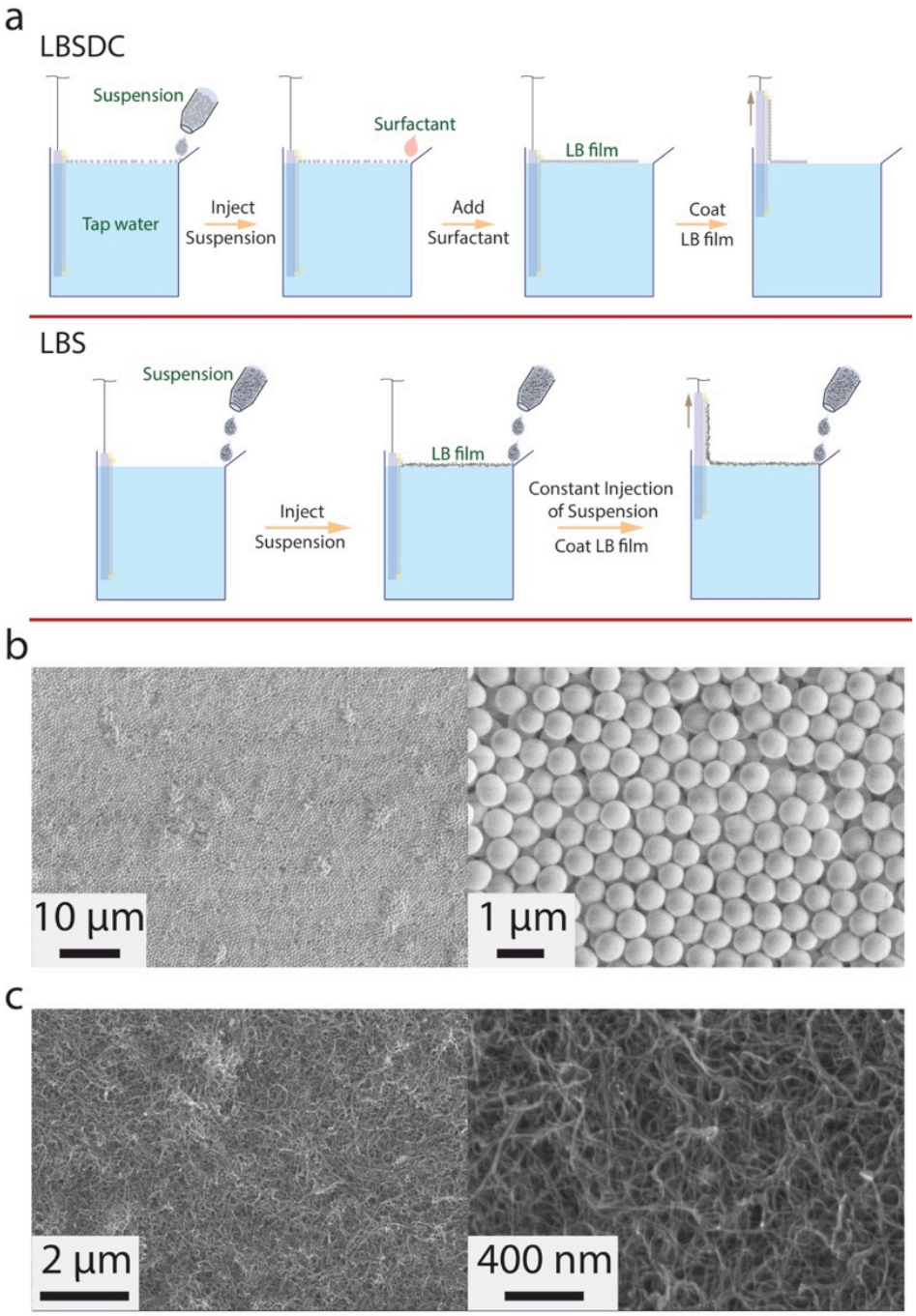

Figure 3.2. LBSDC and LBS coating method schematics and SEM images of multilayer coatings of silica nanospheres and MWCNTs on polypropylene separators. (a) Schematic illustrations of LBSDC and LBS coating methods. (b) SEM images of three monolayers of silica nanospheres coated separator using LBSDC and c, three coating layers of MWCNT coated separator using LBS.

Second, in practice Li-S cells fail to deliver on these high expectations for two stubborn, fundamental reasons: **(i)** sulfur and its reduction compounds with lithium are such poor conductors that unless the electrochemical reactions between Li^+ and sulfur occur in solution near a conductive substrate or in subnanometer-sized pores of a conductive host material such as microporous carbon, only a small fraction of the active sulfur material in the cathode is electrochemically accessible; and **(ii)** the reaction between Li^+ and S_8 is a multi-step reaction[20], in which the higher molecular weight intermediate species Li_2S_x ($x \geq 4$), collectively termed lithium polysulfides (LiPS), are soluble whereas the lower molecular weight ones ($x < 3$) are not. Dissolution of LiPS in an electrolyte means that a substantial fraction of the active material can be lost before it is fully reduced to Li_2S, if the LiPS diffuses too far from the conductive substrate in the cathode. An even greater concern is that once in the electrolyte, LiPS can diffuse to the lithium metal anode and undergo chemical reduction to form polysulfides of lower order, some of which are insoluble and deposit on the anode, causing time-dependent loss of both lithium and sulfur in a parasitic process termed shuttling.

Finally, a variety of approaches have been investigated for controlling LiPS dissolution, diffusion, and shuttling in Li-S cells. Methods ranging from sequestering the sulfur in porous carbon structures in nanospheres[21], nanotubes/nanofibers[22], graphene/graphene oxide sheets[23,24] all utilize the strong affinity of sulfur for carbon-based materials to limit dissolution. Other workers have shown that strong specific interactions of LiPS with amine-containing molecular[25,26] and inorganic chalcogenide[27], particulate additives can

be used to reduce sulfur loss to the electrolyte[28,29]. Even in the best cases, however, there is a finite, equilibrium concentration of LiPS dissolved in the electrolyte such that chemical potential of LiPS in the cathode is equal to that in the electrolyte[18,25,]. As a result, the dissolved LiPS are still able to diffuse to the Li anode, react with it, and increase the interfacial resistance of the anode. Very recently, Hendrickson et al showed that a substantial amount of LiPS is also lost by adsorption in the pores of the separator and that this source of loss can be removed in model Li-S cells run in a separator-/membrane-free configuration, but at the price of very high interfacial impedances at the anode[30]. Other works have shown that incorporation of carbon,[31–42] metal-oxide,[43,44] and polymer[45–47] coatings on separators can reduce LiPS loss, but the electrolyte must still be reinforced with additives such as $LiNO_3$ thought to limit LiPS reaction with metallic lithium, for stable cell cycling over extended periods or in practical lithium- and electrolyte-lean Li-S cell designs.

A broad range of materials such as SP carbon[36–38], KB carbon[37], carbon nanofibers/tubes[32-35], mesoporous carbon[31], alumina[48] and graphene[39-43] were coated on Celgard, and the electrochemical performances of Li-S cells based on these separators are investigated in literatures. To note the versatility and adaptability of the developed coating methods, large selections of a material with one or more different coating materials (Supplementary Figure S5) are coated on the separator and are suitable for different substrates (Supplementary Figure S6 & S7). The thickness of a single layer coating of MWCNT, KB, and SP is ~80 nm, ~350 nm, and ~850 nm, respectively (Supplementary Figure S4). The corresponding gravimetric coverage of a single layer of MWCNT, KB, SP, and ~350 nm silica nanospheres is ~5 μg cm^{-2}, ~17 μg cm^{-2}, ~20 μg

cm^{-2}, and ~25 μg cm^{-2}, respectively (Supplementary Figure S8). The negligible weight gained per coating layer with high uniformity is best appreciated by comparison to literature results, where carbon materials are coated using the vacuum filtration[32-34] (Loading: 0.17 to 0.35 mg cm^{-2}, Thickness: 20 to 25μm) or doctor-blade[31,36-37] (Loading: 0.26 to 0.53 mg cm^{-2}, Thickness: 6.7 to 27 μm) methods. As illustrated in Supplementary Figure S9, LBS coatings on Celgard are single-sided and exhibit high mechanical strength absence of chemical binders (Supplementary Figure S10). The effectiveness of LBS-coated Celgard comprised of 1-10 coating layers of silica nanospheres, MWCNT, KB, and SP were systematically studied for their ability to improve cycling behavior in Li-S cells. As shown in Supplementary Figure S11, Li-S cells based on the carbon coated separator yield superior capacity and retention rates, compared with pristine Celgard separator. Specifically, the capacity retention after 100 cycles is improved from 31% for the pristine separator to 63%, 71%, 63%, and 49% for ten coating layers of MWCNT, KB, SP, and silica nanospheres, respectively. The initial capacity for the pristine separator, 10LR MWCNT, 10LR KB, 10LR SP, and 10LR are 1067 mAh g^{-1}, 1535 mAh g^{-1}, 1594 mAh g^{-1}, 1541 mAh g^{-1}, and 1588 mAh g^{-1}, respectively at 0.5C for the first four and 0.2C for the last.

Our results show that carbon-coated Celgard is far more effective than the silica-coated material in stabilizing cycling performance of Li-S cells. We attribute this behavior to the stronger adsorption of LiPS on the SiO_2 coating layer by physical and covalent bonds[28] and the inability to utilize the trapped LiPS. Our results also confirm observations reported by Yao et al[37], that MWCNT and KB are particularly effective as separator

coatings because the interconnected porous structure of coatings based on these carbon materials allow for both trapping of LiPS and utilization of the trapped materials in electrochemical cycling. It is important to note, however, that the weight of MWCNT per coating layer is only 25% that of KB, implying that the MWCNT coating is by far the most efficient of the carbon materials studied.

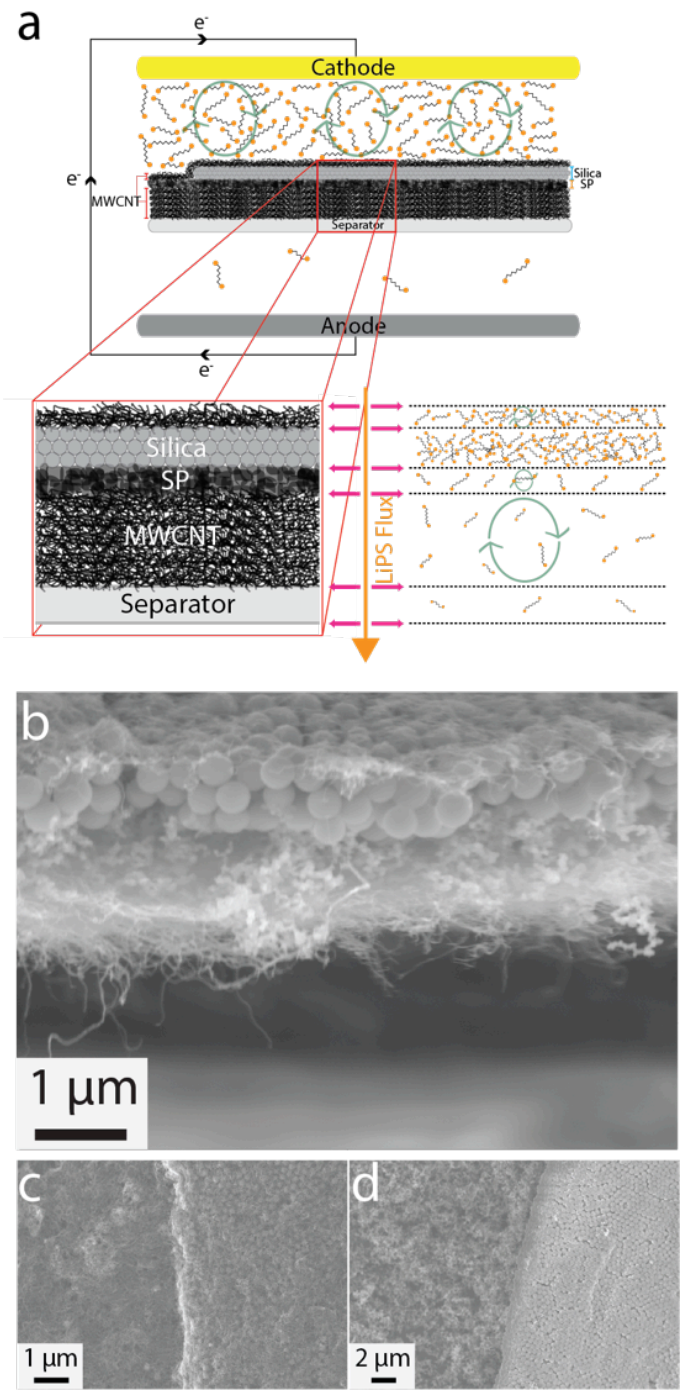

Figure 3.3. Clip configuration coating schematic illustration and SEM images of the clip coated separator. (a) Clip configuration architecture design and LiPS flux diagram across the separator during the discharge of Li-S cell. (b) Cross-sectional SEM image of the clip coated separator. (c) SEM image of the clip coated separator at the silica-SP boundary layer. d, SEM image of the clip coated separator at the boundary without final MWCNT coating.

A separator coating design that offers a combination of the strong LiPS binding attributes of a close-packed array of SiO_2 particles and high utilization of trapped LiPS evident for MWCNT would seem ideal for Li-S cells. This perspective is at odds with the work of Yao et al[37], which previously demonstrated that a Li-S battery separator coated with a mixture of ceramic nanoparticles and Super-P (SP) carbon, using the doctor-blade coating method, yields cells with poorer electrochemical performance than those in which a simple SP coating layer was used. Here, we take advantage of the spatial control afforded by the LBS and LBSDC coating strategy to create a multifunctional separator coating with the configuration shown in Figure 3.3a. In this so-called *clip* configuration multiple layers of closely packed silica particles are surrounded by a conductive fibrous network based on MWCNT. The location of the silica layer is designed such that under compression in a battery, the two MWCNT coatings contact each other (like the clasps of a clip) and also make contact with the cathode so as to ensure maximum electrochemical access to LiPS trapped in any of the coating layers that comprise the clip. As a proof of concept, we created and studied clip coating designs comprised of five coating layers of MWCNT and three monolayers of silica. The quality and mechanical strength of these coatings are illustrated in Supplementary Figure S12. Figure 3.3b shows the cross section of the clip configuration, where it is seen that the material has a consistent structure and a thickness of ~3μm. The clip configuration of the coating has also been confirmed by SEM image at the silica-carbon layer boundary (Figure 3.3c). Figure 3.3c then shows a uniform thin fibrous morphology of the coating surface after the final layer of MWCNT coverage is established over the three layers of silica nanosphere film (Zoomed-in SEM images is shown in Supplementary Figure S13). We observed the immersion of close-

packed silica layers at the third layer on top of the SP layer of the clip coating (Figure 3.3d). For reference, one monolayer of silica nanospheres is also shown in Supplementary Figure S14.

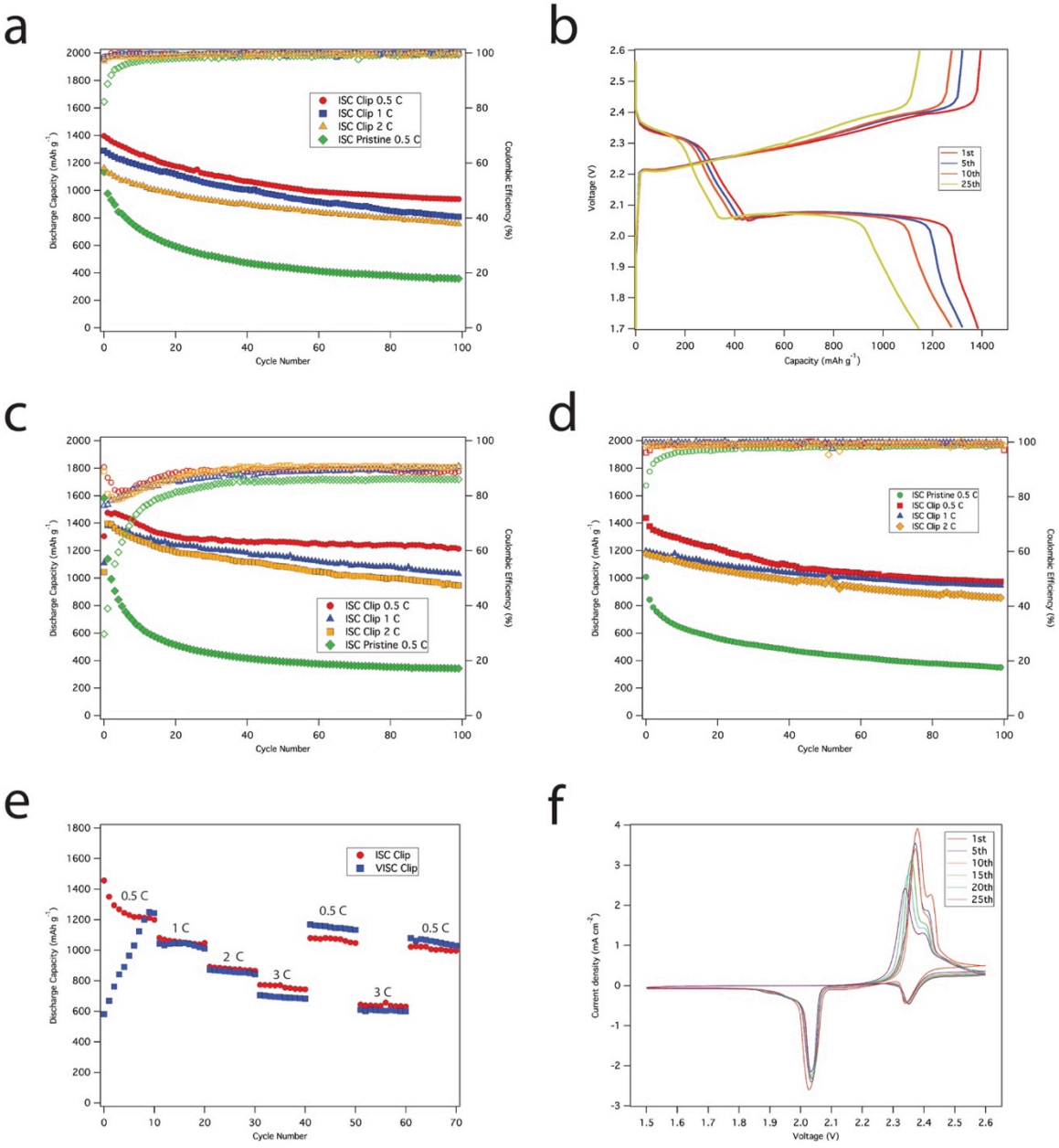

g

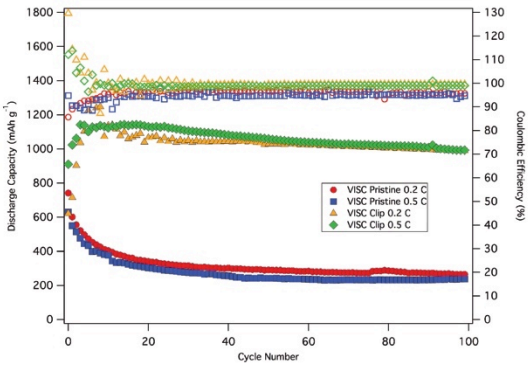
VISC Pristine 0.2 C
VISC Pristine 0.5 C
VISC Clip 0.2 C
VISC Clip 0.5 C
Discharge Capacity (mAh g-1)
Coulombic Efficiency (%)
Cycle Number

h

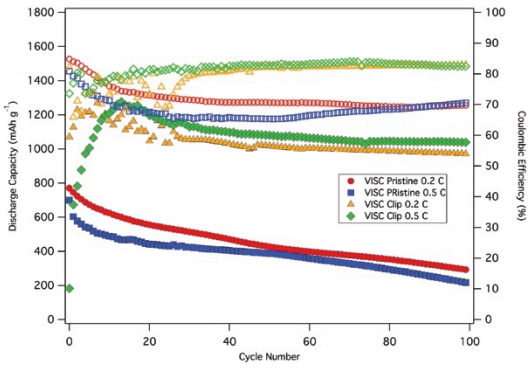
VISC Pristine 0.2 C
VISC PRistine 0.5 C
VISC Clip 0.2 C
VISC Clip 0.5 C
Discharge Capacity (mAh g-1)
Coulombic Efficiency (%)
Cycle Number

i

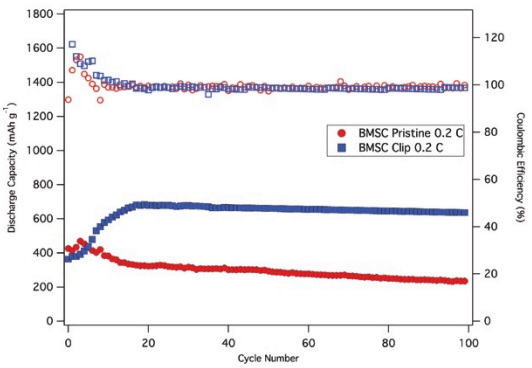
BMSC Pristine 0.2 C
BMSC Clip 0.2 C
Discharge Capacity (mAh g-1)
Coulombic Efficiency (%)
Cycle Number

j

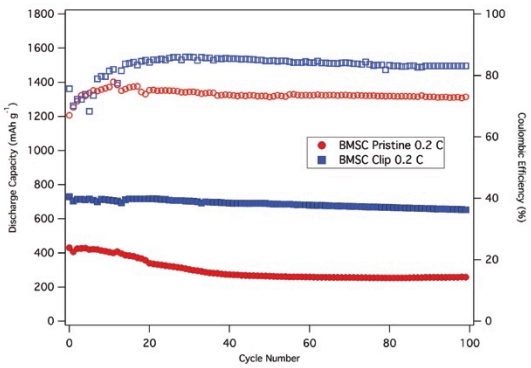
BMSC Pristine 0.2 C
BMSC Clip 0.2 C
Discharge Capacity (mAh g-1)
Coulombic Efficiency (%)
Cycle Number

k

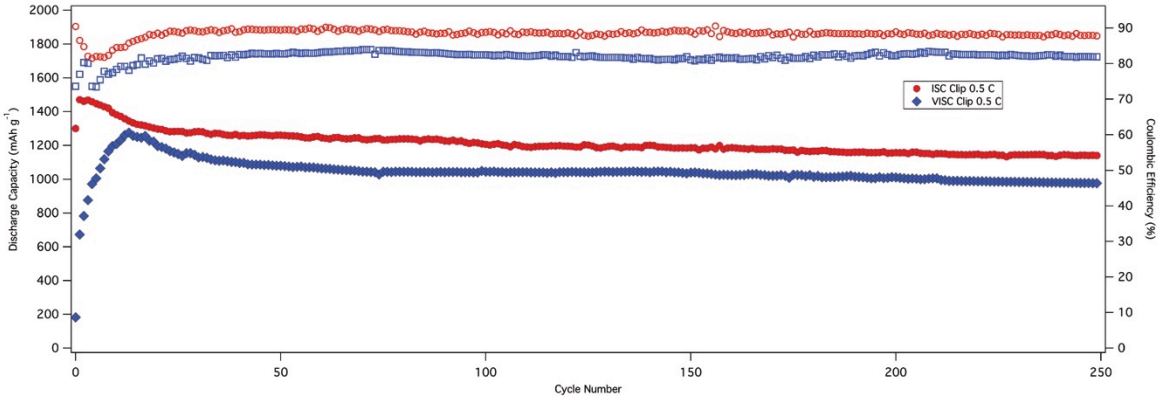
ISC Clip 0.5 C
VISC Clip 0.5 C
Discharge Capacity (mAh g-1)
Coulombic Efficiency (%)
Cycle Number

Figure 3.4. Electrochemical performance of the clip coated separator Li-S cells with various cathodes. (a) Cycling performance of the pretreated Li anode Li-S cell with/without the clip coated separator and with ISC at three different C rates. (b) Discharge-charge voltage profiles of the pretreated Li anode Li-S cell with the clip coated separator and with ISC at 0.5 C. (c) Cycling performance of pristine Li anode of the Li-S cell with/without the clip coated separator and with ISC at three different C rates without $LiNO_3$ in the electrolyte. (d) Cycling performance of pristine Li anode of the Li-S cell with/without the clip coated separator and with ISC at three different C rates with 0.05M $LiNO_3$ in the electrolyte. (e) Cycling performance of pristine Li anode with the clip coated separator Li-S cells with ISC and VISC at various C rates without $LiNO_3$ in the electrolyte. (f) Cyclic voltammograms of the pristine Li anode with the clip coated separator Li-S cell with ISC at 0.1 mV s^{-1} for various cycles. (g) Cycling performance of the pristine Li anode Li-S cells with/without the clip coated separator, with VISC, and 0.3M $LiNO_3$ in the electrolyte at two different C rates. (h) Cycling performance of the pristine Li anode Li-S cells with/without the clip coated separator and with VISC at two different C rates without $LiNO_3$ in the electrolyte. (i) Cycling performance of the pristine Li anode Li-S cells with/without the clip coated separator, with BMSC, and 0.3M $LiNO_3$ in the electrolyte at 0.2 C. (j) Cycling performance of the pristine Li anode Li-S cells with/without the clip coated separator and with BMSC at 0.2 C without $LiNO_3$ in the electrolyte. (k) Cycling performance of the clip coated separator Li-S cells no $LiNO_3$ in the electrolyte and with ISC and VISC at 0.5 C for 250 cycles.

In order to investigate the electrochemical performance of the clip-coated separator, three different cathodes, infused sulfur cathode (ISC), vapor infused sulfur cathode (VISC), and ball-milled sulfur cathode (BMSC), have been used in this study. Figure 3.4a reports results from galvanostatic cycling studies of the materials in a 1M LiTFSI DOL/DME electrolyte and with ISC. The lithium metal anode used in the study was pretreated in the manner reported in reference[30], by soaking it in an electrolyte containing $LiNO_3$ for 24 hours followed by rigorous drying in an Ar environment. It is immediately apparent that they offer significant advantages. Specifically, in the control case with the pristine (uncoated) separator, the capacity dropped to 360 mAh g^{-1} after 100 cycles at a current rate of 0.5C (838 mA g^{-1}). However, when the separator was coated using the

aforementioned clip configuration, a capacity of ~1000 mAh g^{-1} was obtained. The cells with the clip configuration also exhibit superior performance at high current rates. High initial capacities of 1290 mAh g^{-1} and 1160 mAh g^{-1} were obtained at 1C and 2C with high capacity retentions of 63% and 65%, respectively. Figure 3.4b reports the voltage profile at different cycle numbers for the clip configuration at 0.5C. Two discharge plateaus can be seen over many cycles: The first plateau at 2.35V corresponds to the reduction of the elemental sulfur to high order LiPS, whereas the second plateau at 2.05V indicates the high order LiPS reduction into low order LiPS. Notwithstanding the absence of LiNO3 in the electrolyte, there is no evidence of shuttling and a coulumbic efficiency as high as 99.8 % is observed. The voltage profiles for the uncoated separator control are provided in Figure S15a. Not only are the capacities found to be lower but also the telltale extended charge process associated with LiPS shuttling is observed. Supplementary Figure S15b reports the corresponding voltage profile of the clip configuration at different current rates. It is clear that the voltage plateaus for the discharge and charge processes does not change when the current is increased by 2 or 4 times.

To separate out the Li-S performance improvements derived from pretreating the Li metal anode with those obtained from the clip coated separator, Figure 3.4c reports performance of Li-S cells with the clip-coated separator, but in which pristine Li-metal anodes and additive-free electrolyte are used. Comparison of the results with those in Figure 3.4a indicates that comparable capacity is obtained when a pristine lithium metal anode is used. The comparison of the voltage profile of the cells utilizing the pristine separator and the clip coating separator is shown in Supplementary Figure S16. To

facilitate comparisons with literature results, we also performed studies using a conventional Li-S electrolyte containing 0.05M $LiNO_3$ as the additive, and the results are shown in Figure 3.4d and corresponding voltage profiles are shown in Supplementary Figure S17. Figure 3.4e reports the rate capability of the cells with the clip coated separator are also significantly improved, illustrating that the capacity of the cells can recover after high rate cycles of 1C, 2C, and 3C for 10 cycles respectively. Cyclic voltammograms shown in Figure 3.4f further confirms the stability of the cells in the additive-free electrolyte with pristine Li anode. The discharge and charge peaks are observed to remain at the same position over many cycles, indicative of the stable and reversible electrochemical reaction of sulfur. Furthermore, Figure 3.4g and Figure 3.4h show electrochemical performance of the clip coated/pristine separators with VISC in 0.3M $LiNO_3$ and no $LiNO_3$ additive in the electrolyte. VISC has an areal sulfur loading of 3.5 mg cm^{-2} and a content of 68w%. Figure 3.4g and 4h show effectiveness of the clip coated separator with VISC, and increasing capacity at first several cycles can be observed as reported in literatures for high loadings of sulfur with a upper current collector which confirms that the clip configuration plays a crucial role as the effective upper current collector for harvesting LiPS. Also, Supplementary Figure S18 shows the series of the voltage profiles of Li-S cells with the clip coated/pristine separators and VISC in the electrolyte with/without $LiNO_3$. More, the clip coated separators are also tested in a harsh environment - BMSC which is made via simple ball-milling sulfur powder with a carbon matrix and has a high sulfur loading of 3.5 mg cm^{-2} and 70% (Figure 3.4i and Figure 3.4j). The clear improvements of the electrochemical performance of Li-S with the clip coated separators, the equilibrium capacity of ~700

mAh g^{-1}, are shown considering the mass loading of the clip coated separator, ~130 µg cm^{-2}, and the conditions of the cathode. Supplementary Figure S19 shows the series of the voltage profiles of Li-S cells with the clip coated/pristine separators and BMSC in the electrolyte with/without $LiNO_3$. Overall, the electrochemical performance of the clip coated separators are thoroughly examined using pretreated/pristine Li anode, various cathodes, and the electrolyte with/without $LiNO_3$, and good electrochemical performance of the Li-S cells with the clip coated separators are achieved. Longer cycling performance of clip coated separators with ISC and VISC without $LiNO_3$ in the electrolyte is shown in Figure 3.4k, and stable performance is observed >200 cycles at 0.5 C, which is remarkable with such high sulfur loading and $LiNO_3$ free electrolyte.

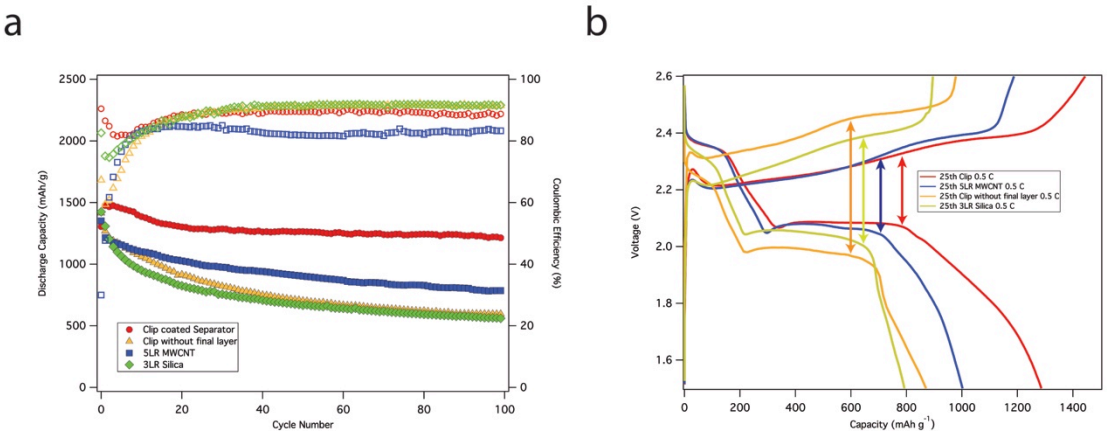

Figure 3.5. Electrochemical performance of the clip multilayer parts. (a) Cycling performance of the pristine Li anode with the clip coated separator, clip coated separator without final MWCNT layer (Same structure as shown in Figure 3.3d), five layers of MWCNT coated separator, and three monolayers of silica nanospheres coated separator Li-S cell with ISC at 0.5 C. (b) Discharge-charge voltage profiles of pristine Li anode with clip coated separator, clip coated separator without final MWCNT layer, five layers of MWCNT coated separator, and three monolayers of silica nanospheres coated separator Li-S cell with ISC for 25th cycle at 0.5 C.

In order to investigate the effect of each compartment in the clip configuration, we compared the electrochemical performance of the clip with five layers of MWCNT coating, three layers of silica, and a clip configuration without the final electrical path MWCNT layer, which is the equivalent structure shown in Figure 3.3d (Figure 3.5a). Significantly, it is noted that without the final MWCNT coating to complete the clip, similar electrochemical performances are observed in Li-S cells using the multifunctional MWCNT-SiO_2 coatings, compared to those based on separators coated with three monolayers of silica. These results underscore the importance of the clip configuration in complementing LiPS adsorption achieved with SiO_2 coatings, with utilization of the trapped LiPS made possible by the MWCNT coating layers. They also validate our hypothesis that a good electrical conductive path is required to efficiently entrap and utilize dissolved LiPS. Figure 3.5b compares the voltage profiles of the cell with the clip configuration done in different steps. Consistent with the previous observation, the capacity is seen to increase progressively as the clip components are sequentially added to complete the structure: 561 mAh g^{-1} at 100^{th} cycle, 596 mAh g^{-1} at 100^{th} cycle, 785 mAh g^{-1} at 100^{th} cycle, and 1214 mAh g^{-1} at 100^{th} cycle when 3LR silica, the multifunctional MWCNT-SiO_2, 5LR MWCNT, and clip are coated on the separator, respectively. Another important observation is that the overpotential of the cell substantially declines when the final layer is involved, which confirms our hypothesis that the silica surface traps LiPS in the separator, which overtime reduces the electrolyte conductivity. Reutilization of the LiPS in the clip configuration eliminates this problem and reduces the overpotential correspondingly.

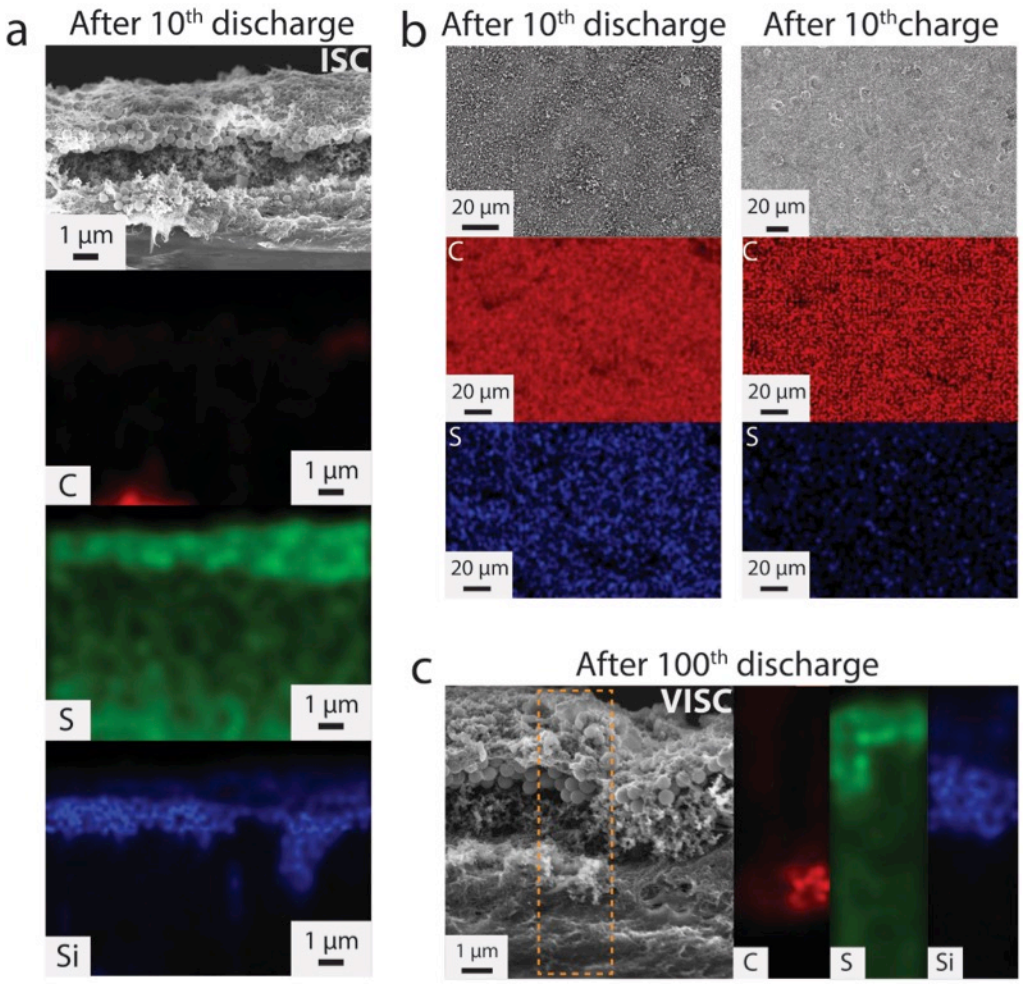

Figure 3.6. Clip coated separator morphology and elemental mappings after several cycles. (a) Cross sectional SEM image of the clip coated separator with ISC after 10th discharge with carbon, sulfur, and silicon maps. (b) Top view SEM image of the clip coated separator with ISC after 10th discharge/charge with carbon and sulfur maps. (c) Cross sectional SEM image of the clip coated separator with VISC after 100th discharge with carbon, sulfur, and silicon maps.

Finally, we investigated the morphology of the coating surface on the clip-coated separator after cycling using SEM. Figure 3.6a shows the morphology of the cross sectional separator after 10th discharge and corresponding energy-dispersed X-ray spectroscopy (EDXS) measurements of elemental mapping of carbon, sulfur, and silicon, in which silicon layer and sulfur distribution in the clip structure is clearly seen. The low

x-ray intensity for carbon is due to high coverage of sulfur after the discharge, indicating carbon layers are efficiently trapping dissolved LiPS. The structure of the clip coating is preserved upon discharge and charge, indicating the robust properties of the coating in both mechanical and chemical aspects. Also EDXS measurements of top view of the clip coated separator show a uniform distribution of carbon and sulfur elements (Figure 3.6b). The fact that the amount of sulfur decreased during the charge process further substantiates the ability of the coating to reutilize the adsorbed species. In addition, the morphology of the clip coated separator with VISC after 100^{th} cycles is shown in Figure 3.6c. This double confirms that the multifunctional coatings remain robust after large number of cycles with the presence of high loading and content of sulfur in the Li-S cells. We have also observed decrease in internal resistance of the Li-S cell for clip coated separator compared to pristine separator (See Supplementary Figure S20). The decreased impedance indicated that the clip design is able to facilitate the electron transfer even the insulating silica particles are involved.

In summary, we have demonstrated two new versatile coating methods, LBSDC and LBS, for creating surface films that utilize the surface tension gradient to create well-ordered monolayer films at an air/water interface. The methods allow multifunctional coatings to be created in a range of designs using a wide selection of individual materials, as well as material combinations, on a variety of substrates, without the need for chemical binders. The utility of the approach is illustrated using the polypropylene membrane separator, Celgard, commonly employed in Li-S batteries as a substrate. Through systematic studies, it is shown how mono-functional coatings based on different metal

oxides and carbon influence reutilization of dissoleved lithium polysulfide species. An unusual coating configuration termed the “clip”, created by stacking an incomplete, but well-formed layer of SiO_2 particles between two complete layers of carbon is used to illustrate both the versatility of the method to create multifunctional coatings with good spatial control and the effectiveness of such coatings in battery separators. In particular, the *clip* coated separator is observed to exhibit largely improved active material utilization, enhanced capacity retention over extended charge/discharge cycling, and attractive high rate capability. These observations are explained in terms of the ability of the multifunctional coatings to simultaneously adsorb and trap LiPS created at the cathode, without loosing electrochemical access to the materials. The new coating approach and configurational design of coating materials synergistically work together to advance Li-S cells and allow us to investigate and optimize the different coating structures.

3.4 Experimental Section

Synthesis

Silica nanospheres: Silica nanospheres were synthesized by the Stober synthesis technique[49]. In this method, 10 ml of amonium hydroxide, 10 ml of water and 75 ml of ethanol are taken in a round bottom flask and stirred using a stir bar to ensure proper mixing. Under smooth stirring conditions, 5.6 ml of tetraethyl orthosilicate (TEOS) was added drop-wise. After 12 hours of stirring, the prepared monodispersed silica nanospheres was purified by alternate centrifuging and sonication in an ethanol-water mixture until the colloidal solution reaches a stable pH of 7. The size of the prepared silica was characterized using the scanning electron microscopy (SEM) technique. The resulting silica nanosphere was determined by means of dynamic light scattering (DLS) and SEM analysis to be approximately 350 nm in diameter.

Suspensions: A Langmuir-Blodgett (LB) film forming suspension was comprised of 1 wt% of a nanomaterial in pure ethanol (Decon, 200 Proof). Each 1wt% of silica nanosphere, titania nanopowder (Rutile, 99% purity, Advanced Materials^{TM}), multi-walled carbon nanotube (L 6-9 nm x 5 μm, >95% carbon, Sigma Aldrich), Ketjen-Black carbon (Akzo Nobel), and Super-P carbon (TIMCAL) was dispersed in pure ethanol. Then each of the suspension was sonicated for 30 minutes to enhance the dispersion of the particles. Note that the film quality is not sensitive to the weight composition of the nanomaterials in ethanol solvent; 0.5 to 3 wt% of the nanomaterial suspensions yielded the same quality films. However, the film quality heavily depends on the distribution of the dispersed particle sizes; big aggregates or clusters will form a defect during the self-assembled LB film.

Surfactant: The SDS surfactant is made by dissolving 3 wt% of sodium dodecyl sulfate (SDS) in DI water.

Sulfur infused KB composite: Sulfur infused in Ketjen Black carbon composite was prepared by an infusion method. First, sulfur powder and Ketjen Black carbon (2.2:1 by weight) were placed in a hollow glass vial in Ar atmosphere. Then, the end of the glass vial was sealed to avoid water moisture during the infusion process. The composite contained glass vial was heated to 155 ^{o}C for 12 hours to infuse active sulfur into the pores of Ketjen Black carbon and subsequently cooled to room temperature. The resulting composite had a sulfur content of 66 wt% (Supplementary Figure S21).

Cathode preparation: ISC - The sulfur infused Ketjen Black composite (77 wt%) was mixed with Super P (8 wt%) and 10 wt% polyvinylidene fluoride (Sigma Aldrich) dissolved in N-methyl-2-prolidone (15 wt%) in N-methyl-2-prolidone (Sigma Aldrich), and the mixture is ball-milled at 50 rev s^{-1} for 30 minutes. The resulting viscous slurry was coated onto a carbon sprayed aluminum foil as a current collector using doctor-blade method. The coated slurry is then dried in a convection oven at 60 ^{o}C for 5 hours. The prepared electrode is cut into a circular disk, and the electrode has sulfur loading of 0.5 – 0.55 mg cm^{-2} with 50 wt% of active sulfur per cathode. After including conductive carbon components in the clip coated separator (excluding the mass of silica nanospheres), the active sulfur content remains at 47.5%. BMSC - The 70 wt% sulfur powder (Sigma Aldrich) was mixed with Super P (20 wt%) and 10 wt% polyvinylidene fluoride (Sigma Aldrich) dissolved in N-methyl-2-prolidone (15 wt%) in N-methyl-2-prolidone (Sigma Aldrich), and the mixture is ball-milled at 50 rev s^{-1} for 30 minutes. The resulting viscous slurry was coated onto a carbon sprayed aluminum foil as a current

collector using doctor-blade method. The coated slurry is then dried in a convection oven at 60 ^{o}C for 5 hours. The prepared electrode is cut into a circular disk, and the electrode has sulfur loading of 3.5 mg cm^{-2} with 70 wt% of active sulfur per cathode. VISC – this is a carbon-sulfur cathode created by infusion of sulfur in the vapor phase into a carbon fiber matrix.[21] Sulfur cathodes are prepared by coating the composite material onto a carbon coated Al foil. The cathode has a high sulfur loading (68w%) and a high areal density of sulfur (3.5 mg cm^{-2}). After including conductive carbon components in the clip-coated separator (excluding the mass of silica nanospheres), the sulfur contents for BMSC and VISC are 69.31% and 67.35%, respectively. All measurements reported in the study utilize a cathode size of 1.26 cm^{2}.

Coating process

Separator: The commercial polypropylene separator (Celgard 2500) was cut into a 1.6 cm diameter circular disk. The separator was placed onto a 1.8 x 1.8 cm microscope cover glass and the ends taped with Kapton tape to control the coating location (Supplementary Figure S22).

Single component separator coating: Mono/multi layers of Silica nanospheres, multi-walled cabon nanotubes, Ketjen Black carbon, and Super P carbon were coated on the separator using LBS method. Prepared separators are washed with tap water to flush out any impurities stuck onto the surface. One drop of isopropanol (IPA) is applied onto the separator or separator with coating layers to uniformly wet the surface of the separator with water, and the excess IPA on the separator is diluted with water. Then, the fully wetted separator is immersed in water. One of the suspensions is then injected at the

surface of the water until more than half of the surface is saturated with the desired nanomaterial; the separator is subsequently raised up to transfer the film followed by a constant injection of the suspension. After that, the coated separator is dried on a hot plate at 110 ^{o}C for 30 seconds. Note that no IPA wetting step is required for the silica nanosphere coatings. The single layer coating process is repeated until the desired number of layers is achieved. After the final layer coating, the whole separator is dried on the hot plate for one minute at 110 ^{o}C. In the different types and forms substrate coating demonstrations (Supplementary Figure S6 & S7), 1 μm fluorescent silica nanospheres and SP carbon suspensions are used to provide clear visibility of the coating layers.

Clip coating: The clip configuration coating is comprised of five coating layers of MWCNT, one coating layer of SP, three monolayers of silica nanospheres, and one final coating layer of MWCNT. The first five coating layers of MWCNT are coated in the same manner as the single component separator coating. Then, one layer of SP, which acts as an adhesion layer for the silica nanospheres, is coated on top of MWCNT using the LBS method. 80% of the MWCNT and SP carbon coated separator is covered with three monolayers of silica nanospheres using the LBSDC method. During the silica coating, no IPA is used after each coating. For the final layer, the remaining 20% of the separator is wetted with IPA. And after the dilution of IPA, the whole surface of the separator is coated with one coatinglayer of MWCNT. The clip coated separator is then dried on the hot plate at 110 ^{o}C for one minute.

Battery preparation

Li anode pretreatment: Li metal foil was cut into a 1.27 cm diameter circular disk, and the Li metal disks are completely soaked in 0.5M $LiNO_3$ (Sigma-Aldrich) 1,2-dimethoxyethane (DME, Sigma Aldrich) and 1,3-dioxolane (DOL, Sigma Aldrich) (1:1 v/v) electrolyte solutions for 24 hours [30]. Then, the pretreated Li metals were rigorously dried in air/oxygen-free Ar environment.

Electrolyte: Three electrolytes are prepared for this study: **i)** 1M Bis(trifluoromethane)sulfonamide lithium salt (LiTFSI, Sigma Aldrich) in DME:DOL (1:1 v/v) electrolyte, **ii)** 1M LiTFSI with 0.05M $LiNO_3$ in DME:DOL (1:1 v/v), and **iii)** 1M LiTFSI with 0.3M $LiNO_3$ in DME:DOL (1:1 v/v).

Cell assembly: CR2032-type Li-S coin cells are assembled with the polypropylene separators with coating layers, Li-foil disks, as prepared Li-S cathode, stainless-steel springs and spacers, and the electrolytes. A total of 40 μL of the electrolyte is used per cell. The first 20 μL of the electrolyte is added to the coating layers of the separator. Then, the cathode is placed onto the electrolyte-wetted separator facing the coating layers. Another 20 μL of the electrolyte is applied to the other side of the separator and pretreated or pristine Li metal disk is placed. Then the spacer and spring are used to sandwich the anode/separator/cathode, and pressure of 15 MPa is applied to punch the cell. The assembled cell is rested for about 15 minutes before testing. Cell assembly was carried out in an Ar filled glove-box (MBraun Labmaster). The room-temperature cycling characteristics of the cells were evaluated under galvanostatic conditions using Neware CT – 3008 battery testers and the electrochemical process in the cells were studied by cyclic voltammetry using a CHI600D potentiostat.

Characterization

Langmuir-Blodgett trough: Surface pressures of 350 nm Silica colloids, MWCNT, KB, SP, and SDS surfactant are measured using conventional LB trough (KSV NIMA L & LB Troughs). The trough has dimension of 7.5 cm x 32.4 cm (Supplementary Figure S2). The trough was cleaned using pure ethanol and DI water and fully dried with nitrogen gas. The trough was filled with DI water and a 0.5 ml of suspension is injected at the ends of the trough to float particles. After the injection of the suspension, rest time of ~7 minutes was needed to evaporate excess ethanol from the suspension. Then the resulting film is compressed at the rate of 3 mm min^{-1} to collect the surface pressure profiles. For obtaining the pressure profile of LBDSC and LBS, ~35 cm^2 and ~25 cm^2 areas are set to mimic actual coating process occurs at the surface from the 50 ml glass beaker. To collect LBDSC surface profile, ~35 cm^2 of the surface is saturated with the silica colloids and rested about 5 minutes to evaporate remaining ethanol. Then, 5 μL of the surfactant is added and the pressure profile is collected at the compression rate of 3 mm min^{-1}. For LBS surface profiles, ~25 cm^2 area is fully covered by MWCNT, KB, and SP, and without the rest time, the surface pressure profiles are collected at the compression rate of 3 mm min^{-1}. The surfactant surface pressure profile is measured at four different areas (7 cm^2, 11 cm^2, 19 cm^2, 38 cm^2) without compressing the barriers, and the 5 μL of the surfactant surface pressures are measured over time.

Galvanostatic charge/discharge: Neware battery testing system is used to perform cycling testing of the Li-S cells. 1.5V to 2.6V and 1.7V to 2.6V voltage windows are used for without/with $LiNO_3$ electrolyte systems, respectively. 1.7V to 2.6V voltage window is chosen for the $LiNO_3$ system to preserve $LiNO_3$ passivation layer on the Li.

CV: CHI600D potentiostat is used to perform cyclic voltammetry analysis of the cell. 0.1 mV s^{-1} scan rate with the voltage window of 1.5V to 2.6V are chosen as the parameters.

SEM: The morphology of the coating layers on the separator is analyzed using Keck scanning electron microscope (LEO 1550 FESEM) at 3 kV acceleration voltage.

EDXS: Energy dispersive X ray spectroscopy (EDXS) is performed on Keck scanning electron microscope to investigate the chemistry of the coatings on the separator.

TGA: Thermogravimetric analysis (TGA) was used to determine the content of sulfur in the S-KB composite. Morphologies of the electrodes were studied using Keck SEM.

ACI: Alternating current impedance (ACI) was measured versus frequency using a Novocontrol N40 broadband dielectric spectroscopy.

3.5 Supporting Information

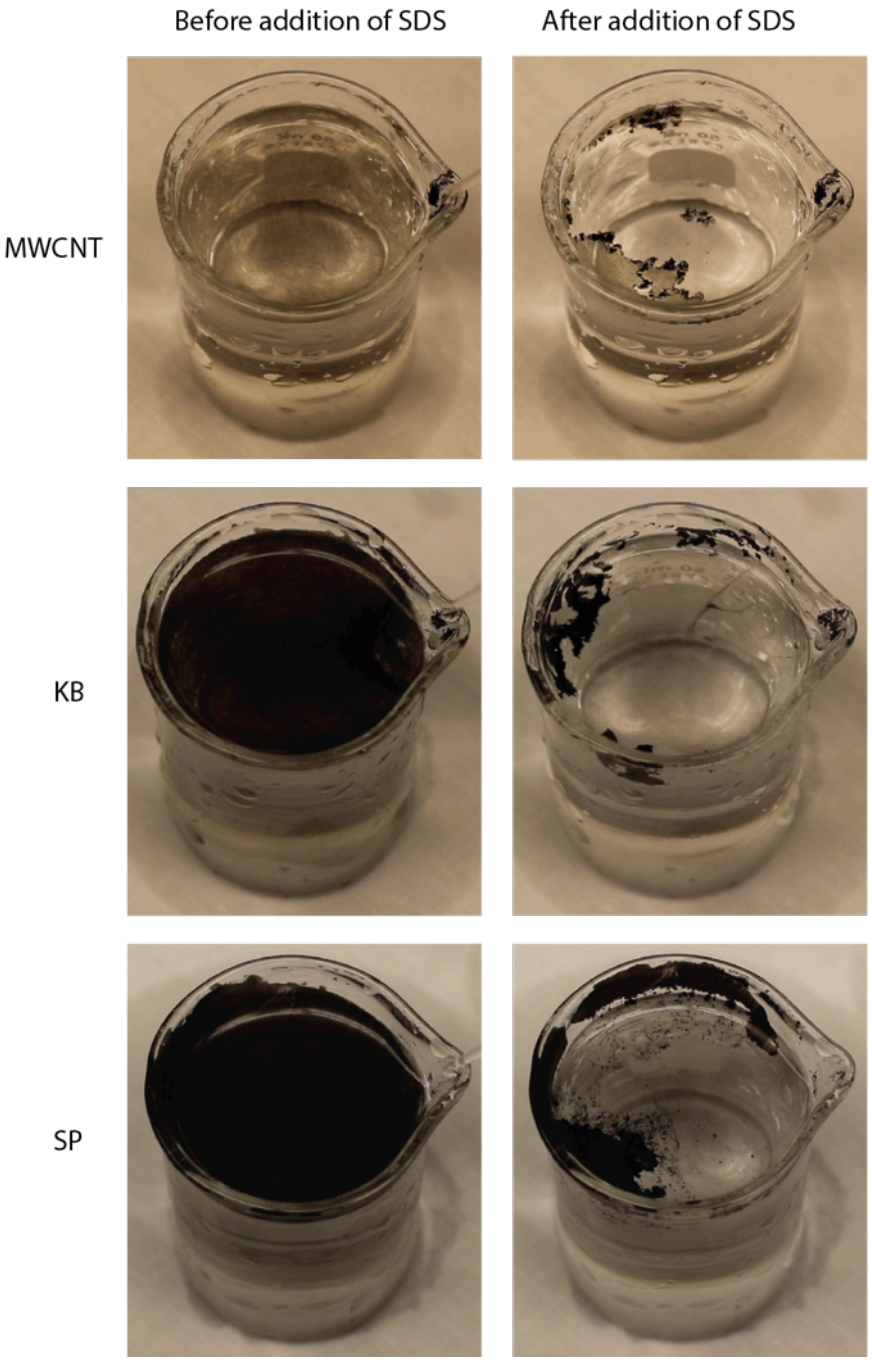

Supplementary Figure S1: Collapsing self-assembled LB film in the presence of SDS surfactant. The self-assembled MWCNT, KB, and SP films are formed at the surface of water using LBS coating method, and images of the films before and after adding a one-drop of SDS surfactant at the neck of the beaker are shown.

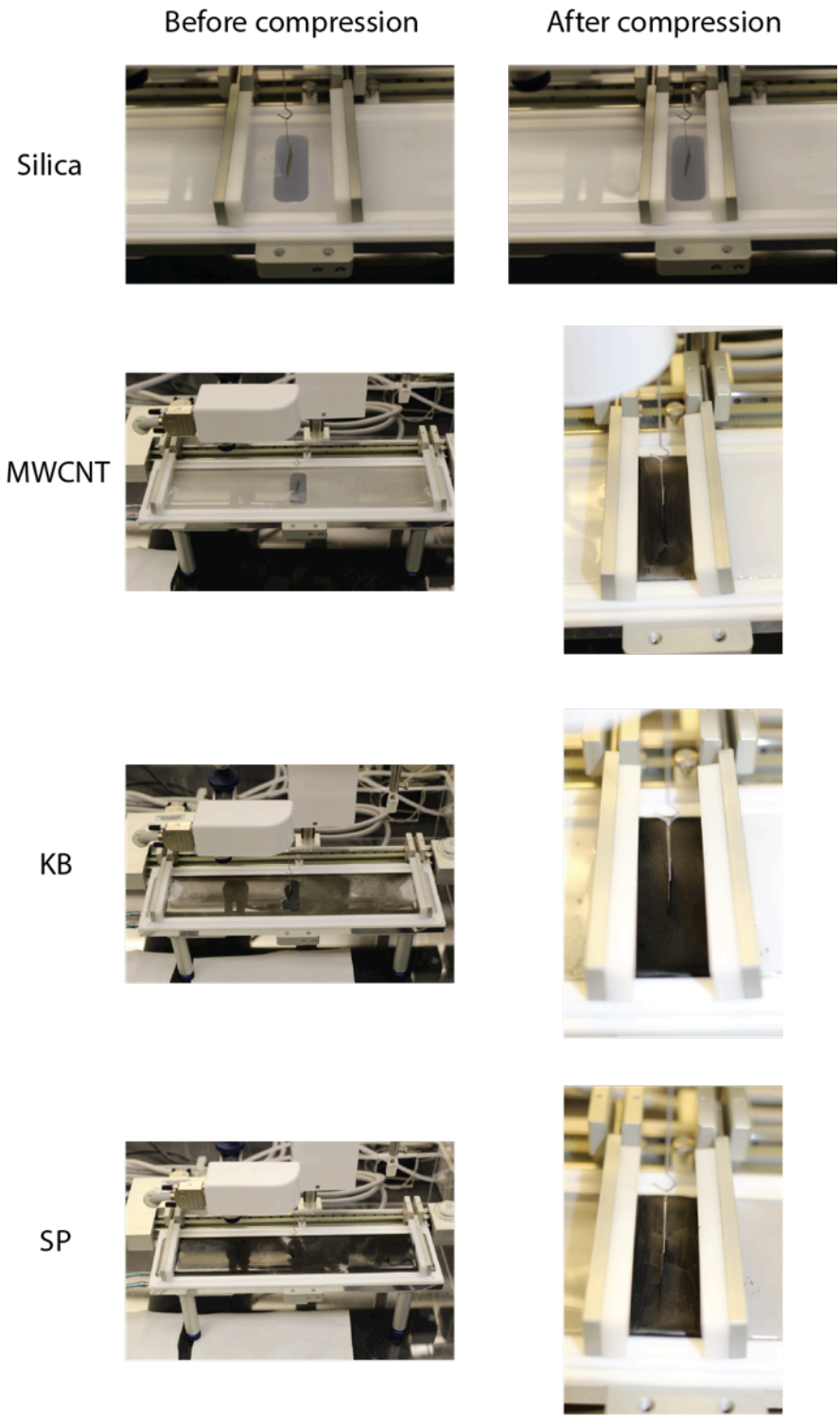

Supplementary Figure S2: Langmuir-Blodgett trough experiment for surface pressure measurements. Images of compressing silica nanospheres, MWCNT, KB, and SP are shown. Note that no materials are lost during the compression of the LB films, and folding of the films is observed instead of particles sinking.

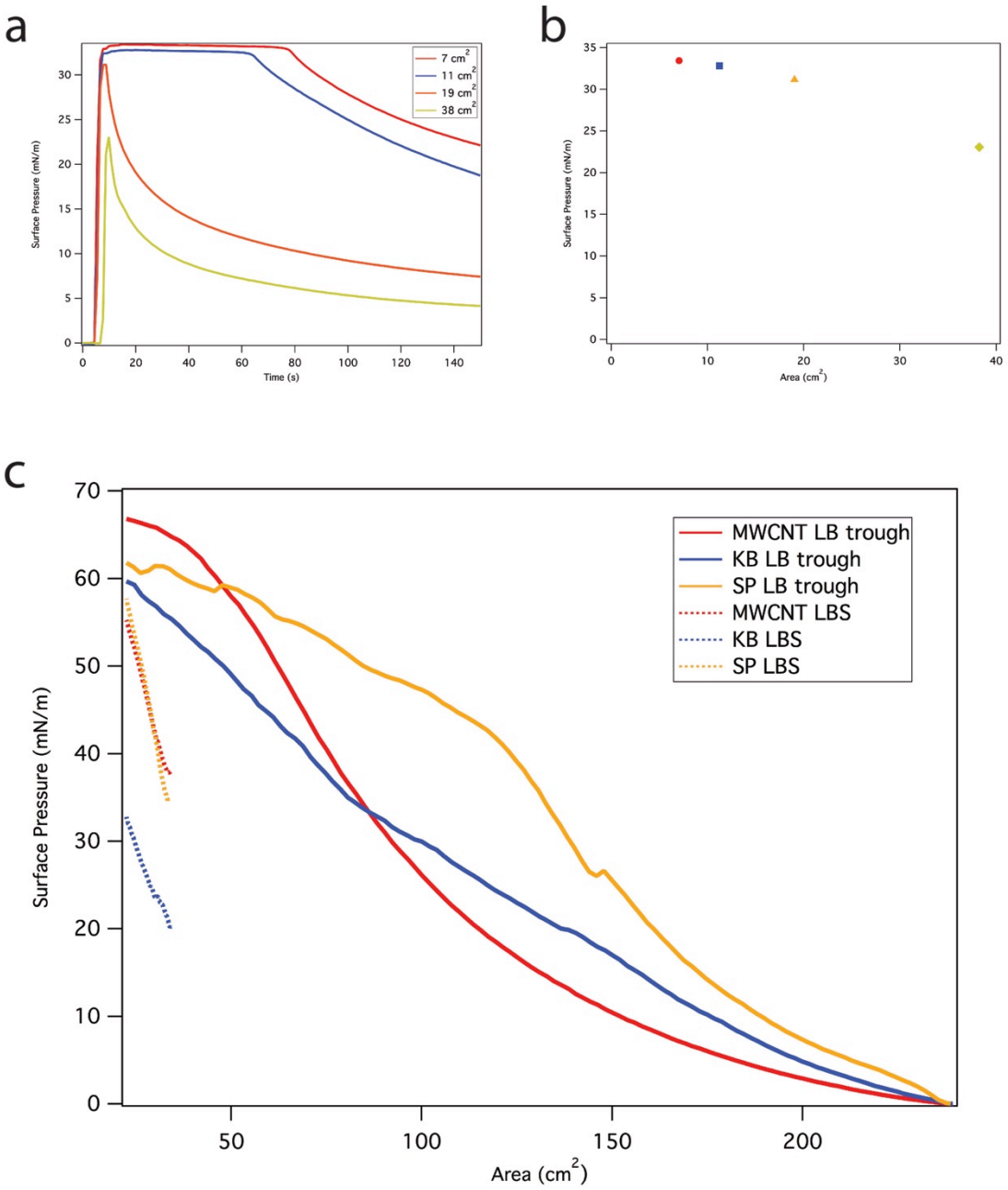

Supplementary Figure S3: SDS surfactant and carbon surface pressure profiles. (a) Surface pressures of SDS surfactant versus time for the surface area of 7 cm^2, 11 cm^2, 19 cm^2, and 38 cm^2. (b) Maximum surface pressures exerted by the surfactant for the surface area of 7 cm^2, 11 cm^2, 19 cm^2, and 38 cm^2. (c) MWCNT, KB, and SP surface pressure profiles obtained from conventional LB trough and LBS methods.

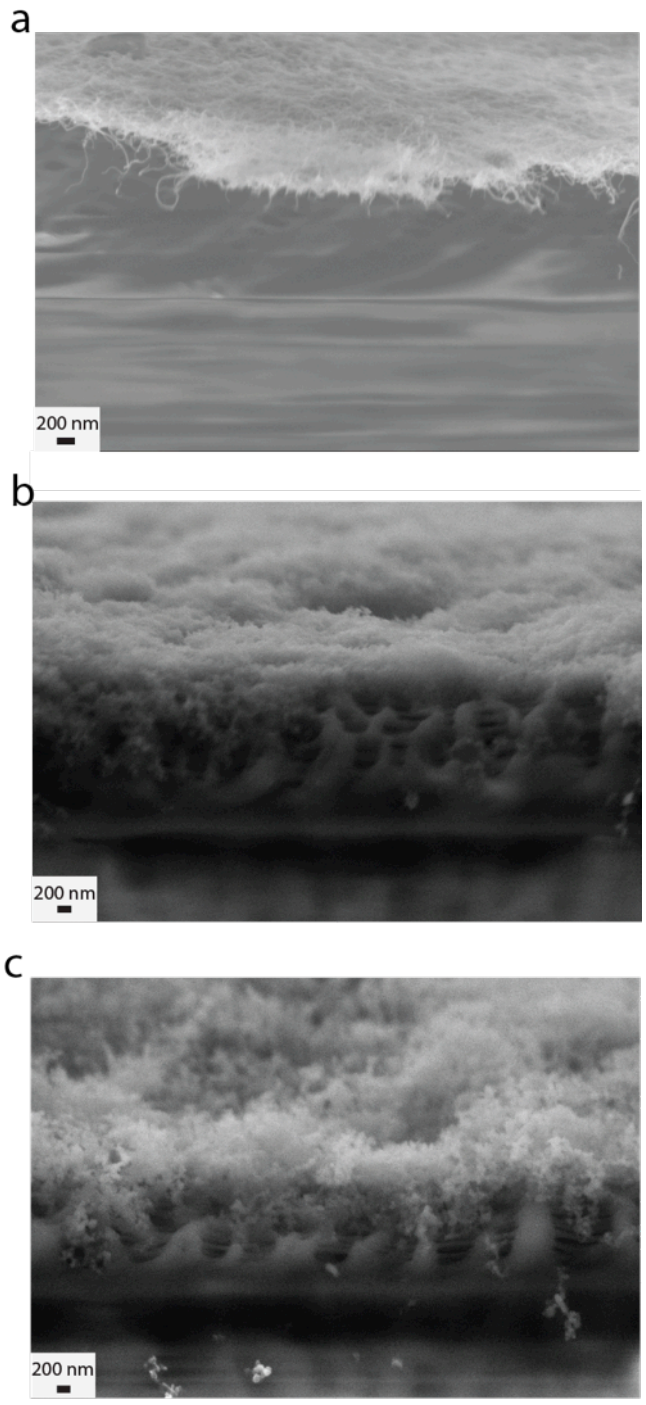

Supplementary Figure S4: Thickness of single coating layer carbon films. Cross-sectional SEM images of a single layer coating of (a) MWCNT, (b) KB, and (c) SP on the separator using LBS method.

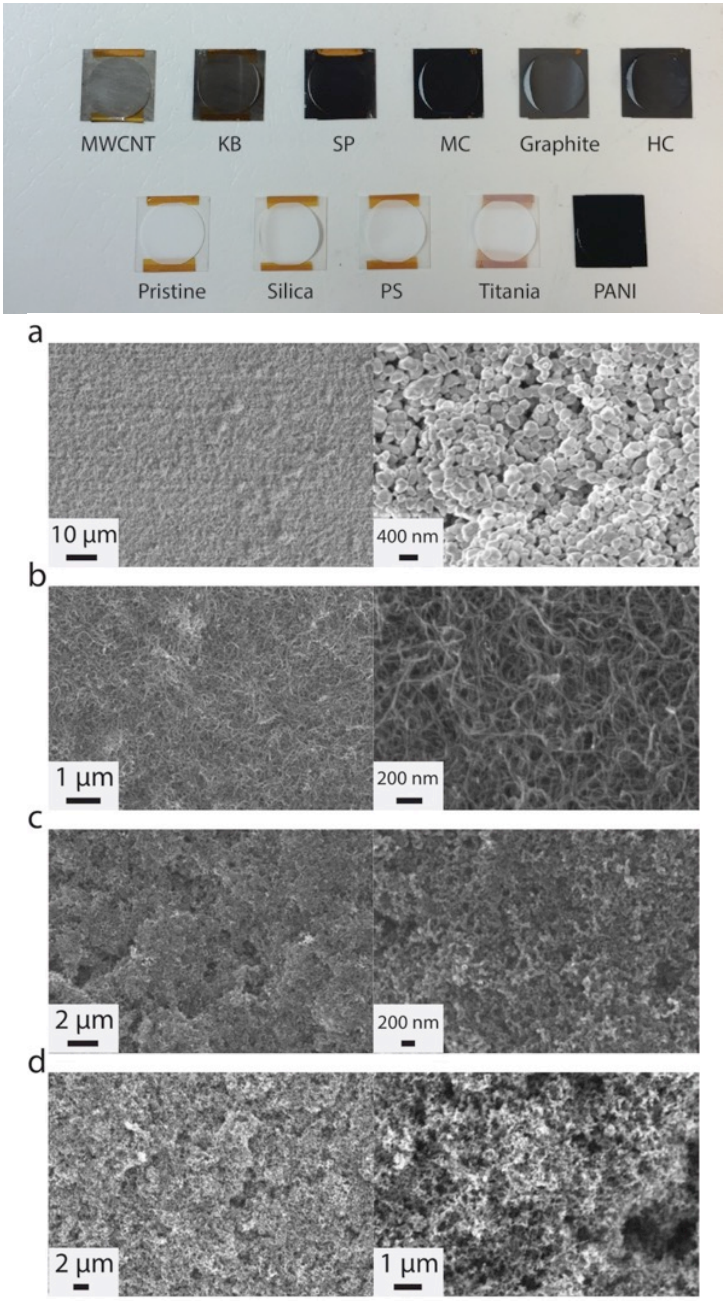

Supplementary Figure S5: Demonstration of coating various materials onto the separator using LBS method. Images of single coating layer of Multi-walled carbon nanotube (MWCNT), Ketjen Black carbon (KB), Super P carbon (SP), Microporous carbon (MC), Graphite, Hard carbon (HC), 350 nm silica nanospheres, 1µm polystyrene spheres (PS), titania nanopowder, and polyaniline (PANI) on the separator are shown. SEM images of three coating layers of (a) titania nanopowder, (b) MWCNT, (c) KB, and (d) SP coated on the separator.

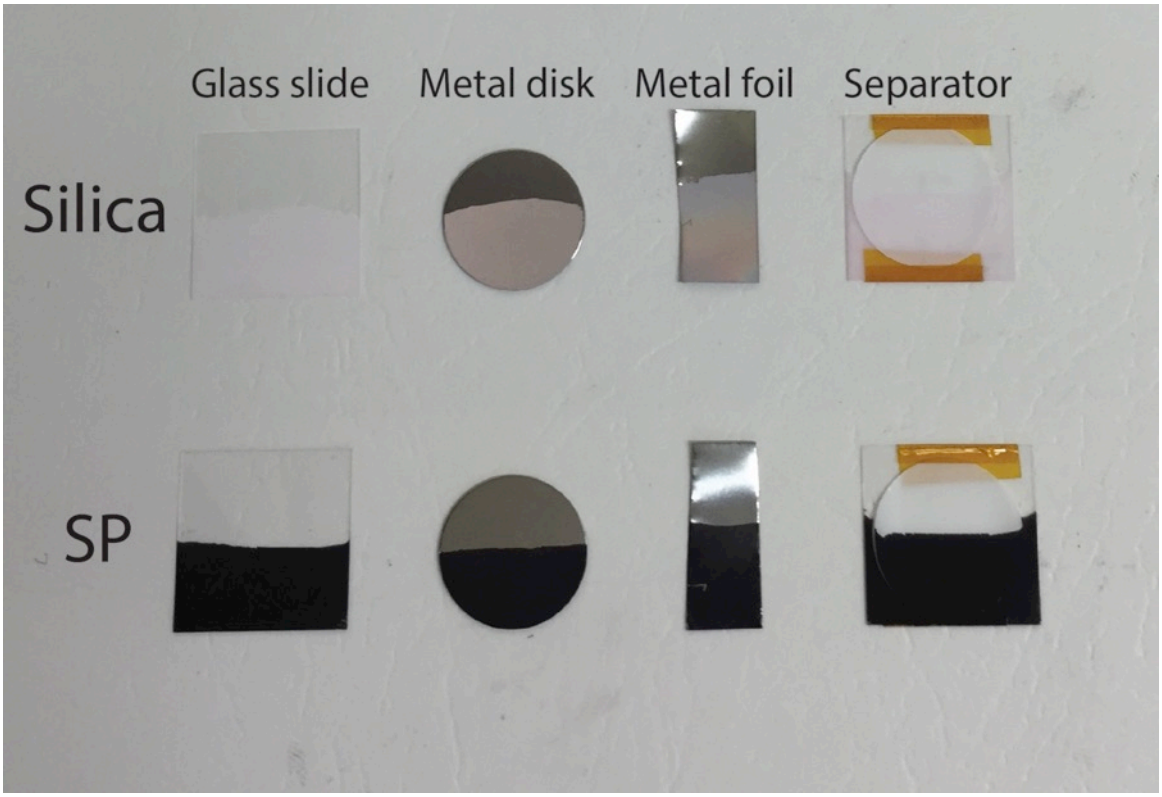

Supplementary Figure S6: Uniform substrate coating demonstration. Images of fluorescent 1µm silica nanosphere and Super P carbon coatings on various uniform substrates using LBS coating method are shown. Note that other materials can also be coated on these substrates.

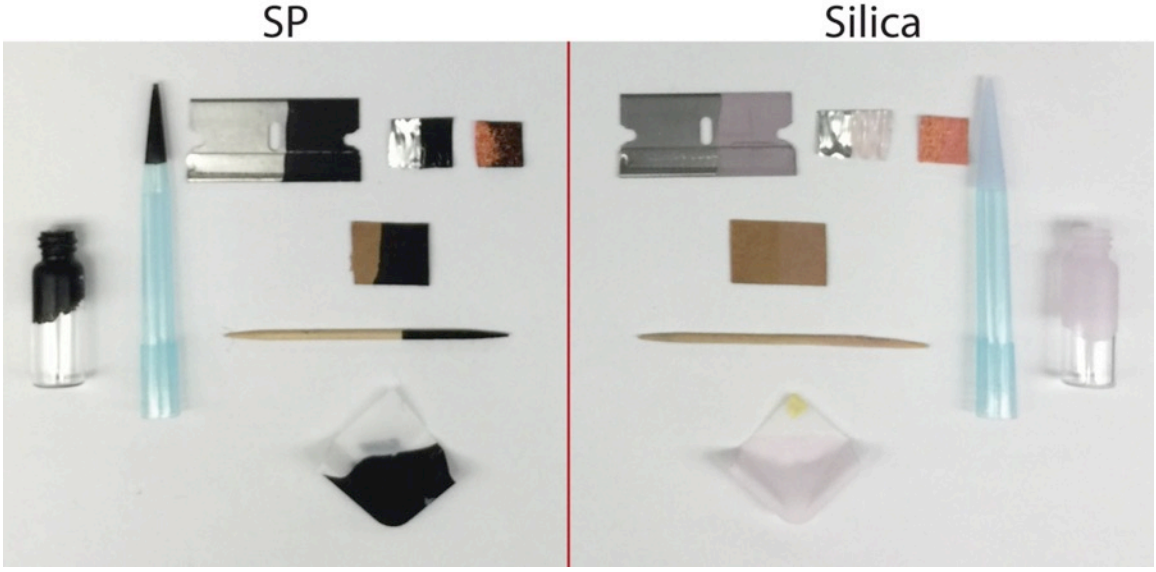

Supplementary Figure S7: Non-uniform substrate coating demonstration. Images of Super P carbon and fluorescent 1µm silica nanosphere coatings on razor blade, rough metallic strip, metallic foam, paper, wood toothpicks, curved plastic, tip of glass vials, and micropipette tips using LBS coating method are shown. Note that other materials can also be coated on these substrates.

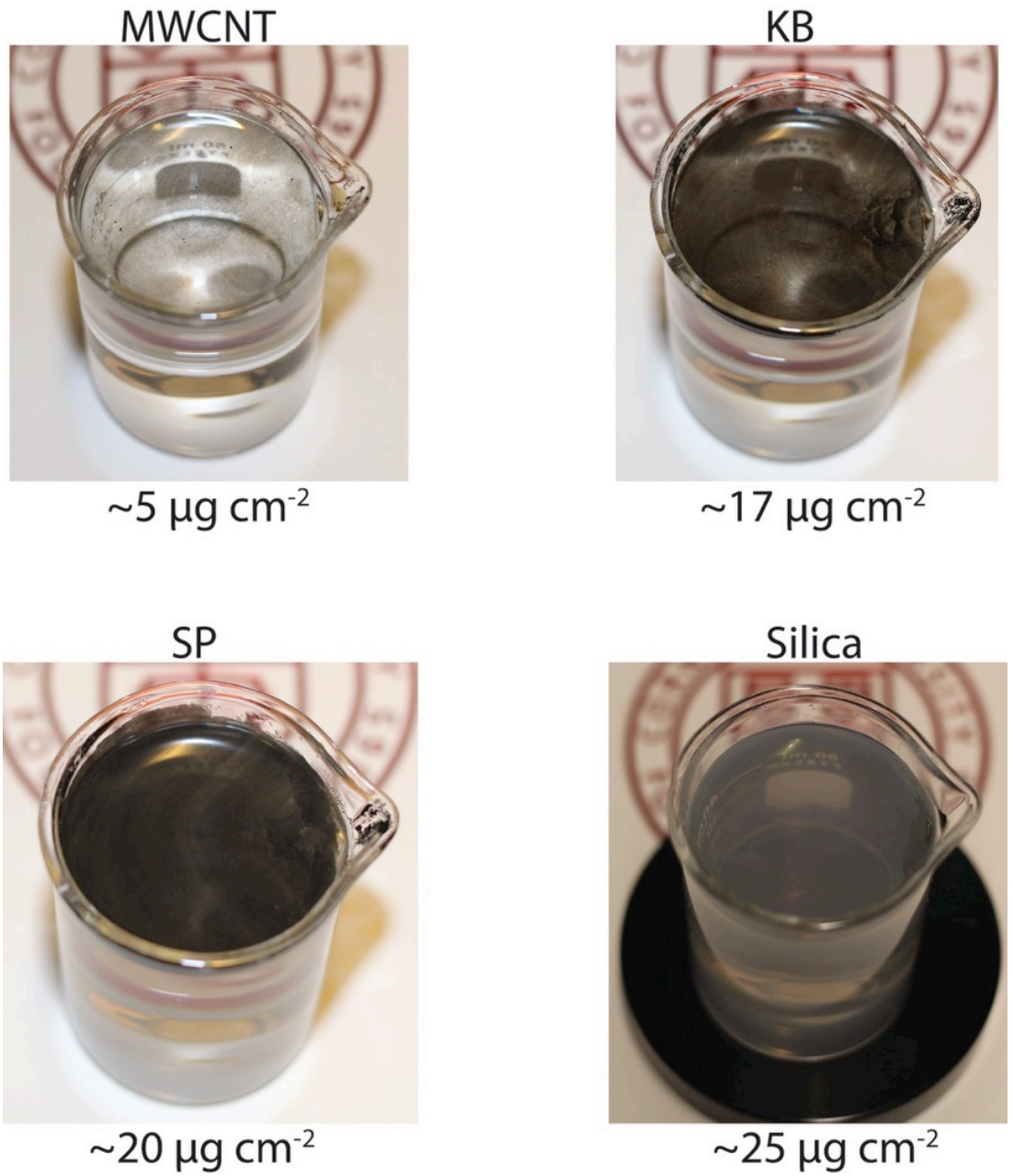

Supplementary Figure S8: Self-assembled Langmuir-Blodgett films. Single coating layer of multi-walled carbon nanotube (MWCNT), Ketjen Black carbon (KB), Super P carbon (SP), and silica nanosphere is shown with gravimetric areal density of the LB films.

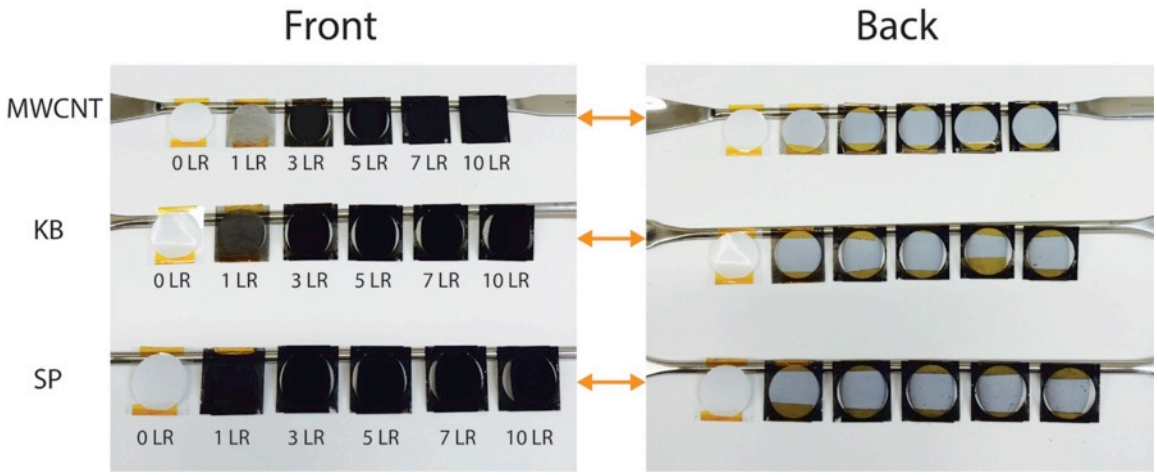

Supplementary Figure S9: Single-sided separator coating demonstration. Images of zero to ten coating layers of multi-walled carbon nanotube (MWCNT), Ketjen Black carbon (KB), and Super P carbon (SP) on the separator using LBS method are shown.

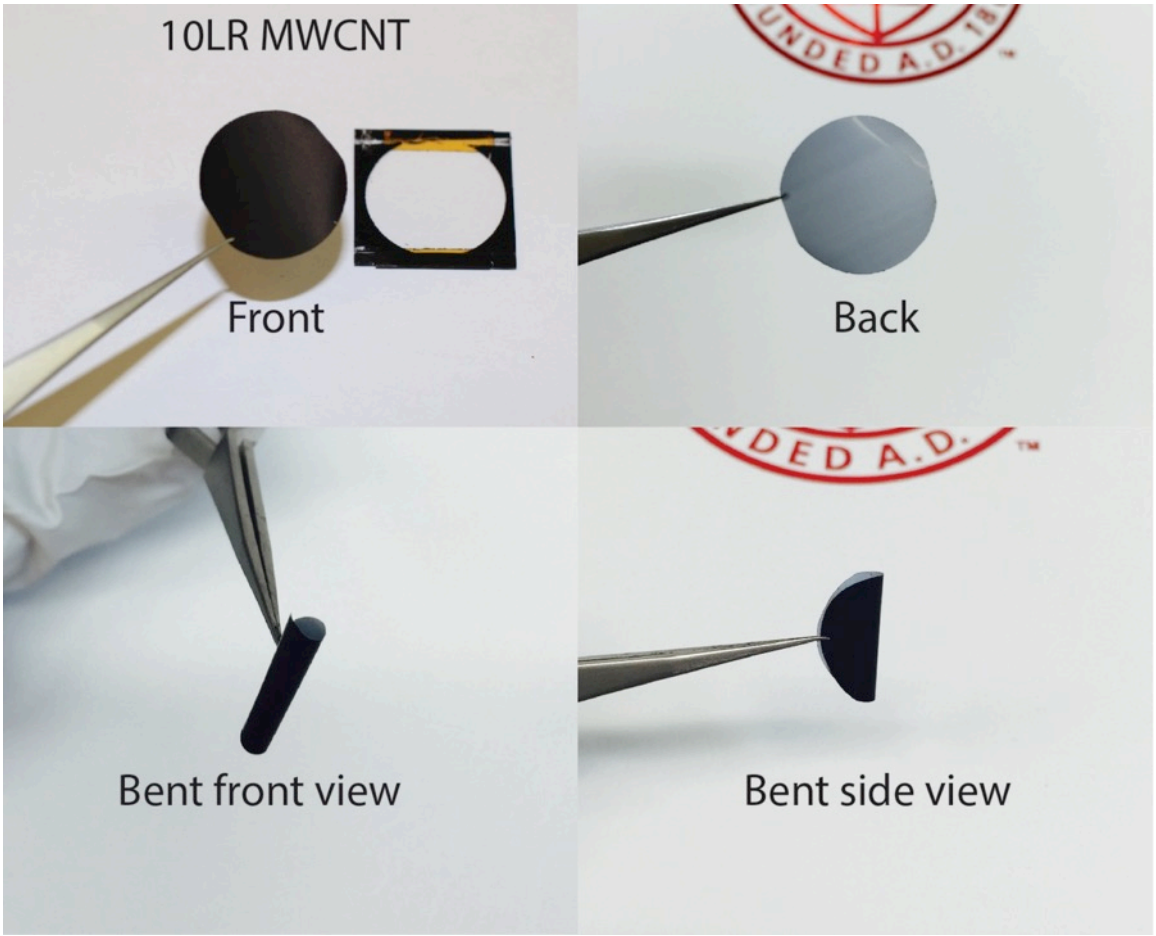

Supplementary Figure S10: MWCNT separator coating quality demonstration. Ten coating layers of MWCNT on the separator are shown.

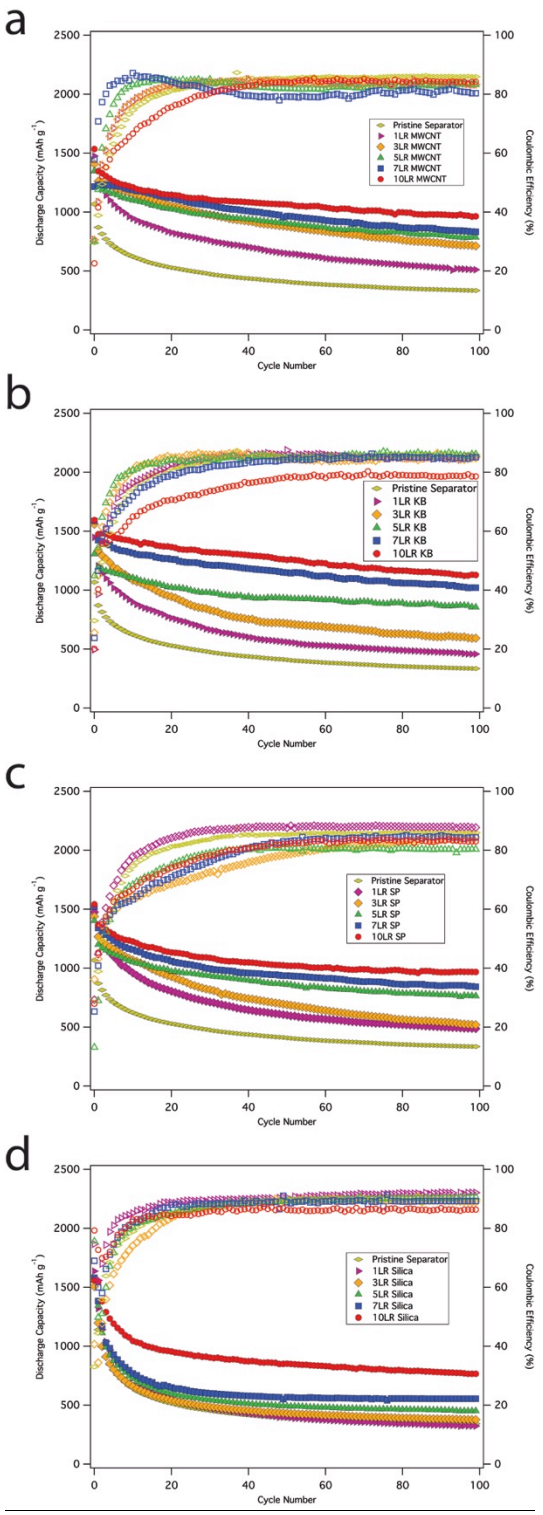

Supplementary Figure S11: Electrochemical performances of silica and carbon coated separators with ISC. Electrochemical performance of zero to ten coating layers of (a) MWCNT, (b) KB, (c) SP coated separators Li-S cells at 0.5 C. (d) Cycling performance of zero to ten monolayers of silica nanospheres coated separators Li-S cells at 0.2 C.

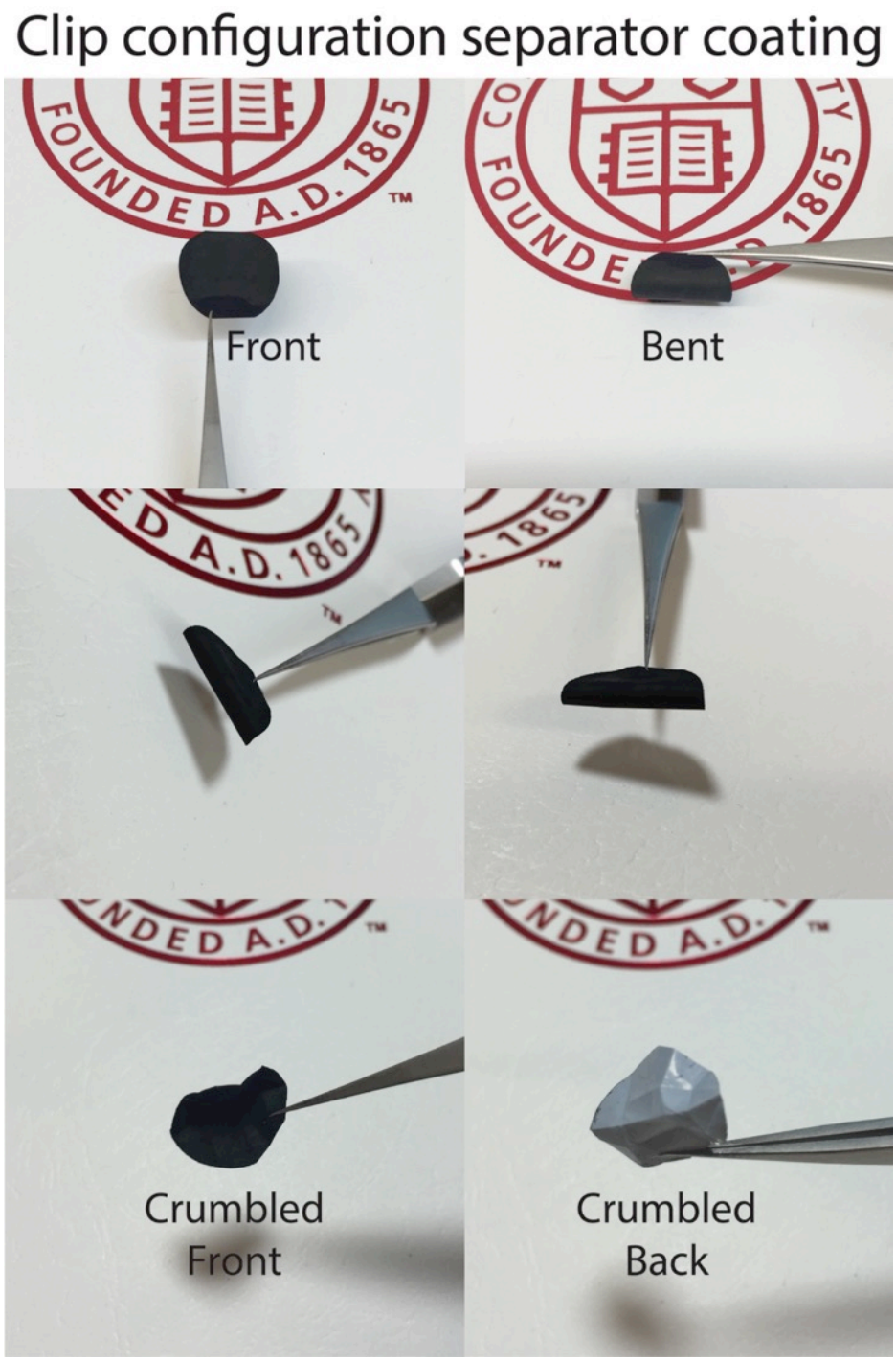

Supplementary Figure S12: Coating quality and mechanical strength demonstration of clip coated separator.

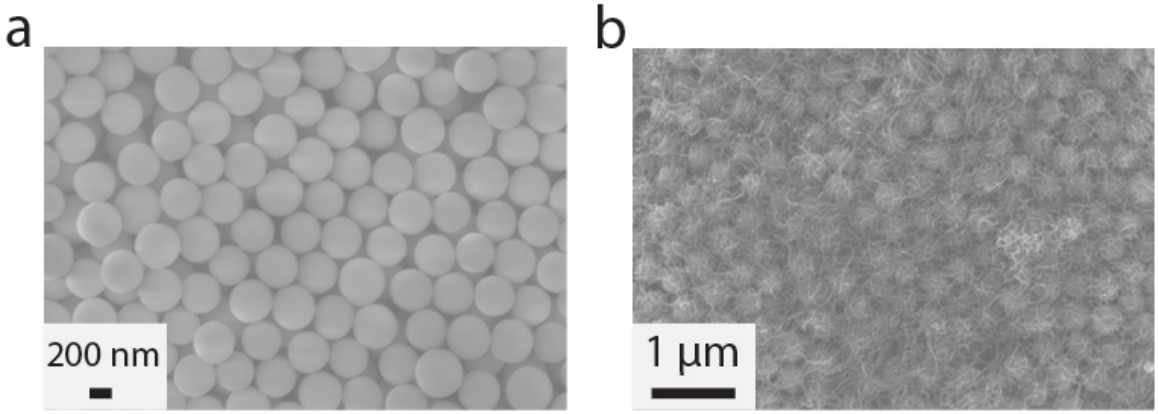

Supplementary Figure S13: Top-view SEM images of (a) three monolayers of silica nanospheres coated on top of SP-MWCNT coated separator and (b) the clip.

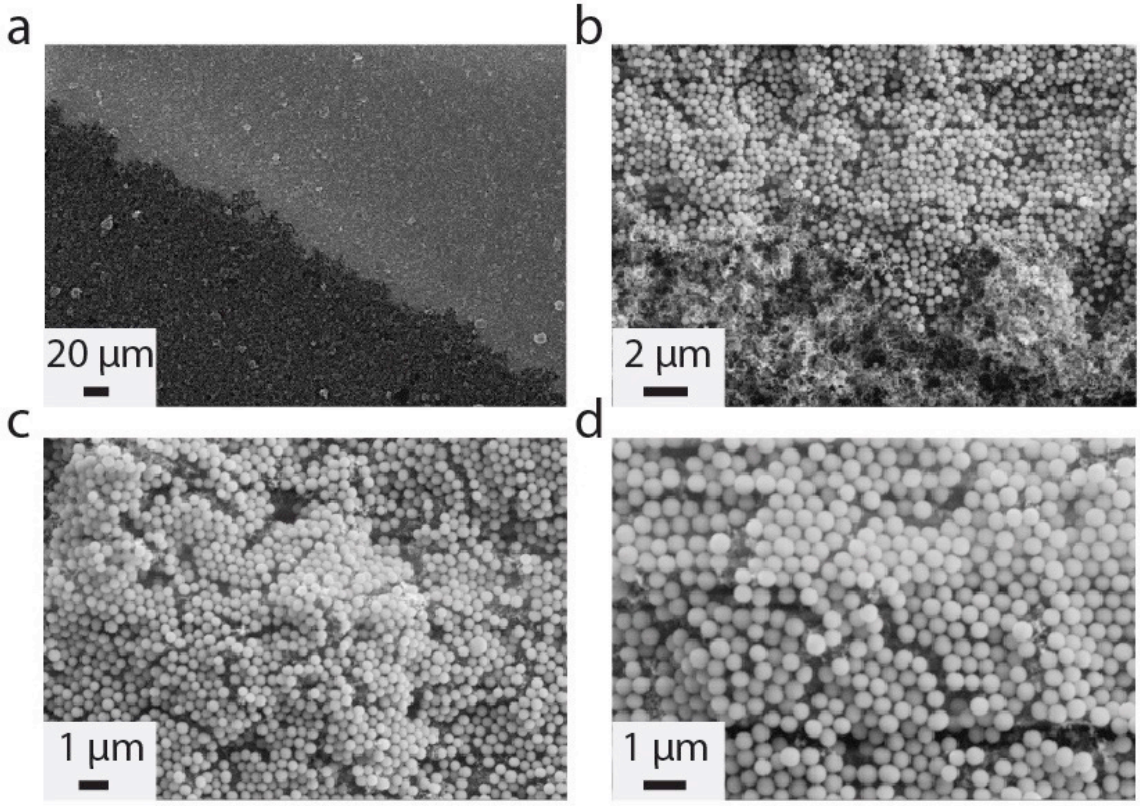

Supplementary Figure S14: SEM images of a monolayer of silica nanospheres coated on SP-MWCNT layer. Silica-SP layer boundary region (a) wide-view and (b) close-view. A monolayer of silica coating on top of the SP-MWCNT layer (c, d).

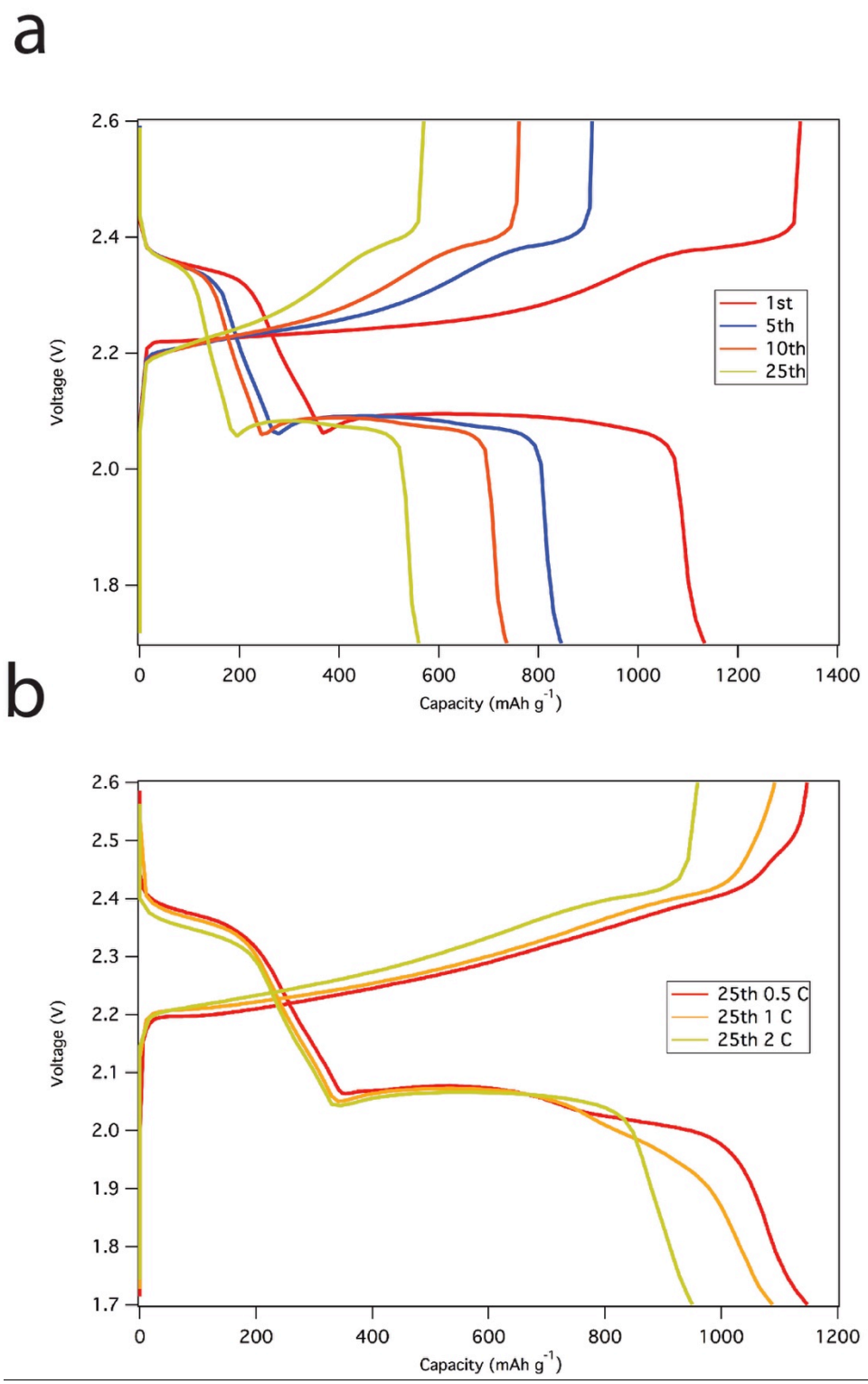

Supplementary Figure S15: Discharge-charge voltage profiles of clip coated separator Li-S cell with the pretreated Li anode and with ISC for (a) various cycles at 0.5C and (b) various C rates at 25th cycle.

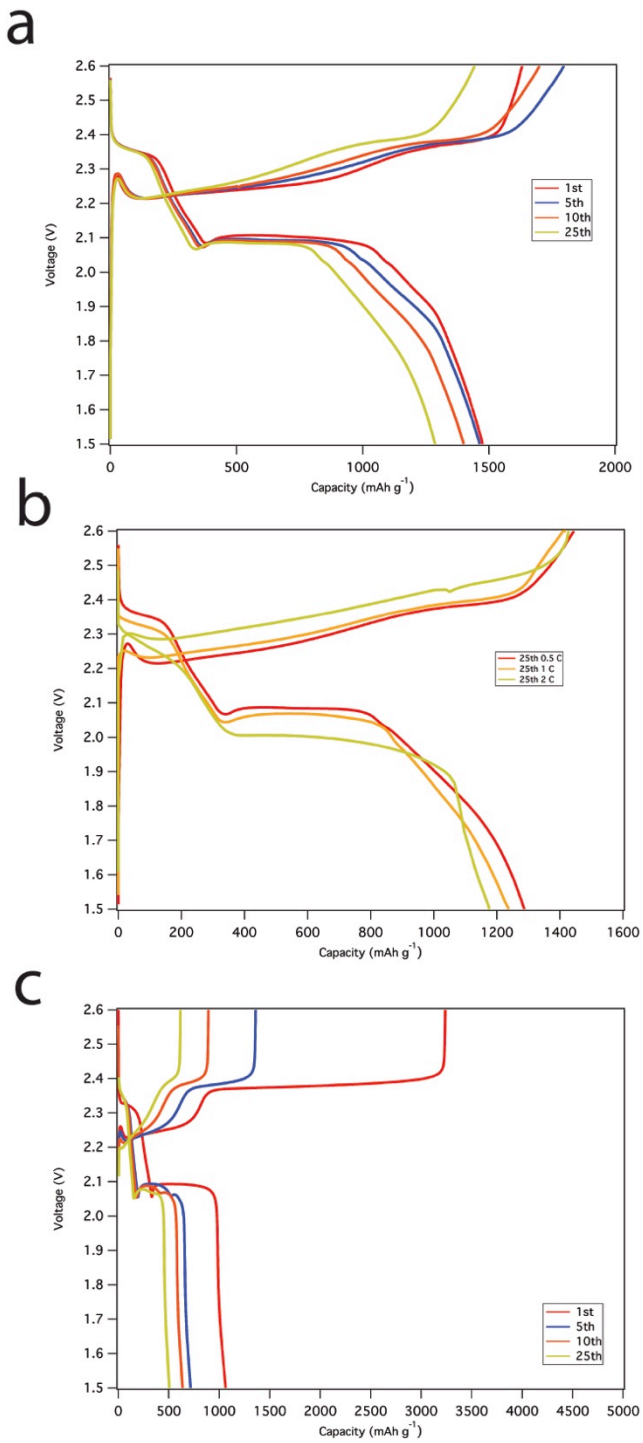

Supplementary Figure S16: Voltage profiles of Li-S cells with clip coated separator and ISC.(a) Discharge-charge voltage profiles of the pristine Li anode Li-S cell with the clip coated separator and ISC for various cycles at 0.5 C. (b) Discharge-charge voltage profiles of pristine Li anode Li-S cell with the clip coated separator and ISC at 25th cycle for various C rates. (c) Discharge-charge voltage profiles of pristine Li anode Li-S cell with the pristine separator and ISC at 0.5 C for various cycles.

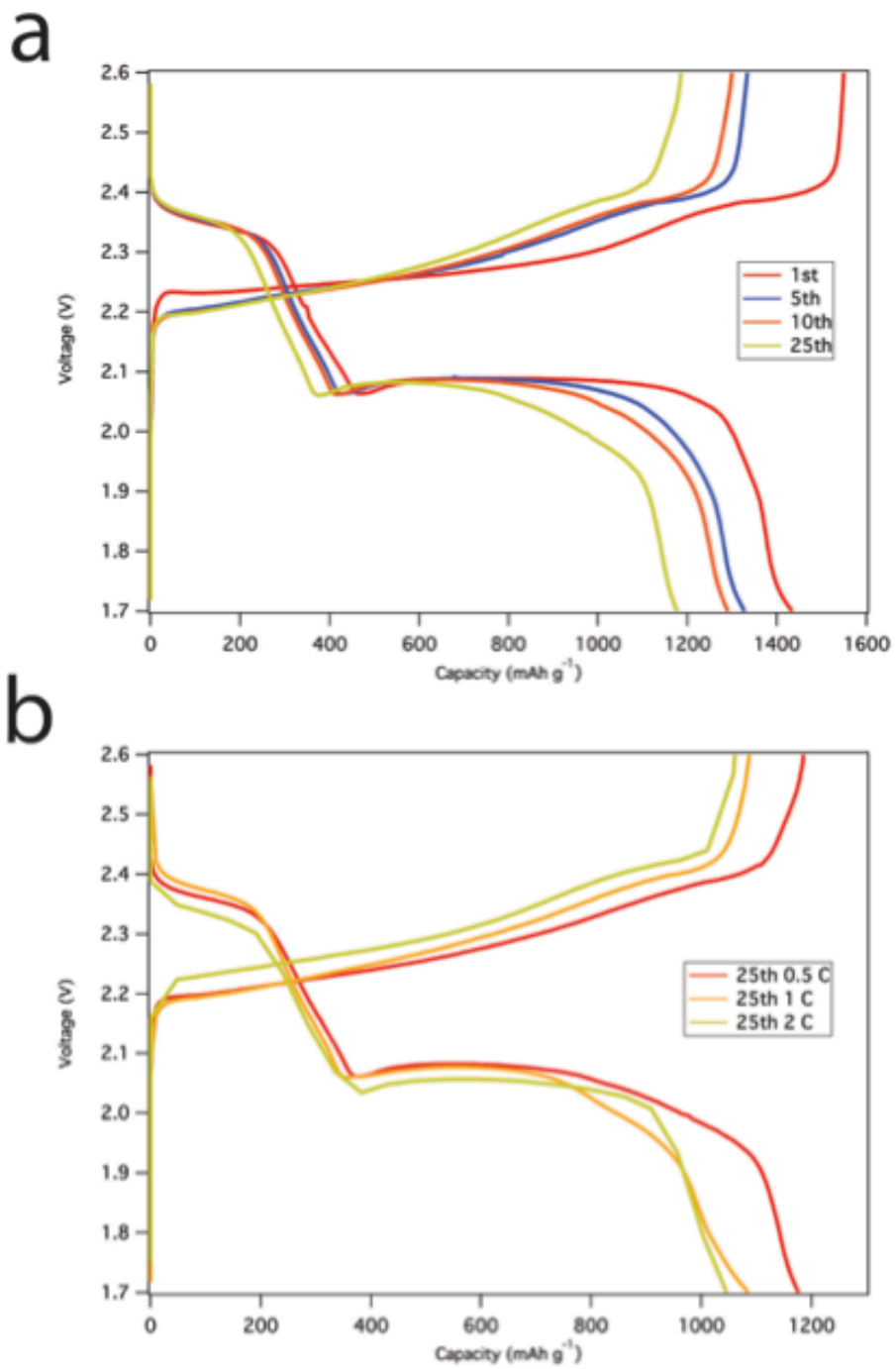

Supplementary Figure S17: Cycling performance and voltage profiles of Li-S cells with clip coated separator, ISC, and 0.05M $LiNO_3$ in the electrolyte. (a) Discharge-charge voltage profiles of clip coated separator Li-S cell with 0.05M $LiNO_3$ added in the electrolyte and with ISC for various cycles at 0.5 C. (b) Discharge-charge voltage profiles of the clip coated separator Li-S cell with 0.05M $LiNO_3$ in the electrolyte and with ISC at 25^{th} cycle at various C rates.

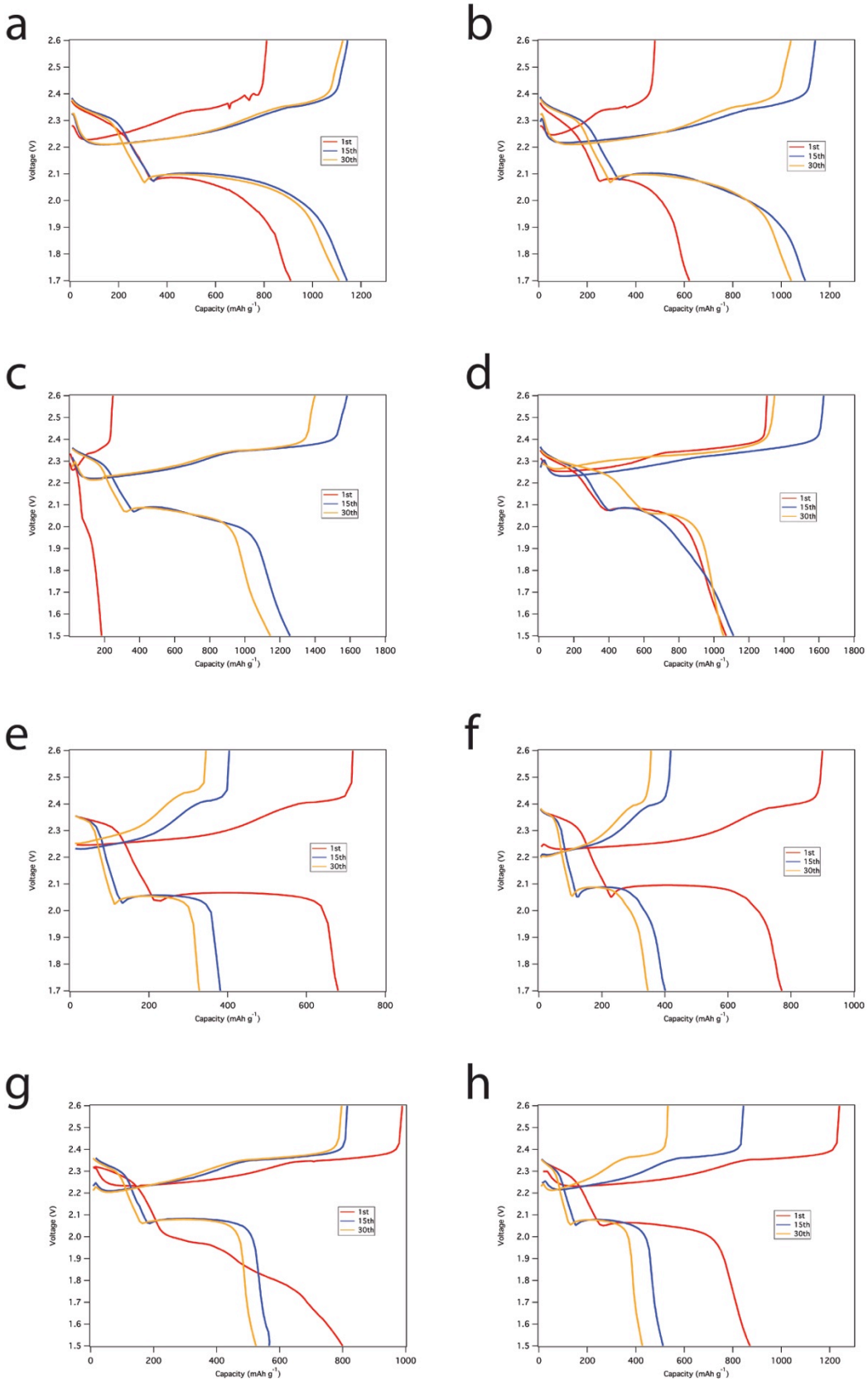
a
b
c
d
e
f
g
h
Voltage (V)
Capacity (mAh g-1)
1st
15th
30th

Supplementary Figure S18: Voltage profiles of Li-S cells with clip coated separator and VISC. (a) Discharge-charge voltage profiles of clip coated separator Li-S cell with VISC and 0.3M $LiNO_3$ added in the electrolyte for various cycles at 0.5 C. (b) Discharge-charge voltage profiles of clip coated separator Li-S cell with VISC and 0.3M $LiNO_3$ added in the electrolyte for various cycles at 0.2 C. (c) Discharge-charge voltage profiles of clip coated separator Li-S cell with VISC for various cycles at 0.5 C. (d) Discharge-charge voltage profiles of clip coated separator Li-S cell with VISC for various cycles at 0.2 C. (e) Discharge-charge voltage profiles of pristine separator Li-S cell with VISC and 0.3M $LiNO_3$ added in the electrolyte for various cycles at 0.5 C. (f) Discharge-charge voltage profiles of pristine separator Li-S cell with VISC and 0.3M $LiNO_3$ added in the electrolyte for various cycles at 0.2 C. (g) Discharge-charge voltage profiles of pristine separator Li-S cell with VISC for various cycles at 0.5 C. (f) Discharge-charge voltage profiles of pristine separator Li-S cell with VISC for various cycles at 0.2 C.

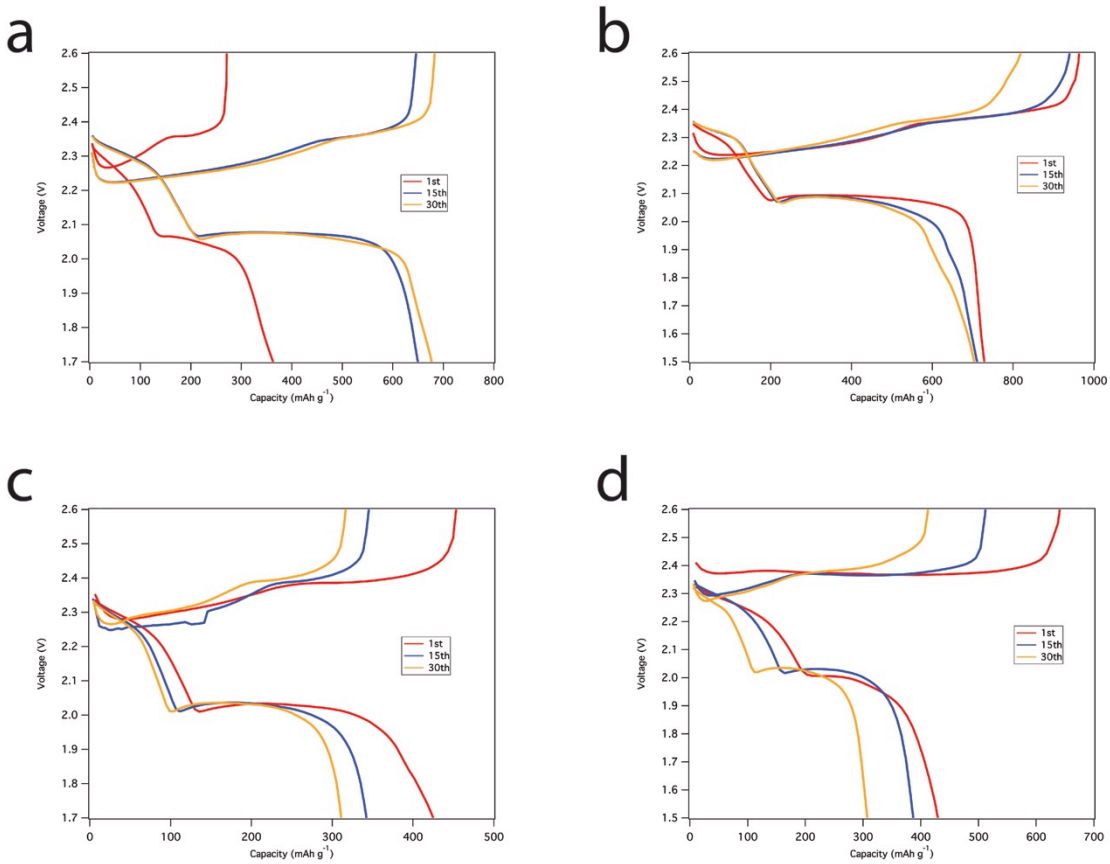

Supplementary Figure S19: Voltage profiles of Li-S cells with clip coated separator and BMSC. (a) Discharge-charge voltage profiles of clip coated separator Li-S cell with BMSC and 0.3M $LiNO_3$ added in the electrolyte for various cycles at 0.2 C. (b) Discharge-charge voltage profiles of clip coated separator Li-S cell with BMSC for various cycles at 0.2 C. (c) Discharge-charge voltage profiles of pristine separator Li-S cell with BMSC and 0.3M $LiNO_3$ added in the electrolyte for various cycles at 0.2 C. (d) Discharge-charge voltage profiles of pristine separator Li-S cell with BMSC for various cycles at 0.2 C.

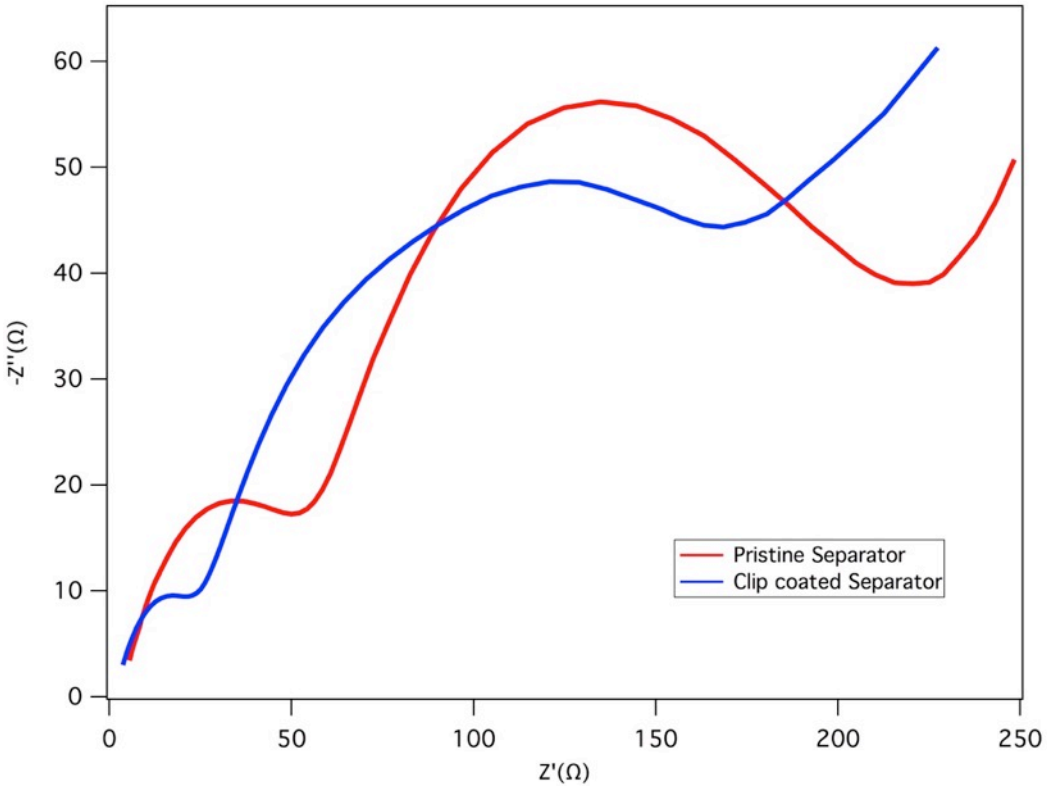

Supplementary Figure S20: AC impedance spectroscopy analysis of the clip coated separator and pristine separator Li-S cells with ISC.

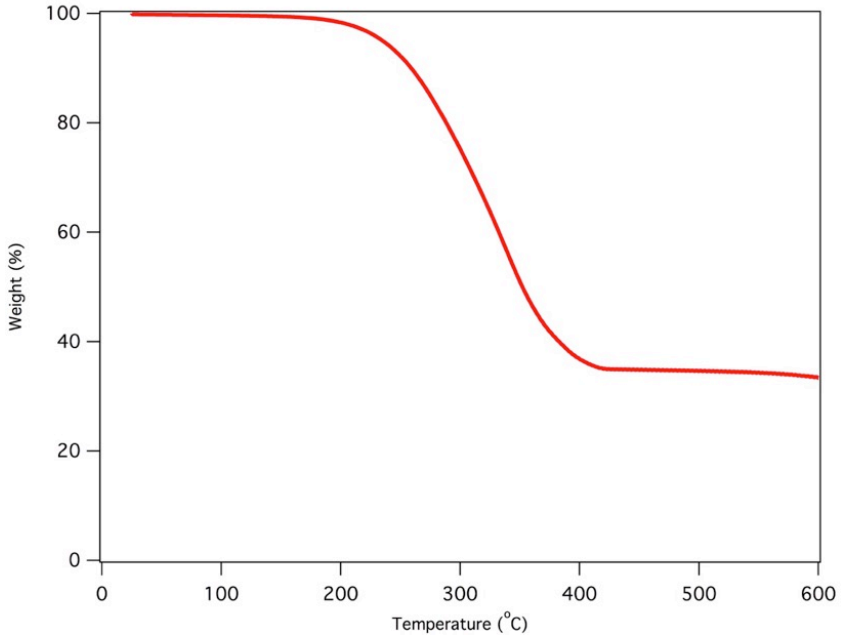

Supplementary Figure S21: Thermogravimetric analysis of sulfur infused in KB composite in a N_2 gaseous atmosphere with a heating rate of 10 ^{o}C min^{-1}, exhibiting 66 wt% sulfur content.

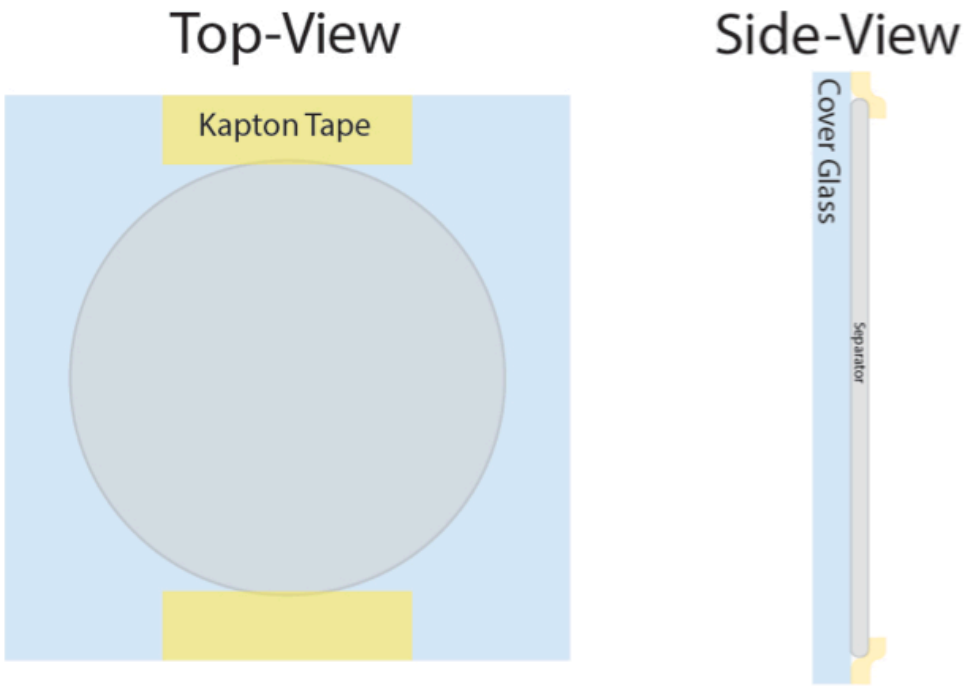

Supplementary Figure S22: Schematic illustration of as-prepared separator for the LBS and LBSDC coating.

REFERENCES

1. D. & Bucher, H. K. H. M. *Early days of molecular electronics*. **1 (3b),** (1972).

2. Delamarche, E. *et al.* Golden Interfaces: The Surface of Self- Assembled Monolayers. *Adv. Mater.* **8,** 719–729 (1996).

3. Meyer E., Howald L., Overney R.M., Heinzelmann H., Frommer J., Guntherodt H.-J., Wagner T., Schier H., R. S. Molecular-resolution images of Langmuir-Blodgett films using atomic force microscopy. *Nature* **349,** 398–400 (1991).

4. Gleiche, M., Chi, L. & Fuchs, H. Nanoscopic channel lattices with controlled anisotropic wetting. *Nature* **403,** 173–5 (2000).

5. Chen, X., Lenhert, S., Hirtz, M., Lu, N. a N. & Fuchs, H. Langmuir – Blodgett Patterning : A Bottom – Up Way To Build Mesostructures over Large Areas. *Acc. Chem. Res.* **40,** 393–401 (2007).

6. Li, X. *et al.* Highly conducting graphene sheets and Langmuir-Blodgett films. *Nat. Nanotechnol.* **3,** 538–542 (2008).

7. Cote, L. J., Kim, F. & Huang, J. Langmuir - Blodgett Assembly of Graphite Oxide Single Layers. *J. Am. Chem. Soc.* **131,** 1043–1049 (2009).

8. Huang, J., Kim, F., Tao, A. R., Connor, S. & Yang, P. Spontaneous formation of nanoparticle stripe patterns through dewetting. *Nat. Mater.* **4,** 896–900 (2005).

9. Paul, S. *et al.* Langmuir-Blodgett film deposition of metallic nanoparticles and their application to electronic memory structures. *Nano Lett.* **3,** 533–536 (2003).

10. Yang, P. Wires on water. *Nature* 243 (2003).

11. Kim, F., Kwan, S. & Akana, J. Langmuir - Blodgett Nanorod Assembly. *J. Am. Chem. Soc.* **123,** 4360–4361 (2001).

12. Murata, S., Kuriyama, N. & Kushida, M. Density control of aligned carbon nanotubes from controlled deposition of Fe catalyst nanoparticles using the filler-added Langmuir–Blodgett technique. *Thin Solid Films* **589,** 115–119 (2015).

13. Nie, H.-L., Dou, X., Tang, Z., Jang, H. D. & Huang, J. High-Yield Spreading of Water-Miscible Solvents on Water for Langmuir–Blodgett Assembly. *J. Am. Chem. Soc.* **137,** 10683–10688 (2015).

14. Huang, J., Tao, A. R., Connor, S., He, R. & Yang, P. A general method for assembling single colloidal particle lines. *Nano Lett.* **6,** 524–529 (2006).

15. Lu, Y. *et al.* Self-assembly of mesoscopically ordered chromatic polydiacetylene/silica nanocomposites. *Nature* **410,** 913–917 (2001).

16. Cao, Q. *et al.* Arrays of single-walled carbon nanotubes with full surface coverage for high-performance electronics. *Nat. Nanotechnol.* **8,** 180–186 (2013).

17. Ji, X., Lee, K. T. & Nazar, L. F. A highly ordered nanostructured carbon-sulphur cathode for lithium-sulphur batteries. *Nat. Mater.* **8,** 500–506 (2009).

18. Ma, L., Hendrickson, K. E., Wei, S. & Archer, L. A. Nanomaterials: Science and applications in the lithium–sulfur battery. *Nano Today* **10,** 315–338 (2015).

19. Manthiram, A., Fu, Y., Chung, S., Zu, C. & Su, Y. Rechargeable Lithium − Sulfur Batteries. *Chem. Rev.* **114,** 11751–11787 (2014).

20. Barchasz, C. *et al.* Lithium/sulfur cell discharge mechanism: An original approach for intermediate species identification. *Anal. Chem.* **84,** 3973–3980 (2012).

21. Jayaprakash, N., Shen, J., Moganty, S. S., Corona, A. & Archer, L. A. Porous hollow carbon@sulfur composites for high-power lithium-sulfur batteries. *Angew. Chemie* **50,** 5904–5908 (2011).

22. Cheng, X. B. *et al.* Aligned carbon nanotube/sulfur composite cathodes with high sulfur content for lithium-sulfur batteries. *Nano Energy* **4,** 65–72 (2014).

23. Wang, H. *et al.* Graphene-Wrapped Sulfur Particles as a Rechargeable Lithium – Sulfur Battery Cathode Material with High Capacity and Cycling Stability. *Nano Lett.* **11,** 2644–2647 (2011).

24. Zhou, W. *et al.* Amylopectin Wrapped Graphene Oxide / Sulfur for Improved Cyclability of Lithium - Sulfur Battery. *ACS Nano* **7,** 8801–8808 (2013).

25. Ma, L. *et al.* Tethered Molecular Sorbents: Enabling Metal-Sulfur Battery Cathodes. *Adv. Energy Mater.* **4,** 390–399 (2014).

26. Ma, L. *et al.* Enhanced Li–S Batteries Using Amine-Functionalized Carbon Nanotubes in the Cathode. *ACS Nano* **10,** 1050–1059 (2015).

27. Ma, L. *et al.* Hybrid cathode architectures for lithium batteries based on TiS 2 and sulfur. *J. Mater. Chem. A* **3,** 19857–19866 (2015).

28. Evers, S., Yim, T. & Nazar, L. F. Understanding the nature of absorption/adsorption in nanoporous polysulfide sorbents for the Li-S battery. *J. Phys. Chem. C* **116,** 19653–19658 (2012).

29. Ji, X., Evers, S., Black, R. & Nazar, L. F. Stabilizing lithium-sulphur cathodes using polysulphide reservoirs. *Nat. Commun.* **2,** 325 (2011).

30. Hendrickson, K. E., Ma, L., Cohn, G., Lu, Y. & Archer, L. A. Model Membrane-Free Li-S Batteries for Enhanced Performance and Cycle Life. *Adv. Sci.* **2,** 68–77 (2015).

31. Balach, J. *et al.* Functional Mesoporous Carbon-Coated Separator for Long-Life, High-Energy Lithium-Sulfur Batteries. *Adv. Funct. Mater.* **25,** 5285–5291 (2015).

32. Chung, S.-H., Han, P., Singhal, R., Kalra, V. & Manthiram, A. Electrochemically Stable Rechargeable Lithium-Sulfur Batteries with a Microporous Carbon Nanofiber Filter for Polysulfide. *Adv. Energy Mater.* (2015). doi:10.1002/aenm.201500738

33. Chung, S.-H. & Manthiram, A. Bifunctional Separator with a Light-Weight Carbon-Coating for Dynamically and Statically Stable Lithium-Sulfur Batteries. *Adv. Funct. Mater.* **24,** 5299–5306 (2014).

34. Chung, S. & Manthiram, A. High-Performance Li − S Batteries with an Ultra-lightweight MWCNT- Coated Separator. *Phys. Chem. Lett.* **5,** 1987–1983 (2014).

35. Wang, G., Lai, Y., Zhang, Z., Li, J. & Zhang, Z. Enhanced rate capability and cycle stability of lithium–sulfur batteries with a bifunctional MCNT@PEG-modified separator. *J. Mater. Chem. A* **3,** 7139–7144 (2015).

36. Zhang, Z., Lai, Y., Zhang, Z. & Li, J. A functional carbon layer-coated separator for high performance lithium sulfur batteries. *Solid State Ionics* **278,** 166–171 (2015).

37. Yao, H. Bin *et al.* Improved lithium-sulfur batteries with a conductive coating on the separator to prevent the accumulation of inactive S-related species at the cathode-separator interface. *Energy Environ. Sci.* **7,** 3381 (2014).

38. Wei, H., Li, B., Zuo, Y. & Xia, D. Enhanced Cycle Performance of Lithium-Sulfur Battereis Using a Separator Modified with a PVDF-C Layer. *ACS Appl. Mater. Interfaces* **6,** 20276–20281 (2014).

39. Li, F. *et al.* A graphene-pure-sulfur sandwich structure for ultrafast, long-life lithium-sulfur batteries. *Adv. Mater.* **26,** 625–631 (2014).

40. Zhang, Y. *et al.* A graphene-oxide-based thin coating on the separator: an efficient barrier towards high-stable lithium–sulfur batteries. *2D Mater.* **2,** 024013 (2015).

41. Fang, R., Zhou, G., Pei, S., Li, F. & Cheng, H.-M. Localized polyselenides in a graphene-coated polymer separator for high rate and ultralong life lithium–selenium batteries. *Chem. Commun.* **51,** 3667–3670 (2015).

42. Lin, W. *et al.* Enhanced Performance of Lithium Sulfur Battery with a Reduced Graphene Oxide Coating Separator. *J. Electrochem. Soc.* **162,** 1624–1629 (2015).

43. Xiao, Z. *et al.* A Lightweight TiO2/Graphene Interlayer, Applied as a Highly Effective Polysulfide Absorbent for Fast, Long-Life Lithium-Sulfur Batteries. *Adv. Mater.* **27,** 2891–2898 (2015).

44. Xu, Q., Hu, G. C., Bi, H. L. & Xiang, H. F. A trilayer carbon nanotube/Al2O3/polypropylene separator for lithium-sulfur batteries. *Ionics (Kiel).* **21,** 981–986 (2014).

45. Chen, Y. *et al.* Chitosan as a functional additive for high-performance lithium–

sulfur batteries. *J. Mater. Chem. A* **3,** 15235–15240 (2015).

46. Zhang, Z., Zhang, Z., Li, J. & Lai, Y. Polydopamine-coated separator for high-performance lithium-sulfur batteries. *J. Solid State Electrochem.* **19,** 1709–1715 (2015).

47. Huang, J.-Q. *et al.* Ionic shield for polysulfides towards highly-stable lithium–sulfur batteries. *Energy Environ. Sci.* **7,** 347 (2014).

48. Zhang, Z., Lai, Y., Zhang, Z., Zhang, K. & Li, J. Al2O3-coated porous separator for enhanced electrochemical performance of lithium sulfur batteries. *Electrochim. Acta* **129,** 55–61 (2014).

49. Rossi, L. M., Shi, L., Quina, F. H. & Rosenzweig, Z. Stober synthesis of monodispersed luminescent silica nanoparticles for bioanalytical assays. *Langmuir* **21,** 4277–4280 (2005).

CHAPTER 4

MULTIFUNCTIONAL AND CONFIGURATIONAL STRUCTURE SEPARATOR COATINGS FOR HIGH PERFORMANCE LITHIUM SULFUR BATTERIES

4.1 Introduction

Electrochemical energy storage systems that are cost-effective, safe, environmentally-friendly and possess long cycle/shelf-life are needed in multiple fields of technology, including transportation, portable devices, robotics, and power generation from intermittent sources. Currently, Li-ion (150 Wh kg^{-1}) and Li-ion-polymer (180 Wh kg^{-1}) batteries[1] are the most promising storage platforms for many applications. It is understood however that the intercalation-based cathodes used in these technologies provide limited opportunities for the sort of advancement in specific energy required to keep pace with growing demand.[2–4] Replacing cathodes with conversion materials such as sulfur, oxygen, or carbon-dioxide, removes these limitations, but introduce new challenges associated with dissolution, transport, and parasitic reactions between battery anodes and redox products in cathodes.[2,5] Lithium-sulfur (Li-S) battery is the most studied and arguably the most promising candidate for commercial use for at least three reasons: i) The Li-S battery offers tenfold higher energy storage capacity (Specific capacity 1675 mAh g^{-1} and Theoretical energy density 2600 Wh kg^{-1}) than any of the commercial Li-ion batteries; ii) sulfur is earth abundant and inexpensive (\$0.02 g $sulfur^{-1}$), leading to low cost high-energy batteries;[6,7] iii) sulfur is environmentally benign, reacts spontaneously and reversibly with lithium.[5,8,9] Despite these benefit, Li-S cells suffer from poor cycling efficiency and short lifetimes stemming from the complex solution chemistry of lithium sulfide and lithium polysulfide (LiPS) products from the cathode.[10–13] The most successful efforts have been devoted to cathode configurations/materials to provide physical confinement[11,14,15] and chemical adsorption[16–18] for LiPS to prevent its

dissolution and uncontrolled redox reaction with lithium metal.

Membranes able to regulate diffusion of cathode products, without compromising ion transport between anode and cathode provide a means for controlling LiPS loss from the cathode and for preventing shuttling in the Li-S cells.[19–31] For instance, carbon and ceramic coatings on the porous separator using slurry/tape casting methods have been argued to provide a mechanism for blocking passage of LiPS to the anode, while providing a mechanism for electrochemical utilization and adsorption of the LiPS during the cycle.[20–29] A persistent challenge has been how to implement these changes in the basic Li-S cell design in such a manner to not add significantly to the mass of coating materials in the cell.

This article reports on the fabrication of membranes by coating inorganic particles, polymers, and carbon on polyolefin separators. Specifically, a binder-free coating method, termed Langmuir-Blodgett-Scooping (LBS), is used to rapidly create multifunctional coatings on commercial Celgard separators with single-particle thickness resolution, using polyaniline (PANI), titania nanoparticles (titania NP), and multi-walled carbon nanotube (MWCNT). PANI is an electron conducting polymer that contains amine/imine groups able to interact strongly and specifically with LiPS via electrostatic interactions. Membranes based on this material are therefore able to bind to and thereby hinder transport of LiPS between the cathode and anode of Li-S cells, and at the same time allow the adsorbed LiPS to remain electrochemically accessible during cycling.[32] PANI was previously used in Li-S cathodes to encapsulate sulfur in yolk-shell[33], nanotubes[32],

nanorods[34] structures, and coat thin layer of PANI on S/C composites.[35] In this work, PANI is applied directly to the separator without any additional treatment and under ambient conditions.

4.2 Results and Discussion

There are a variety of coating methods suitable for materials of specific geometries with most methods requiring use of a binder material for cohesion. The coating method developed in the present work takes advantage of Marangoni stresses and self-assembly at the air/water interface to create highly organized monoparticle layers on non-reactive substrates. Application of thes approaches for fabricating titania NPs, PANI, and MWCNT in layer-by-layer, laminated format provides strategies for creating membranes with low material content and in a porous 3D network morphology able to suppress loss of LiPS, while simultaneously maintaining electrochemical access to the material.[36] The laminated PANI structure used in the study is comprised of 80nm thick MWCNT adhesion layer for PANI, followed by ~6μm thick PANI, ~1μm thick titania NP, and ~3μm thick PANI (overall thickness of ~10μm) with total material loading of ~400μg cm^{-2}. When used in Li-S batteries with low and high material loadings, we show that the prepared membranes lead to high reversible capacities (1220 mAh g^{-1}, 1150 mAh g^{-1}, and 1000 mAh g^{-1} at 0.5C, 1C, and 2C, respectively), with stable and high Columbic efficiencies (~97% at the 100^{th} cycle), without the need for common $LiNO_3$ additives in the electrolyte.

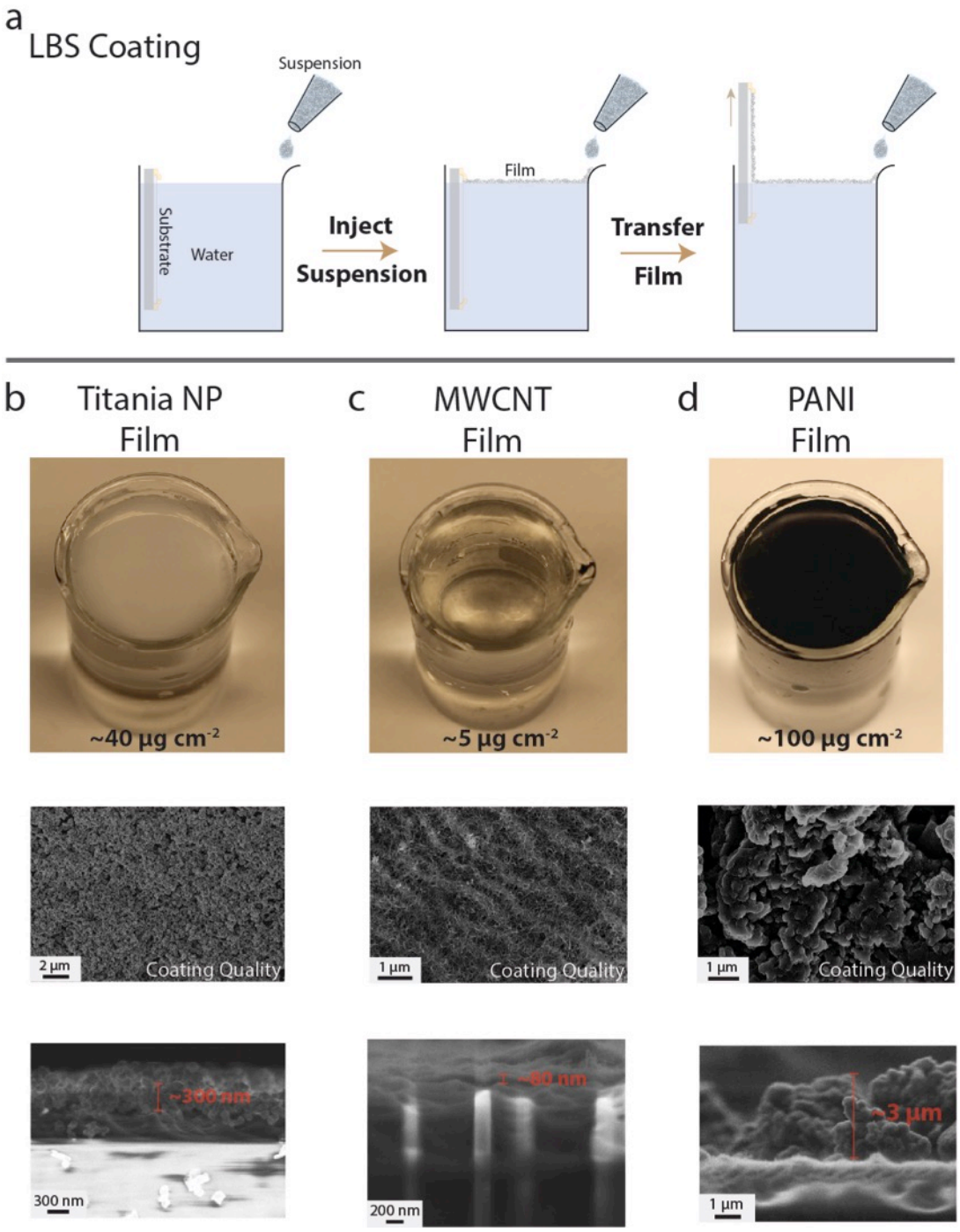

Figure 4.1. (a) Schematic illustration of LBS coating process. Physical images of self-assembled films at the surface of water with the gravimetrical density of (b) Titania NP, (c) MWCNT, (d) PANI, and their coating quality SEM images on Celgard separators as well as LBS coating film thicknesses per material coating layer are shown.

Figure 4.1a illustrates the LBS method. The approach utilizes self-assembly of particles to form a well-packed film (Supplementary Videos). The self-assembly is induced by spreading and mixing of water miscible solvent at the surface of water[37] and surface tension gradients.[38] Briefly, a volatile and water miscible solvent is injected at the air-water interface, induces strong flows at the surface that drive the spreading of the solvent by the combined effect of surface tension gradient from the two different fluids, known as Marangoni effect.[39] The spreading pressure leads to rapid and highly ordered assembly of structures present at the air-water interface, which can be transferred to any non-reactive substrates by immersion and removal of the substrate from the liquid. Because of its speed (<10 sec), the method can be applied repeatedly to create multilayer ordered coatings of a variety of materials in layer-by-layer format. For the coating process, only ethanol with nanopowders and water are required. Figure 4.1b shows a self-assembled film of titania nanoparticles (NPs) with gravimetrical density of 40 μg cm^{-2} and thickness of approximately 300 nm created using the approach. Figure 4.1c and 1d illustrate analogous results for coating of MWCNT and PANI with gravimetrical density and thickness of ~5 μg cm^{-2}, ~100 μg cm^{-2} and ~80 nm and ~3 μm, respectively. In all cases, it is apparent that the obtained coatings are of high quality.

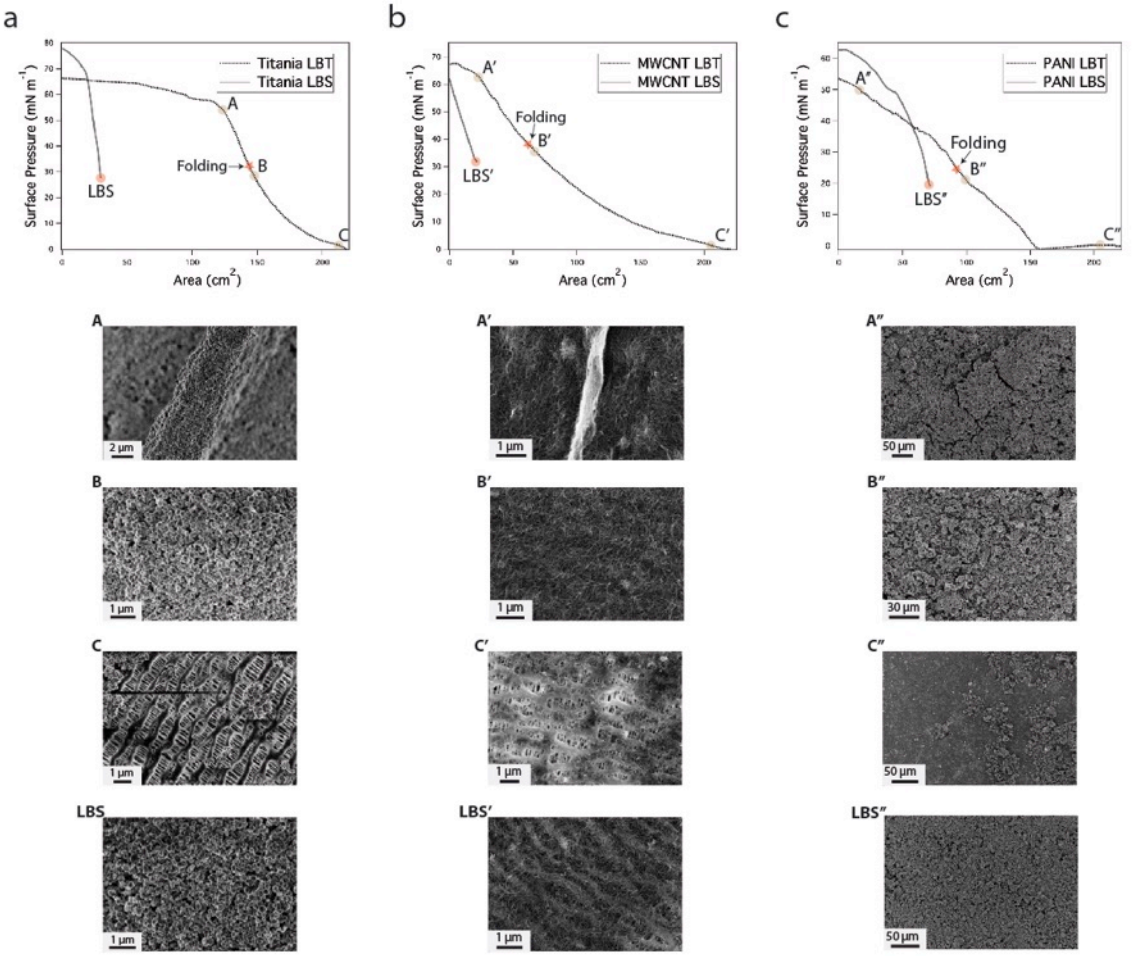

Figure 4.2. (a) Titania NP, (b) MWCNT, (c) PANI surface pressure profiles of conventional LBT and LBS coating methods with the coating quality SEM at designated surface pressures. Titania NP: A=54 mN m^{-1}, B=28 mN m^{-1}, C=1 mN m^{-1}, LBS=28 mN m^{-1}, Folding=31 mN m^{-1}. MWCNT: A'=63 mN m^{-1}, B'=35 mN m^{-1}, C'=2 mN m^{-1}, LBS'=32 mN m^{-1}, Folding=37 mN m^{-1}. PANI: A''=50 mN m^{-1}, B''=21 mN m^{-1}, C''=3 mN m^{-1}, LBS''=20 mN m^{-1}, Folding=24 mN m^{-1}.

To understand the fundamental processes responsible for self-assembled titania NP, MWCNT, and PANI films, surface pressure profiles of the three materials were measured using a conventional Langmuir-Blodgett trough (LBT) as shown in Figure 4.2. To facilitate comparisons, profiles obtained using LBS and LBT are compared, and three surface pressures are chosen for each material coincident with the overly packed, fully packed, and poorly packed states. The full spectrum of surface film packing densities are

apparent from the LBT profiles, including a regime of film buckling and folding at high surface pressures (See Figure S1). The onset of folding behavior is evident as an inflection point where the concavity of the profile curve changes, which provide a convenient means of assessing achievement of fully packed high quality films.

Figure 4.2a shows the surface pressure profiles of titania NP using LBT and LBS methods. Three surface pressures are chosen (A=54 mN m^{-1}, B=28 mN m^{-1}, C=1 mN m^{-1}) to observe the titania NP coatings on the separator. A, B, and C represents the surface pressures where the nanoparticles are overly packed, fully packed, and poorly packed, respectively. Analysis of the SEM images for titania NP coated separators, highest coating quality is made at point B. This means that around surface pressure of 28 mN m^{-1}, which is around the inflection point at 31 mN m^{-1}, will yield highly packed particle film on the water surface. The information is then used to verify the coating quality of LBS method. For the self-assembled films using LBS method, we have measured the surface pressure profiles of the resulting films. In Figure 4.2a, LBS surface pressure profile starts at a surface pressure of 28 mN m^{-1}, and no inflection point is observed. The starting surface pressure indicates that the self-assembly process exerts the pressure of 28 mN m^{-1}, and absence of the inflection point in the LBS profile verifies that the LBS method starts at highly-packed state. Hence, the uniform titania NP coating on the separator is made as shown in Figure 4.2a SEM at LBS that matches well with the coating at point B. Analogous measurements for MWCNT (Figure 4.2b) and PANI (Figure 4.2c) were used to assess the state of order in these films. The surface pressures of A'=63 mN m^{-1}, B'=35 mN m^{-1}, C'=2 mN m^{-1} for MWCNT and A''=50 mN m^{-1}, B''=21 mN m^{-1}, C''=3 mN m^{-1}

for PANI are chosen to investigate the film qualities. Highest coating qualities are obtained for B' and B'' for MWCNT and PANI. The folding point for MWCNT and PANI are 37 mN m^{-1} and 24 mN m^{-1}, and around these surface pressures yield optimized coating films. As results, LBS coating of MWCNT and PANI at LBS' (32 mN m^{-1}) and LBS'' (20 mN m^{-1}) yield high qualities as we see in Figure 4.2b and Figure 4.2c.

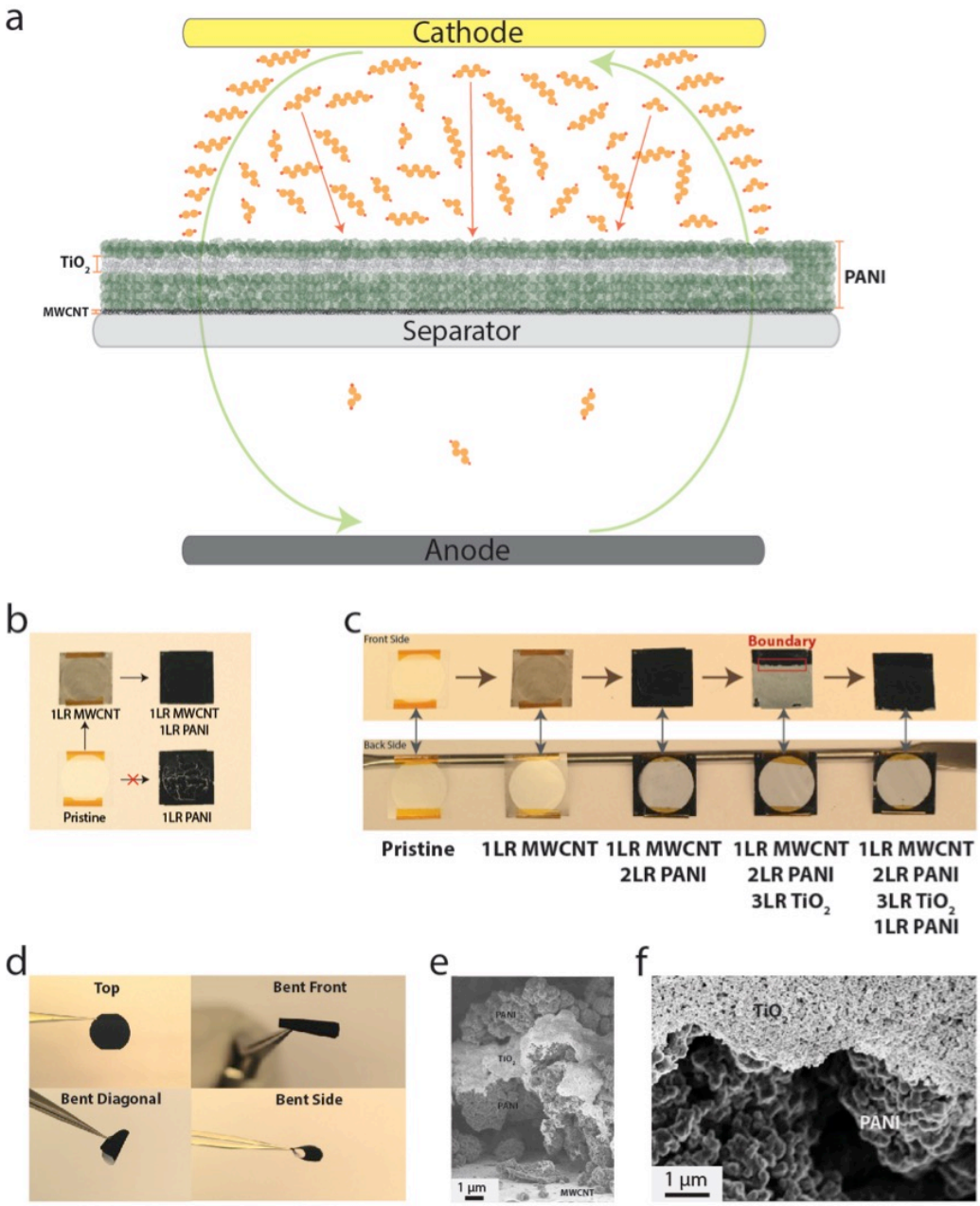

Figure 4.3. (a) Schematic illustration of laminated configured separator coating structure (laminated PANI) and LiPS flux diagram during the charge/discharge of the Li-S cell. (b) Demonstration of thin layer of MWCNT as an effective adhesion layer for PANI coating. (c) Demonstration of single-sided LBS coatings and the layer-by-layer coating process to fabricate the laminated PANI separator. (d) Mechanical strength demonstration of the laminated PANI separator. (e) Cross sectional SEM image of the laminated PANI separator. (f) SEM image of the titania NP-PANI boundary (3 coating layers of titania NP on top of PANI coatings, see the red box in Figure 4.3c)

Building upon these fundamental studies, we employed the LBS method to create membranes in which the titania NP layers are sandwiched by PANI layers (See Figure 4.3a) adhered to Celgard by thin MWCNT layer. As discussed earlier, this design was motivated by the hypothesis that a flexible membrane in a clip-like configuration in which two electronically conductive layers bracket sorbent NP layer would facilitate efficient trapping of LiPS in the membrane and utilization of the trapped LiPS by the conductive layers for high active material utilization. Figure 4.3c shows the layer-by-layer configuration of the coatings. As illustrated in Figure 4.3d and Figure S2 the membranes are mechanically strong and their structure is completely preserved after mechanical distortion. Figure 4.3e shows the cross sectional image of laminated PANI structure which is ~10μm thick. To observe the boundary region that is indicated with the red box in Figure 4.3c, we imaged this region using SEM. It is apparent that a very compact and porous 3D titania NP network is present on the top of PANI coatings.

To investigate the effectiveness of the resultant membranes in regulating LiPS transport and utilization in Li-S cells, membranes based on the individual components with 1 to 5 layers (~3μm to ~15μm thick) were studied as separators in Li-S cells and the results compared with those based on the laminated MWCNT-PANI/titania/PANI design. Figure S3 reports the cycling performance of the Li-S cells with 1, 3, and 5 coating layers of PANI alone on the separator, with 1M LiTFSI in a 1:1 DME/DOL solvent mixture with no $LiNO_3$ as electrolyte, polyethylenimine-MWCNT-sulfur composite cathode (PEISC)[18] and Li metal anode. It is apparent in Figure S3 that improved capacity retention and higher Coulombic efficiency (CE) are achieved as the number of PANI

coatings increases on the separator. For the 5LR PANI separator, a capacity of ~1000 mAh g^{-1} and 96% CE are achieved at the 100^{th} cycle for a fixed 0.5C discharge/charge rate. This can be compared to the results for the uncoated/pristine separator, which exhibits a capacity of 430 mAh g^{-1} and CE of 80% after the 100^{th} cycle at 0.5C. The voltage profiles of 5LR PANI separator are shown in Figure S3. Figure S4 provides a more comprehensive account of the electrochemical cycling behaviors of the Li-S cells with 5LR PANI separator where results at three different C rates: 0.5C, 1C, and 2C are reported. At the 100^{th} cycle, capacities of ~1000 mAh g^{-1}, ~860 mAh g^{-1}, ~740 mAh g^{-1}, and ~97% CE are obtained for 0.5C, 1C, and 2C, respectively. The voltage profiles of 5LR PANI at three different C rates are shown in Figure S4. For comparison, Figure S5 shows the cycling performance of Li-S cells with 5LR PANI separator at 0.5C, 1C, and 2C when 0.05M $LiNO_3$ is added in the electrolyte. Li-S cells with the 5LR PANI on the separator achieved ~99.9% CE for 100^{th} cycles with the small amount of $LiNO_3$ in the electrolyte. The control's CE, however, remained ~91% in the presence of small amount of $LiNO_3$ due to more severe shuttling effect compare to that of the modified separator cells. The capacity retention, on the other hand, increased in the control due to the large number of amine groups in PEI chains, which anchor LiPS in the cathode.[18] With the 5LR PANI coated separator at 100^{th} cycle, capacities of ~1000 mAh g^{-1}, ~900 mAh g^{-1}, ~830 mAh g^{-1}, and ~99.9% CE are obtained for 0.5C, 1C, and 2C, respectively. The voltage profiles of 5LR PANI at three different C rates are shown in Figure S5.

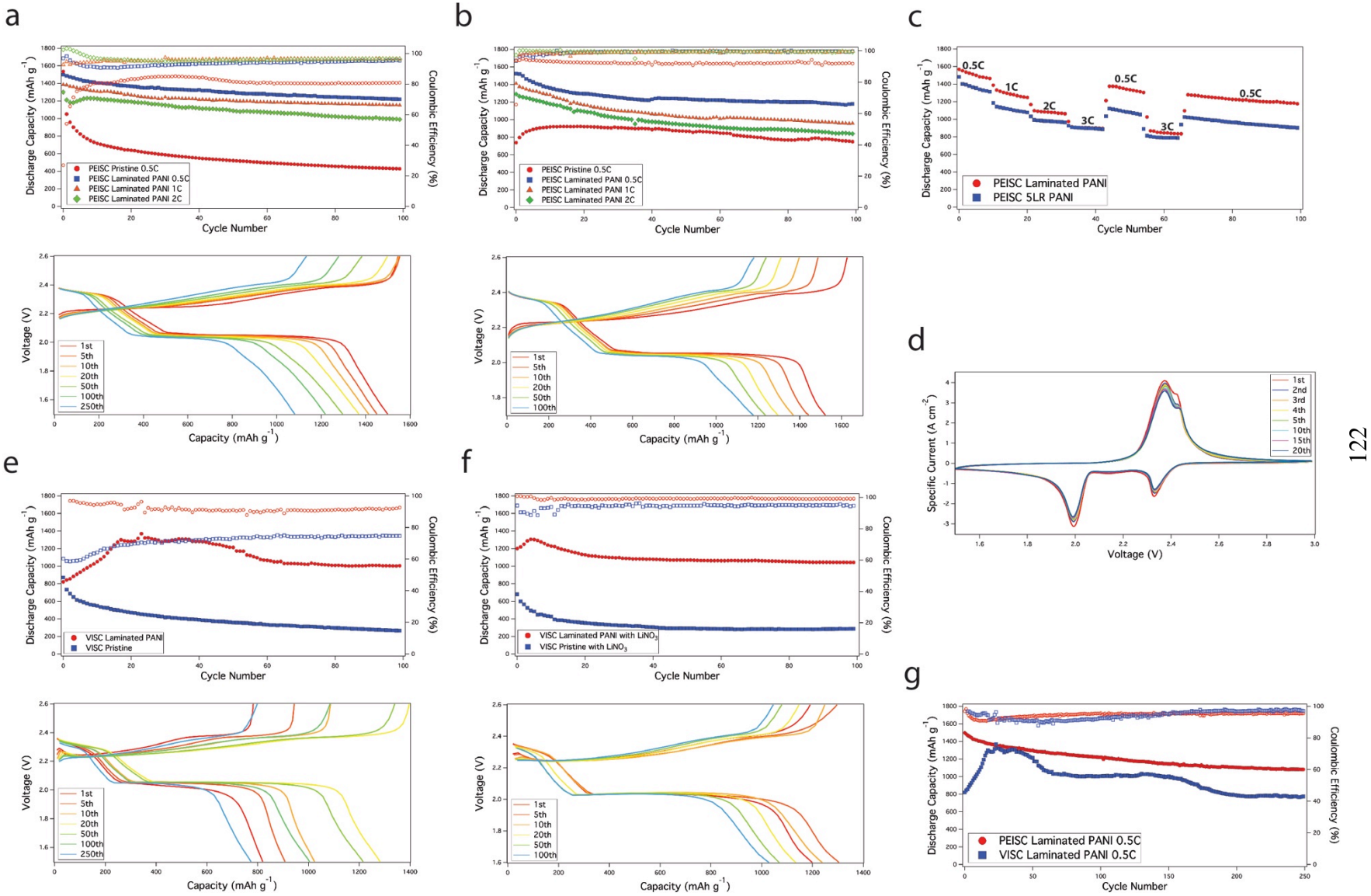
a
b
c
d
e
f
g
Discharge Capacity (mAh g-1)
Coulombic Efficiency (%)
Cycle Number
PEISC Pristine 0.5C
PEISC Laminated PANI 0.5C
PEISC Laminated PANI 1C
PEISC Laminated PANI 2C
Voltage (V)
Capacity (mAh g-1)
1st
5th
10th
20th
50th
100th
250th
0.5C
1C
2C
3C
PEISC Laminated PANI
PEISC 5LR PANI
Specific Current (A cm-2)
2nd
3rd
4th
15th
VISC Laminated PANI
VISC Pristine
VISC Laminated PANI with LiNO3
VISC Pristine with LiNO3
VISC Laminated PANI 0.5C

Figure 4.4. (a) Cycling performance of the laminated PANI separator and pristine separator with PEISC and no $LiNO_3$ in the electrolyte Li-S cells for 100 cycles at three different C rates and the voltage profiles of the laminated PANI separator with PEISC at 0.5C for various cycles. (b) Cycling performance of the laminated PANI separator and pristine separator with PEISC and 0.05M $LiNO_3$ in the electrolyte Li-S cells for 100 cycles at three different C rates and the voltage profiles of the laminated PANI separator with PEISC at 0.5C for various cycles. (c) Various C rate cycling performances of PEISC with the laminated PANI separator and 5LR PANI coated separator with no $LiNO_3$ in the electrolyte Li-S cells for 100 cycles. (d) Cyclic voltammetry measurement of the laminated PANI separator with PEISC and no $LiNO_3$ in the electrolyte Li-S cell. (e) Cycling performance of the laminated PANI separator and pristine separator with VISC and no $LiNO_3$ in the electrolyte Li-S cells for 100 cycles at 0.5C and the voltage profiles of the laminated PANI separator with VISC at 0.5C for various cycles. (f) Cycling performance of the laminated PANI separator and pristine separator with VISC and 0.05M $LiNO_3$ in the electrolyte Li-S cells for 100 cycles at 0.5C and the voltage profiles of the laminated PANI separator with VISC at 0.5C for various cycles. (g) Long time cycling performances of the laminated PANI separators with PEISC and VISC without $LiNO_3$ in the electrolyte Li-S cells at 0.5C.

Next, we consider Li-S cells based on the laminated membrane composed of ~80nm thick (1LR) MWCNT, ~9μm thick (3LR) PANI, and ~900nm thick (3LR) titania NP on Celgard. In comparison to the single-component 5LR PANI (thickness of ~15μm and mass loading of ~500μg cm^{-2})-based membranes assessed in the last section, the laminated PANI coating though more complex is thinner (~10μm) and introduces a lower material mass (400μg cm^{-2}) to the Li-S cell. Figure 4.4a reports cycling performance and voltage profiles for Li-S cells based on these laminated membranes. It is seen that capacities of 1220 mAh g^{-1}, 1150 mAh g^{-1}, and 1000 mAh g^{-1} are obtained at 0.5C, 1C, and 2C, respectively, with ~97% CE at 100^{th} cycle. Comparison with the results from the uncoated membranes shows that the capacity has approximately doubled and the CE increased markedly. It is instructive to compare these results with analogous ones reported for other materials configurations, e.g. cation-shield (CE ~95%)[30] and ionomer film (CE~97%)[31] reported previously for regulating LiPS mass transport and shuttling in

Li-S cells. It is apparent that the CE values achieved for the laminated PANI membranes are comparable with those reported for single ion conductors. A small amount of $LiNO_3$ (0.05M) was added in the electrolyte to observe its effect on electrochemical performance of Li-S cells with laminated membranes. As expected, (Figure 4.4b) CE values approaching 99.9% are achieved without affecting cell capacity and cycling stability. Voltage profiles of the laminated PANI separator Li-S cells at three different C rates with/without $LiNO_3$ in the electrolyte is shown in Figure S6. Moreover, various C rate performance is measured with the laminated PANI separator with no $LiNO_3$ in the electrolyte (See Figure 4.4c). As the C rates increase (0.5C to 1C, 1C to 2C, 2C to 3C), 14%, 15%, and 17% decrease in the capacity is observed with the recovery capacity of 1310 mAh g^{-1}, which is 10% decrease from the previous 0.5C cycling, after cycling the cell from 0.5C to 3C for 10 cycles at each C rates. Comparing this result with the Li-S cell with 5LR PANI separator, higher recovery capacity is obtained (Laminated PANI: 1310 mAh g^{-1} & 5LR PANI: 1110 mAh g^{-1}) for the laminated PANI without loosing the high C rate performances even though lesser amount of PANI is used. Together, these results provide strong support for our hypothesis that membranes based on laminated PANI structures simultaneously provide a path towards high energy and high power Li-S cells by regulating transport of LiPS without compromising active material utilization in the cathode.

Figure 4.4d report cyclic voltammograms of the Li-S cell with laminated PANI separator for $LiNO_3$ free system. Scan rate of 0.1 mV s^{-1} and voltage window of 1.5V-3V is used to perform the measurement. The cathodic scans show distinctive voltage plateaus at 2.3V

and 2V. The first peak at 2.3V represents cyclic sulfur breaking and forming high order LiPS ions whereas the next peak at 2V represents the reduction of high order LiPS ion to low order LiPS. This voltage plateaus are typical for Li-S cells that represent two-step reduction process of elemental sulfur. For the anodic scans, the distinctive voltage plateaus, oxidation peaks, are observed at 2.37V and 2.43V based on the phase transition mechanism. [10] Stable anodic and cathodic peak positions are achieved for several cycles. Hence, highly reversible electrochemical reactions are confirmed for the Li-S cell with laminated PANI separator without $LiNO_3$ in the electrolyte.

A disadvantage of the PEISC cathode is relatively low sulfur loading (1.2 mg cm^{-2} S and content of 50% S). State-of-the-art Li-S cells require substantially higher sulfur loadings and content in the cathode. As more rigorous tests of the laminated PANI membranes, we also assessed the materials, vapor infused sulfur cathode (VISC), in Li-S cells with higher sulfur loading (3.5 mg cm^{-2} S and 68% S), created by a previously reported vapor infusion method.[11] Figure 4.4e reports cycling performance and voltage profiles of Li-S cells with both the pristine and laminated PANI separator membranes, with VISC and no $LiNO_3$ in the electrolyte. The control Li-S cell exhibits a capacity of ~270 mAh g^{-1} and 74% CE after 100^{th} cycles at 0.5C. In contrast the laminated PANI separator displays a capacity of ~1000 mAh g^{-1} and 94% CE after the 100^{th} cycle at 0.5C. Closer inspection of the cycling results for the VISC using the laminated PANI membrane separator show initial increase in the discharge capacity. This behavior is understood to be a manifestation of the laminated coatings capacity to reutilize LiPS as it is built up in the sorbent layer in the membrane.[40] Our results therefore verify that the laminated PANI

membrane separator is capable of cycling high sulfur loading cathodes in cells without $LiNO_3$ in the electrolyte. As before, we also performed studies in which 0.05M $LiNO_3$ is used in the electrolyte (See Figure 4.4f). The results show that while similar capacity is observed as for the $LiNO_3$ free case, ~99.9% CE is achieved. Figure 4.4e and Figure 4.4f report voltage profiles for the VISC cells with and without $LiNO_3$ in the electrolyte, it is apparent that they are stable in both cases. Figure 4.4g shows that these favorable results are preserved in longer term cycling experiments, where Li-S cells with PEISC and VISC and no $LiNO_3$ are observed to yield discharge capacities of 1090 mAh g^{-1} and 96% CE (PEISC) and 780 mAh g^{-1} and 97% CE (VISC) after the 250^{th} discharge cycle at 0.5C. We therefore conclude that membranes based on the proposed laminated PANI configuration using existing Celgard separator as a substrate provide a promising path towards Li-S cells with stable electrochemical performance. The results also show that compact layers of PANI and titania NPs created by LBS work synergistically to improve membrane performance.

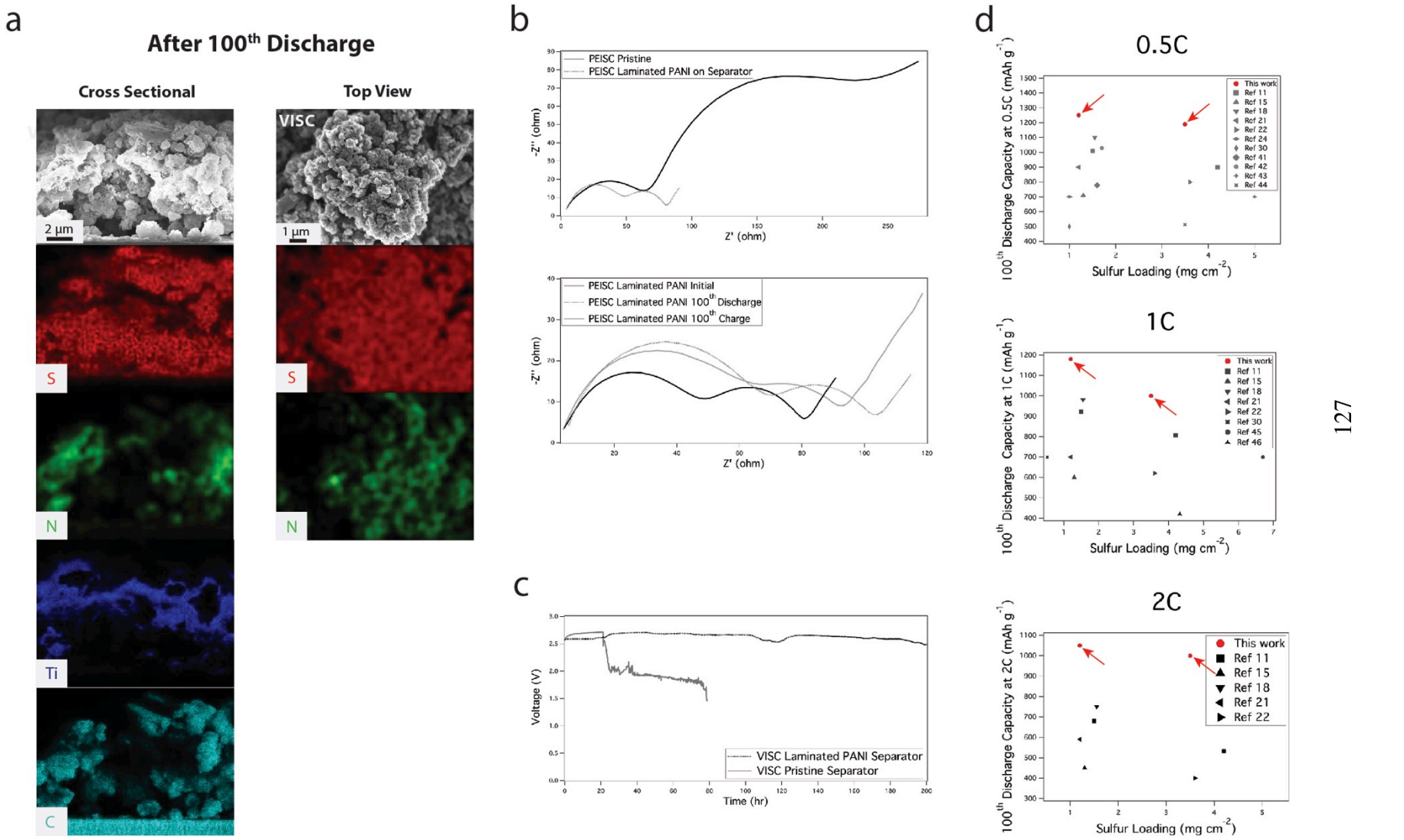
a
After 100th Discharge
Cross Sectional
Top View
2 µm
1 µm
VISC
S
N
Ti
C
b
PEISC Pristine
PEISC Laminated PANI on Separator
-Z'' (ohm)
Z' (ohm)
PEISC Laminated PANI Initial
PEISC Laminated PANI 100th Discharge
PEISC Laminated PANI 100th Charge
c
Voltage (V)
Time (hr)
VISC Laminated PANI Separator
VISC Pristine Separator
d
0.5C
1C
2C
100th Discharge Capacity at 0.5C (mAh g-1)
100th Discharge Capacity at 1C (mAh g-1)
100th Discharge Capacity at 2C (mAh g-1)
Sulfur Loading (mg cm-2)
This work
Ref 11
Ref 15
Ref 18
Ref 21
Ref 22
Ref 24
Ref 30
Ref 41
Ref 42
Ref 43
Ref 44
Ref 45
Ref 46

Figure 4.5. (a) SEM and EDXS (Cross sectional elemental mapping: Sulfur, Nitrogen, Titanium, and Carbon & Top-view elemental mapping: Sulfur and Nitrogen) of the cycled laminated PANI separator with VISC. (b) AC impedance measurements of non-cycled Li-S cells without $LiNO_3$ in the electrolyte and PEISC with the pristine and the laminated PANI separator-upper data and cycled corresponding Li-S cell with the laminated PANI separator after 100^{th} discharge and charge-bottom data. (c) Self-discharge of pristine and the laminated PANI separators with VISC and no $LiNO_3$ in the electrolyte Li-S cells. (d) Li-S cells comparison data of 100^{th} discharge capacity versus sulfur loading at three different C rates for our work and other literature works.[11,15,18,20,21,23,29,30,41–46]

The cycled laminated PANI membranes were investigated via SEM and energy-dispersive X-ray spectroscopy (EDXS). Figure 4.5a shows cross sectional and top view SEM and elemental mapping of sulfur, nitrogen, titanium, and carbon on the laminated PANI separator that is cycled 100 times with VISC and no $LiNO_3$ in the electrolyte. The laminated structure is observed to be well maintained after complete 100^{th} cycles. This is due to the property of the PANI, which is known as soft polymer that could withstand the pressures from volumetric expansion of sulfur during the charge-discharge process.[32] A strong field map of sulfur is also apparent in the cross sectional and top view of the laminated PANI-based membranes.

Figure 4.5b shows the AC impedance (ACI) of Li-S cells with pristine and the laminated PANI separators with VISC and no $LiNO_3$ in the electrolyte for before and after cycling. The upper ACI data shows the impedance comparison between the Li-S cells with the laminated PANI and pristine separator before cycling, and lower impedance is measured for the laminated PANI separator Li-S cell indicating that the high conductivity of PANI helps to reduce the interfacial impedance. The bottom ACI data shows the impedance data of the laminated PANI separator Li-S cell before and after 100^{th} cycle. Slight

increase of impedance is observed after 100th discharge. This is because the laminated PANI coatings adsorb LiPS which increases the interfacial impedance. After 100th charge, the impedance gets lower than that of 100th discharge but higher than that of initial. This is due to the adsorbed LiPS is reutilized during the charge process which lowers the interfacial impedance, and since sulfur is present on the surface of the coatings on the separator, higher impedance is measured compared to the initial impedance measurement which the surfaces are free from LiPS and sulfur. Hence, reutilization and lower impedance of adsorbed LiPS is observed with the laminated PANI separator. We have also performed self-discharge experiment with the laminated PANI separator Li-S cells with VISC and no $LiNO_3$ in the electrolyte (See Figure 4.5c). With the laminated PANI separator, the Li-S cell can stably remains as initial state >200 hours where as the Li-S cell with the pristine separator fails after 20 hours. This indicates that the top surface of PANI on the cathode provides a protection layer to alleviate the loss of sulfur during shelf time.

We have compared our results with current literature values as shown in Figure 4.5d. It is apparent that the Li-S cell performances achieved with the proposed membranes stand out among current literature works in terms of the capacity and high rate performances achievable for high sulfur loadings in the cathode.[11,15,18,20,21,23,29,30,41–46] The effect of the membranes are seen to be more dramatic at high current rates – at 2C, for example, the results obtained using the laminated membrane separators are superior to all other literature reports at comparable sulfur loading.

In this study, we report utilization of LBS coating method to fabricate sophisticated

coating structure with the successful integration of polymer/ceramic hybrid separator coatings for LiPS reservoir for the advancement of Li-S cells. Yielding high quality coatings of PANI and titania NP via LBS method and optimizing the coating configuration, capacity of ~1220 mAh g^{-1}, ~1150 mAh g^{-1}, and ~1000 mAh g^{-1} are obtained at 0.5C, 1C, and 2C, respectively, with ~97% CE at 100th cycle in additive-free electrolyte. Hence, simple multifunctional separator is fabricated that can maintain stable cycling performance with high CE without $LiNO_3$ in the electrolyte. More sophisticated configurations and well-nanostructured materials can be therefore used for the separator coating in the future to further advance state-of-the-art Li-S systems.

4.3 Experimental Section

Preparation of nanomaterial suspensions: The titania NP (99% purity, Rutile, Advanced Materials^{TM}), MWCNT (>95% carbon, L: 6-9 nm x 55 μm, Sigma Aldrich) and PANI (average M_w >15,000, emeraldine salt, Sigma Aldrich) suspensions are prepared using pure ethanol (Decon, 200 Proof) and selections of materials above (1wt%). After mixing the particles with pure ethanol, all the suspensions are sonicated for 10 minutes to allow good dispersion of particles.

Preparation of PEISC and VISC*:* PEISC – The sulfur is infused to PEI attached MWCNT matrix as described in previous report [18]. The S@C composite (80 wt%) was mixed with Super P (10 wt%) and polyvinylidene fluoride (10 wt%) dissolved in N-methyl-2-prolidone (15 wt%) in N-methyl-2-prolidone, and the mixture is ball-milled at 50 rev s^{-1} for 30 minutes. The resulting viscous slurry was coated onto a carbon sprayed

aluminum foil as a current collector using doctor-blade method. The coated slurry is then dried in a convection oven at 60 ^{o}C for 5 hours. The prepared electrode (1.2 mg cm^{-2} S & 50% S) is cut into a circular disk. VISC – sulfur was vapor-infused into the carbon fiber matrix via high temperature method [11]. The S@C composite (85 wt%) was mixed with vapor grown carbon fiber (10 wt%) and polyvinylidene fluoride (5 wt%) dissolved in N-methyl-2-prolidone (15 wt%) in N-methyl-2-prolidone, and the mixture is ball-milled at 50 rev s^{-1} for 30 minutes. The sulfur cathodes (3.5 mg cm^{-2} S and 68% S) are prepared by coating the composite onto a carbon sprayed Al foil. Including coating materials of the laminated PANI, the sulfur contents for PEISC (43% S) and VISC (63% S) are achieved. The cathode size (1.266 cm^{2}) is used for the cathodes.

Coating Process*:* Separator (Celgard 2500) is cut into a circular disk (1.6 cm diameter). A cover glass (1.8 by 1.8 cm) is used as a substrate for the cutted separators. The separator is placed on top of the cover glass and the edges of the separator is taped with Kapton tape. LBS method requires tap water, prepared suspensions, a beaker, and micropipette. Prepared separator is quickly rinsed with running water. The suspension (<1mL) is injected at the surface water via a neck of the beaker. During the self-assembly process, the separator is slowly raised followed by constant injection of the suspension (See supplementary videos). After single coating layer of desired material is coated on the separator, the coated separator is then dried on a hotplate (110 ^{o}C) for less then a minute. After coating a single layer, a drop of isopropanol (IPA) is applied to the coated separator to uniformly wet the surface with water, and the separator is remained in clean water about 10~20 seconds. After fully wetting the coated separator, another LBS coating

is performed until desired number of layers and materials are coated. After desired numbers of coatings are achieved, the separator is dried on the hotplate (125 ^{o}C) for 1 minute to fully remove any moisture on the separator. To fabricate the laminated PANI structure, single coating of MWCNT is applied on the separator. After drying, a drop of IPA is used to fully wet the separator surface and remained inside of the clean water ~15 seconds. After MWCNT coating, 2 coatings of PANI are made on the separator followed by 3 coating layers of titania NP and ending with another layer of PANI. Each coating methods is same as mentioned above to coat these materials. After the final drying, the separator is removed from the cover glass substrate and used to fabricate Li-S cells.

Battery assembly: CR2032-type coin cells are used to make Li-S cells. Prepared separators, Li foil disks (0.5 inch in diameter), prepared cathodes, stainless-steel springs and spacers, and the electrolytes (40 μL, 1M Bis(trifluoromethane)sulfonamide lithium salt (LiTFSI, Sigma Aldrich) in DME:DOL (1:1 v/v) electrolyte with/without 0.05M $LiNO_3$) are used to assemble Li-S cells. First, electrolyte (20 μL) is applied onto coated side of the separator, and cathode is placed on top of the separator. Then, another half amount of the electrolyte is applied at the other side of the separator, and Li foil is placed. On top of the Li, stainless steel disk is placed, and the spring is placed next. After all the components are assembled, the coin cell is punched (15 MPa). The cell is rested around 15 minutes before testing. The assembly process is carried out in Ar filled gaseous environment (MBraun Labmaster).

***Characterization**:* The assembled Li-S cells are tested at room-temperature and evaluated under galvanostatic conditions using Neware CT – 3008 battery testers. Two voltage windows are chosen for Li-S systems that involve $LiNO_3$ co-salt in the electrolyte. Without the co-salt, 1.5V to 2.6V voltage window is chosen whereas with the co-salt, 1.7V to 2.6V voltage window is chosen to prevent the degradation on the passivation layer formed by $LiNO_3$ at the surface of Li. Cyclic voltammetry measurements are done by CHI600D potentiostat, and scan rate (0.1 mV s^{-1}) and voltage window (1.5V to 3V) is used during the analysis. LEO 1550 FESEM is used for SEM and EDXS analysis with 5 kV and 10 kV acceleration voltages. AC impedance spectroscopy is measured using Novocontrol N40 broadband dielectric spectroscopy. KSV NIMA L & LB Troughs equipment is used to characterize the films qualities and measure surface pressure profiles of the materials. The trough (7.5 cm x 32.4 cm, See Figure S1) is cleaned using pure ethanol and DI water to rinse off all contaminants. The trough is filled up with DI water. For LBT measurement, suspension (~3 mL) is spread at the surface of water and rested about 5 to 7 minutes to evaporate remaining ethanol from the suspension. The floating particles are compressed via mechanical barriers (3 mm min^{-1}) and the surface pressure profiles are measured. For LBS measurement, the trough area (~25 cm^2) is matched with the side of the beaker to compare actual coating process. The surface pressure profile is measured during the self-assembly process, and the fully formed films are compressed (3 mm min^{-1}) without resting to collect the full profiles.

4.4 Supporting Information

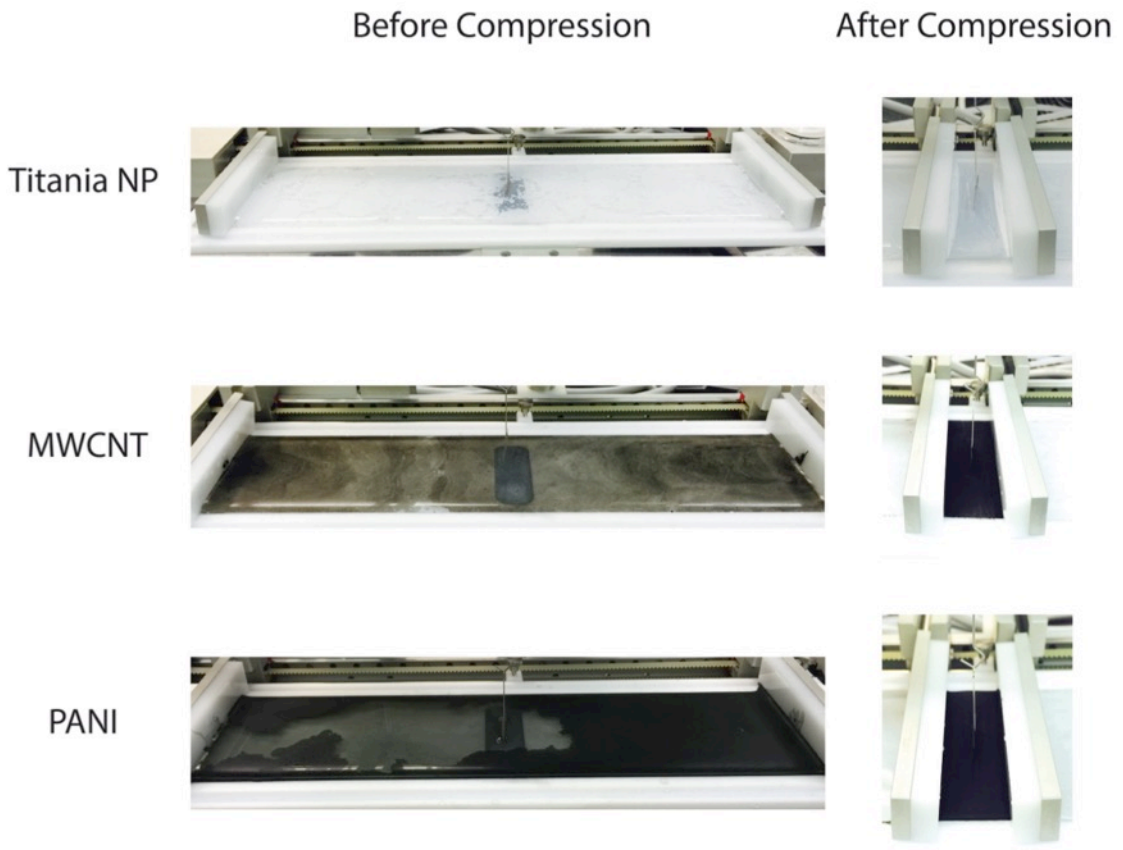

Figure S1. Physical images of Langmuir-Blodgett trough surface pressure profile measurements before and after the compression of the films of Titania NP, MWCNT, and PANI. Note that folding of the films, starting at the mechanical barriers, is shown in "After compression" which indicates that films are stable at liquid-gas interface.

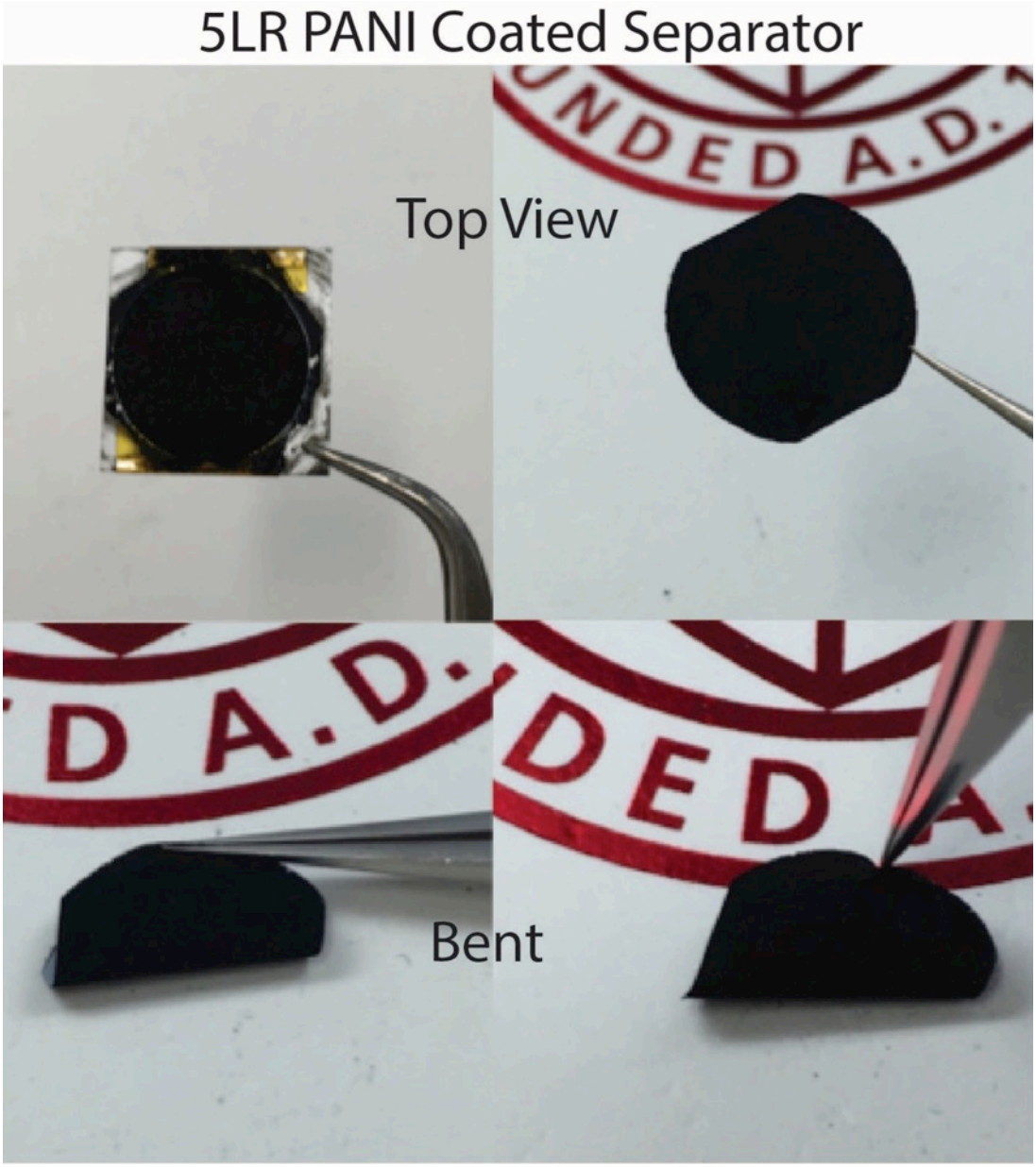

Figure S2. Mechanical strength demonstration of 5LR PANI coated separator.

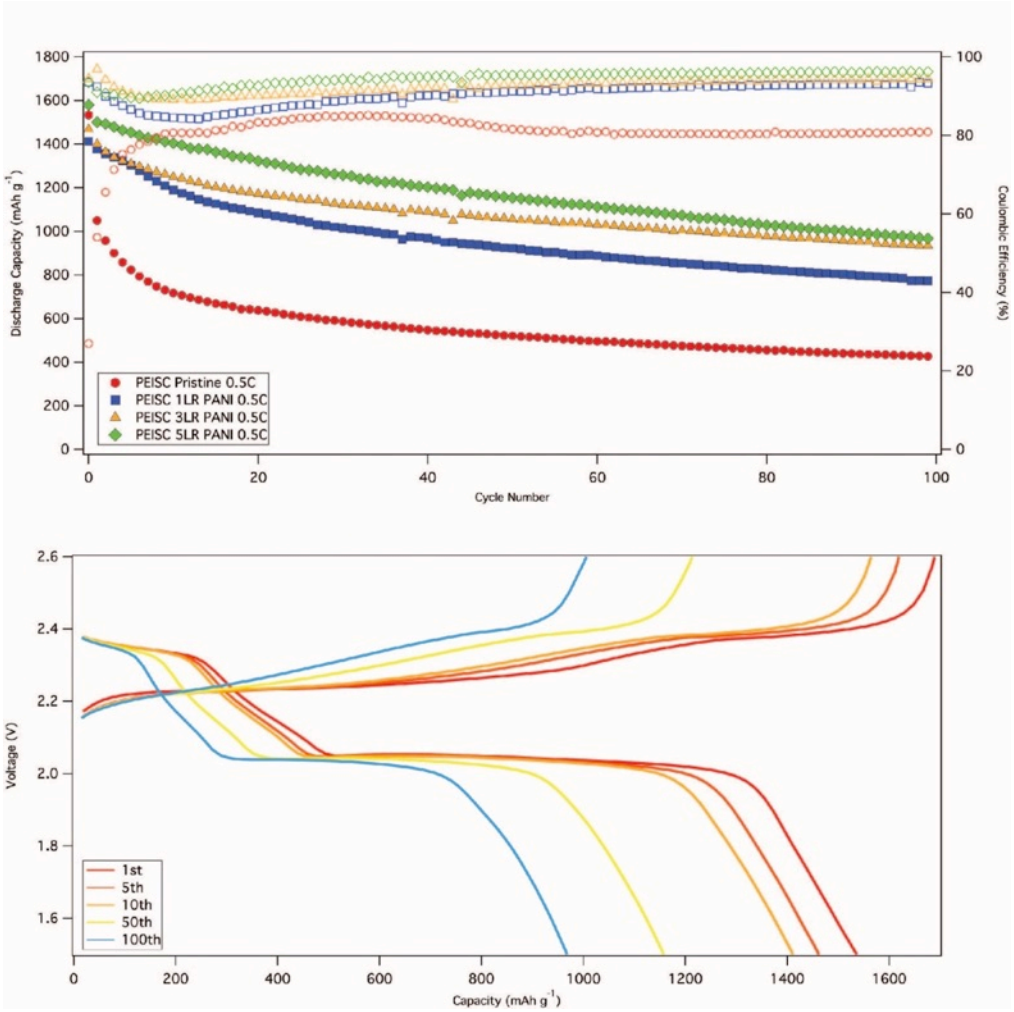

Figure S3. Cycling performance of the 1-5LR PANI coated separators and pristine separator with PEISC and no $LiNO_3$ in the electrolyte Li-S cells at 0.5C for 100 cycles and the voltage profiles of 5LR PANI coated separator Li-S cell at 0.5C for various cycles.

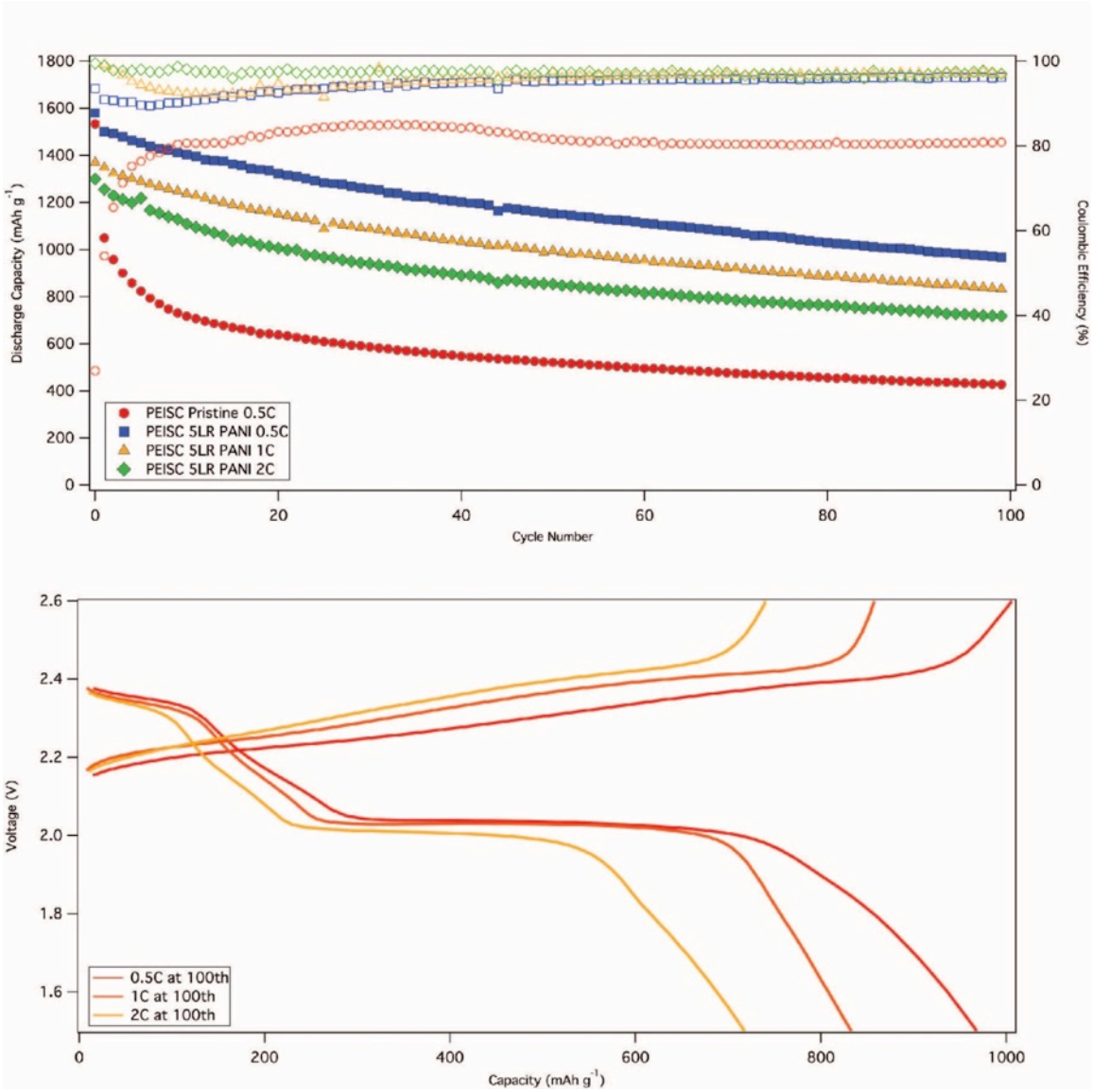

Figure S4. Cycling performance of 5LR PANI coated separators and pristine separator with PEISC and no $LiNO_3$ in the electrolyte Li-S cells for 100 cycles at three different C rates and the voltage profiles of 100th cycled 5LR PANI coated separators with PEISC Li-S cells at three different C rates for various cycles.

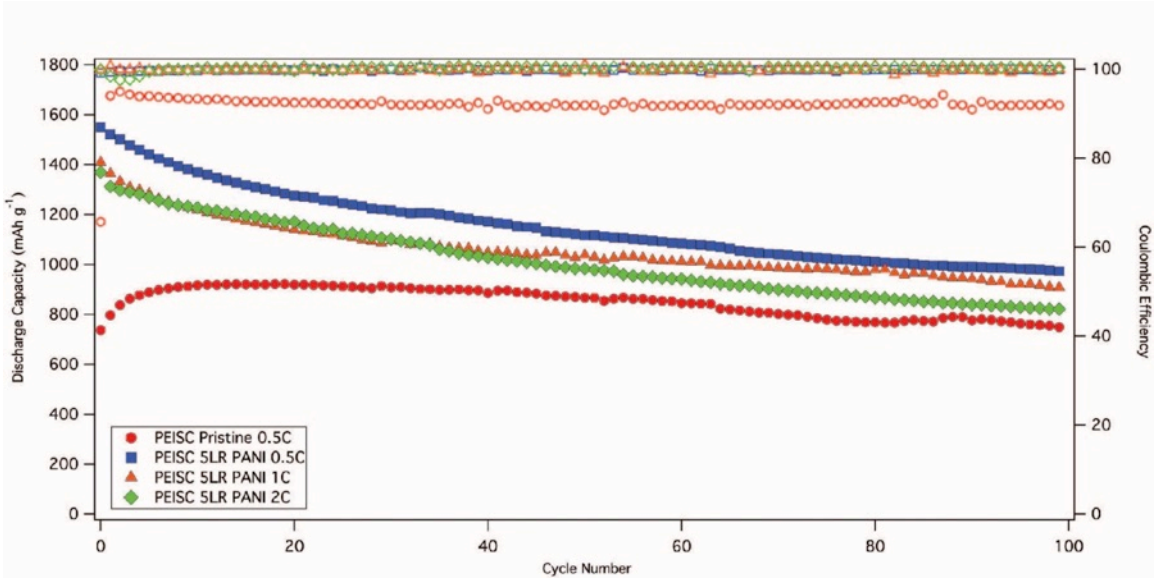

Figure S5. Cycling performance of 5LR PANI coated separators and pristine separator with PEISC and 0.05M $LiNO_3$ in the electrolyte Li-S cells for 100 cycles at three different C rates.

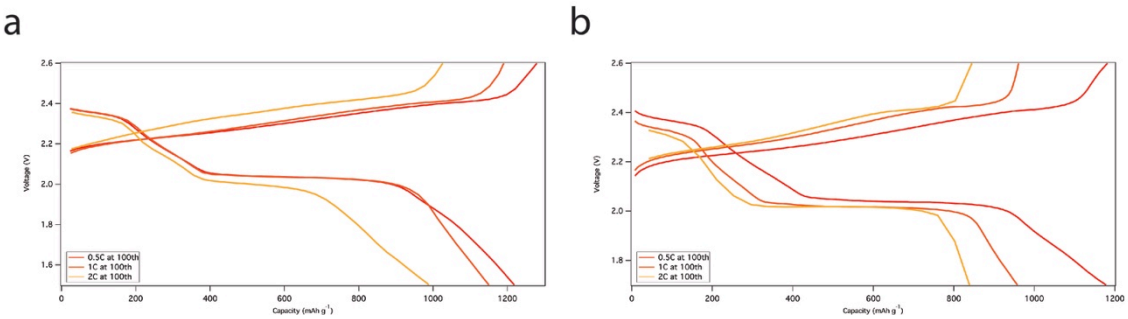

Figure S6. (a) Voltage profiles of the laminated PANI separator with PEISC and without $LiNO_3$ in the electrolyte Li-S cells at 100^{th} cycle for three different C rates. (b) Voltage profiles of the laminated PANI separator with PEISC and with 0.05M $LiNO_3$ in the electrolyte Li-S cells at 100^{th} cycle for three different C rates.

Supporting References:

[1] L. Ma, H. L. Zhuang, S. Wei, K. E. Hendrickson, M. S. Kim, G. Cohn, R. G. Hennig, L. A. Archer. *ACS Nano* **2015**, 10**,** 1050–1059.

[2] N. Jayaprakash, J. Shen, S. S. Moganty, A. Corona, L. A. Archer. *Angew. Chemie* **2011**, 50**,** 5904–5908.

REFERENCES

1. Miller, T. J. Electrical energy storage for vehicles: Targets and metrics. *Ford Mot. Co.* **1,** 1–69 (2009).
2. Armand, M. & Tarascon, J.-M. Building better batteries. *Nature* **451,** 652–657 (2008).
3. Goodenough, J. B. & Kim, Y. Challenges for rechargeable Li batteries. *Chem. Mater.* **22,** 587–603 (2010).
4. Zu, C.-X. & Li, H. Thermodynamic analysis on energy densities of batteries. *Energy Environ. Sci.* **4,** 2614 (2011).
5. Bruce, P. G., Freunberger, S. a., Hardwick, L. J. & Tarascon, J.-M. Li–O2 and Li–S batteries with high energy storage. *Nat. Mater.* **11,** 172–172 (2011).
6. Hassoun, J. & Scrosati, B. Moving to a solid-state configuration: A valid approach to making lithium-sulfur batteries viable for practical applications. *Adv. Mater.* **22,** 5198–5201 (2010).
7. Yang, Z. *et al.* In situ synthesis of lithium sulfide-carbon composites as cathode materials for rechargeable lithium batteries. *J. Mater. Chem. A* **1,** 1433–1440 (2013).
8. Guo, Y. G., Hu, J. S. & Wan, L. J. Nanostructured materials for electrochemical energy conversion and storage devices. *Adv. Mater.* **20,** 2878–2887 (2008).
9. Ma, L., Hendrickson, K. E., Wei, S. & Archer, L. A. Nanomaterials: Science and applications in the lithium–sulfur battery. *Nano Today* **10,** 315–338 (2015).
10. Mikhaylik, Y. V. & Akridge, J. R. Polysulfide shuttle study in the Li/S battery

system. *J. Electrochem. Soc.* **151,** A1969–A1976 (2004).

11. Jayaprakash, N., Shen, J., Moganty, S. S., Corona, A. & Archer, L. A. Porous hollow carbon@sulfur composites for high-power lithium-sulfur batteries. *Angew. Chemie* **50,** 5904–5908 (2011).
12. Nelson, J. *et al.* In operando X-ray diffraction and transmission X-ray microscopy of lithium sulfur batteries. *J. Am. Chem. Soc.* **134,** 6337–6343 (2012).
13. Wei Seh, Z. *et al.* Sulphur-TiO2 yolk-shell nanoarchitecture with internal void space for long-cycle lithium-sulphur batteries. *Nat. Commun.* **4,** 1331 (2013).
14. Ji, X., Lee, K. T. & Nazar, L. F. A highly ordered nanostructured carbon-sulphur cathode for lithium-sulphur batteries. *Nat. Mater.* **8,** 500–506 (2009).
15. Wang, H. *et al.* Graphene-Wrapped Sulfur Particles as a Rechargeable Lithium – Sulfur Battery Cathode Material with High Capacity and Cycling Stability. *Nano Lett.* **11,** 2644–2647 (2011).
16. Ma, L. *et al.* Hybrid cathode architectures for lithium batteries based on TiS 2 and sulfur. *J. Mater. Chem. A* **3,** 19857–19866 (2015).
17. Ma, L. *et al.* Tethered Molecular Sorbents: Enabling Metal-Sulfur Battery Cathodes. *Adv. Energy Mater.* **4,** 390–399 (2014).
18. Ma, L. *et al.* Enhanced Li–S Batteries Using Amine-Functionalized Carbon Nanotubes in the Cathode. *ACS Nano* **10,** 1050–1059 (2015).
19. Hendrickson, K. E., Ma, L., Cohn, G., Lu, Y. & Archer, L. A. Model Membrane-Free Li-S Batteries for Enhanced Performance and Cycle Life. *Adv. Sci.* **2,** 68–77 (2015).
20. Yao, H. Bin *et al.* Improved lithium-sulfur batteries with a conductive coating on

the separator to prevent the accumulation of inactive S-related species at the cathode-separator interface. *Energy Environ. Sci.* **7,** 3381 (2014).

21. Balach, J. *et al.* Functional Mesoporous Carbon-Coated Separator for Long-Life, High-Energy Lithium-Sulfur Batteries. *Adv. Funct. Mater.* **25,** 5285–5291 (2015).
22. Wang, G., Lai, Y., Zhang, Z., Li, J. & Zhang, Z. Enhanced rate capability and cycle stability of lithium–sulfur batteries with a bifunctional MCNT@PEG-modified separator. *J. Mater. Chem. A* **3,** 7139–7144 (2015).
23. Zhang, Z., Lai, Y., Zhang, Z. & Li, J. A functional carbon layer-coated separator for high performance lithium sulfur batteries. *Solid State Ionics* **278,** 166–171 (2015).
24. Wei, H., Li, B., Zuo, Y. & Xia, D. Enhanced Cycle Performance of Lithium-Sulfur Battereis Using a Separator Modified with a PVDF-C Layer. *ACS Appl. Mater. Interfaces* **6,** 20276–20281 (2014).
25. Li, F. *et al.* A graphene-pure-sulfur sandwich structure for ultrafast, long-life lithium-sulfur batteries. *Adv. Mater.* **26,** 625–631 (2014).
26. Xiao, Z. *et al.* A Lightweight TiO2/Graphene Interlayer, Applied as a Highly Effective Polysulfide Absorbent for Fast, Long-Life Lithium-Sulfur Batteries. *Adv. Mater.* **27,** 2891–2898 (2015).
27. Zhang, Z., Lai, Y., Zhang, Z., Zhang, K. & Li, J. Al2O3-coated porous separator for enhanced electrochemical performance of lithium sulfur batteries. *Electrochim. Acta* **129,** 55–61 (2014).
28. Chen, Y. *et al.* Chitosan as a functional additive for high-performance lithium–sulfur batteries. *J. Mater. Chem. A* **3,** 15235–15240 (2015).

29. Zhang, Z., Zhang, Z., Li, J. & Lai, Y. Polydopamine-coated separator for high-performance lithium-sulfur batteries. *J. Solid State Electrochem.* **19,** 1709–1715 (2015).

30. Huang, J.-Q. *et al.* Ionic shield for polysulfides towards highly-stable lithium–sulfur batteries. *Energy Environ. Sci.* **7,** 347 (2014).

31. Jin, Z., Xie, K., Hong, X., Hu, Z. & Liu, X. Application of lithiated Nafion ionomer film as functional separator for lithium sulfur cells. *J. Power Sources* **218,** 163–167 (2012).

32. Xiao, L. *et al.* A soft approach to encapsulate sulfur: Polyaniline nanotubes for lithium-sulfur batteries with long cycle life. *Adv. Mater.* **24,** 1176–1181 (2012).

33. Zhou, W., Yu, Y., Chen, H. & Disalvo, F. J. Yolk − Shell Structure of Polyaniline-Coated Sulfur for Lithium − Sulfur Batteries. *J. Am. Chem. Soc.* 16736–16743 (2013).

34. Li, W., Zhang, Z., Kang, W., Tang, Y. & Lee, C.-S. Rice-like Sulfur/Polyaniline Nanorods Wrapped by Reduced Graphene Oxide Nanosheets as High-Performance Cathode for Lithium-Sulfur Batteries. *ChemElectroChem* **3,** 1–8 (2016).

35. Li, G. C., Li, G. R., Ye, S. H. & Gao, X. P. A Polyaniline-coated sulfur/carbon composite with an enhanced high-rate capability as a cathode material for lithium/sulfur batteries. *Adv. Energy Mater.* **2,** 1238–1245 (2012).

36. Evers, S., Yim, T. & Nazar, L. F. Understanding the nature of absorption/adsorption in nanoporous polysulfide sorbents for the Li-S battery. *J. Phys. Chem. C* **116,** 19653–19658 (2012).

37. Nie, H.-L., Dou, X., Tang, Z., Jang, H. D. & Huang, J. High-Yield Spreading of

Water-Miscible Solvents on Water for Langmuir–Blodgett Assembly. *J. Am. Chem. Soc.* **137,** 10683–10688 (2015).

38. Fanton, X. & Cazabat, A. M. Spreading and Instabilities Induced by a Solutal Marangoni Effect. *Langmuir* **14,** 2554–2561 (1998).

39. Sternling, C. V. & Scriven, L. E. Interfacial turbulence: Hydrodynamic instability and the marangoni effect. *AIChE J.* **5,** 514–523 (1959).

40. Chang, C. H., Chung, S. H. & Manthiram, A. Effective Stabilization of a High-Loading Sulfur Cathode and a Lithium-Metal Anode in Li-S Batteries Utilizing SWCNT-Modulated Separators. *Small* **12,** 174–179 (2016).

41. Ding, Y. L. *et al.* Facile Solid-State Growth of 3D Well-Interconnected Nitrogen-Rich Carbon Nanotube-Graphene Hybrid Architectures for Lithium-Sulfur Batteries. *Adv. Funct. Mater.* **26,** 1112–1119 (2015).

42. Li, Z., Zhang, J. T., Chen, Y. M., Li, J. & Lou, X. W. (David). Pie-like electrode design for high-energy density lithium–sulfur batteries. *Nat. Commun.* **6,** 8850–8858 (2015).

43. Xu, T. *et al.* Mesoporous carbon-carbon nanotube-sulfur composite microspheres for high-areal-capacity lithium-sulfur battery cathodes. *ACS Appl. Mater. Interfaces* **5,** 11355–11362 (2013).

44. Pang, Q., Kundu, D. & Nazar, L. F. A graphene-like metallic cathode host for long-life and high-loading lithium–sulfur batteries. *Mater. Horiz.* **3,** 130–136 (2016).

45. Chung, S. & Manthiram, A. High-Performance Li − S Batteries with an Ultra-lightweight MWCNT- Coated Separator. *Phys. Chem. Lett.* **5,** 1987–1983 (2014).

46. Papandrea, B. *et al.* Three-dimensional graphene framework with ultra-high sulfur content for a robust lithium–sulfur battery. *Nano Res.* **9,** 240–248 (2016).